Control of a Three-phase Shunt Active Power Filter for Unbalanced Conditions

by

Saad Fahad Al-Gahtani

A dissertation submitted to the Graduate Faculty of
Auburn University
in partial fulfillment of the
requirements for the Degree of
Doctor of Philosophy

Auburn, Alabama
December 15, 2018

Keywords: shunt active power filter, instantaneous
reactive power theory, harmonics, unbalanced conditions

Approved by

Dr. Mark Nelms, Chair, Professor of Electrical and Computer Engineering
Dr. Mark Halpin, Professor of Electrical and Computer Engineering
Dr. John Hung, Professor of Electrical and Computer Engineering
Dr. Eduard Muljadi, Professor of Electrical and Computer Engineering

Abstract

The awareness of the quality and reliability of the power system has been increased in recent years due to several reasons. The excessive increasing of the applications of power electronics devices on the grid causes power quality problems including harmonic distortion and unbalancing in the power system. The unbalanced loading and the variations in the loads cause system imbalance. Harmonic distortion and system imbalance weaken the system and make it unstable and unsecured.

Several devices have been introduced for solving power quality problems. Problems such as imbalance and harmonics can be corrected using filters. Because of the increasing of nonlinear loads, the active power filter (APF) have been preferable over passive filters. The shunt APFs are controlled to eliminate power quality problems related to source current. However, some control systems do not operate effectively under unbalanced power system operation.

The extraction of the positive and negative sequence components is important for the control system of shunt APFs. Traditional extraction methods have weak performance under unbalanced conditions. Therefore, a new extraction method is introduced. It operates under any power system conditions, and is intended to extract the positive and negative sequence components from the measured signals. The analysis and evaluation demonstrate the capability of this extraction method.

An improved control method based on instantaneous real and reactive power theory (IRPT) is proposed. Using the proposed extraction method allows the control system to operate under

different power system conditions. Several simulation and experimental tests are presented to validate the work of this control method. Moreover, the system frequency could fluctuate due to changes in the power system. For that, the proposed control method was examined under frequency change. A frequency detection method was designed using the proposed extraction filter. It is aimed to measure the frequency and allow the control system to adapt the system frequency. Several simulation and experimental tests were performed to validate the operation of the proposed control methods. Finally, a voltage sensorless control method is presented. It is intended to reduce the number of the measured signals. The proposed extraction method is used with the source current. The simulation and experimental results show the operation of this control technique.

Acknowledgements

First and foremost I would like to express my deepest gratitude and thanks to my parents, my wife, and my brothers for their endless support, encouragement and patience. I would not achieve anything without them.

It is a pleasure to extend my thanks, appreciations and gratitude to Dr. Nelms for his esteemed guidance, encouragement, friendship and support during my studies.

Additionally, I would like to thank all my professors and colleagues who taught me, gave me valuable comments, and supported me in any way. I would like to thank Mr. Mike Eddy for his technical help and useful suggestions during the study.

Finally, I want to thank my wife again for her outstanding support, encouragement, and unlimited patience while bearing much of the life burden until the completion of this dissertation.

Table of Contents

List of Figures

List of Tables

List of Symbols

APF	Active power filter
IRPT	Instantaneous reactive power theory
VSI	Voltage-sourced inverter
PCC	Point of common coupling
PWM	Pulse-width modulation
THD	Total harmonic distortion
α	Time-delay function of $\frac{1}{90}$ seconds
α^2	Time-delay function of $\frac{1}{180}$ seconds
f_{abc}	Three-phase quantities
f_{012}	Symmetrical components
$f^{(1)}$	Positive sequence quantity
$f^{(2)}$	Negative sequence quantity
p, q	Instantaneous real and reactive powers
$\bar{p}$, $\bar{q}$	Instantaneous average real and reactive powers
$\tilde{p}$, $\tilde{q}$	Instantaneous oscillating real and reactive powers
i_s	Source current
i_L	Load current
i_f	Filter current
i_{ref}	Reference current

v_{pcc}	PCC voltage
v_{α}^{+}, v_{β}^{+}	Positive sequence components of voltage in αβ coordinates
i_{α}^{-}, i_{β}^{-}	Negative sequence components of current in αβ coordinates
L_i	Inverter-side inductor of LCL filter
L_g	Grid-side inductor of LCL filter
C_f	Capacitor of LCL filter
R_d	Damping resistor
NL	Nonlinear load
BLL	Balanced linear load
ULL	Unbalanced linear load

CHAPTER 1: INTRODUCTION

Power quality problems arise from the deviation from ideal conditions of the power system [1]. Non-linear loads cause several power quality issues such as low power factor, low efficiency, electromagnetic interference (EMI), and distortions in the voltage and the current signals [2] [3]. Other issues come from the zero, negative and positive components generated from a single-phase load or unbalanced loads. The awareness of the quality and reliability of the power system has increased in recent years [4] [5]. The impacts of power quality problems are greatly adverse on the power system, and they should be solved in order to have reliable and secure power systems [2].

1.1 Power Quality Problems

Different power systems problems such as current harmonics, voltage and load variations, and frequency variations can be encountered. The impact of each on the system performance, reliability and stability differs. The main problem for the current is the harmonic distortion.

1.1.1 Current harmonics

The advancement in power generation technology including, renewable energy sources installed in the grid network and the highly developed devices at the end users, has increased in power systems [4]. The use of power electronics devices have given more efficiency and flexibility to numerous applications [7]. But, the excessive number of these power electronic devices or non-linear loads on the grid leads to many problems that have become an important concern [7] [8]. Non-linear loads have increased in the industrial and commercial spaces [5]. Examples of non-linear loads are rectifier equipment, appliances, and adjustable speed drives. Non-linear loads cause distortion and unbalance at the supply. Disturbances such as harmonic distortion weaken a power system and makes it unstable and unsecured. The main source of the harmonic distortion in power distribution system is the non-linear load. The harmonic currents flow back in the direction

of the source through the point of common coupling (PCC) [9]. Harmonics have both short-term and long-term impacts on the power system. The short-term impacts are related to excessive voltage distortion. While, long-term impacts are an increase in resistive losses and voltage stresses. Moreover, harmonic currents can interact harmfully with power system equipment causing additional losses, overheating, overloading, and interface with telecommunication lines, and errors in metering devices. Another impact is reducing the system power factor (pf), which can be expressed as:

$$\mathrm{pf} = \frac{\mathrm{P}}{\sqrt{\mathrm{P}^2 + \mathrm{Q}^2}} \qquad (1.1)$$

$$\mathrm{S} = \sqrt{\mathrm{P}^2 + \mathrm{Q}^2} \qquad (1.2)$$

where P is the active power, Q is the reactive power, and S is the apparent power.

As a result, the IEEE (Institute of Electrical and Electronics Engineers) introduced regulating guidelines and standards to manage the accepted limits of the voltage and current harmonics as shown in Table 1.1 [10]. Two important definitions regarding current harmonics are: total demand distortion (TDD) and total harmonic distortion (THD) [11]. The THD is the most used harmonic index for many applications and is calculated as follows:

$$T\mathrm{HD}_{current} = \frac{\sqrt{\mathrm{I}_{\mathrm{RMS}}^2 - \mathrm{I}_1^2}}{\mathrm{I}_1} = \frac{\text{RMS of all harmonic current}}{\text{RMS of the fundamental current}} \qquad (1.3)$$

Table 1.1: IEEE 519-2014 current harmonic distortion limits [10]

Maximum current harmonic distortion in percent of I_L						
Individual harmonic order (Odd harmonics)[a,b]						
I_{SC}/I_L	<11	11≤h<17	17≤h<23	23≤h<35	35≤h	TDD
< 20 [c]	4.0	4.0	4.0	4.0	4.0	4.0
20<50	7.0	7.0	7.0	7.0	7.0	7.0
50<100	10.0	10.0	10.0	10.0	10.0	10.0
100<100	12.0	12.0	12.0	12.0	12.0	12.0
0>1000	15.0	15.0	15.0	15.0	15.0	15.0

a: Even harmonics are limited to 25% of the odd harmonic limits above.
b: Current distortions that result in a dc offset, e.g., half-wave converters, are not allowed.
c: All power generation equipment is limited to these values of current distortion, regardless of actual I_{sc}/I_L.
where I_{sc} = maximum short-circuit current at PCC
I_L = maximum demand load current (fundamental frequency at the PCC under normal load operating conditions

1.1.2 Unbalanced System

Another power quality issue is system imbalance. Three-phase quantities are called balanced when they have equal magnitudes and are displaced from each other by 120°. In a three-phase system, voltages are called unbalanced when either or both the magnitude and phase are different from the definition in the previous sentence [12]. System imbalance is mostly caused by unbalanced loading. Electrical equipment, especially motors and their controllers, will not run reliably under unbalanced voltages in a 3-phase system [13]. The impact of power system imbalance depends on the unbalance ratio and on the nature of the electrical equipment. Voltage unbalance has three definitions addressed by different organizations [12], [14]. The unbalance ratio is defined as the ratio of the negative sequence component to the positive sequence component, and this definition is known as unbalance factor (UF) which is given by:

$$UF = \frac{negative\ sequence\ component}{positive\ sequence\ component} \qquad (1.4)$$

Higher unbalance ratio might cause overheating of components, especially motors, and irregular shutdown of motor controllers. According to [12], the unbalance ratio should not exceed 2% of the lowest voltage. Three-phase quantities are called unbalanced if the unbalance ratio is more than 2%.

1.1.3 Frequency variations

For grid frequency of 60 Hz, the limit of the frequency in the normal conditions should be within 60±2% Hz [15]. When the demand increases, the power consumption fluctuates [16] [17]. As a result, the prime mover of the generator oscillates causing the frequency to deviate.

1.2 Mitigation of Power Quality Problems

Several devices have been developed and introduced to improve of the power quality [1]. The suppression of the current harmonics is important in improving the power quality [4] [5]. A common technique for eliminating the harmonics is using filters. Two types of filters are common for eliminating current harmonics: passive and active filters. Passive filters were an adequate solution. But, the increase in power electronics devices in power networks make passive filters an insufficient solution. As a result, the active power filter (APF) was introduced to solve the problems that passive filters cannot solve.

1.2.1 Passive filters

Passive filters are made of passive components: resistors, capacitors, and inductors [18]. A passive filter is a filter that does not have amplifying elements (transistors, operational amplifiers, etc.). Passive filters have become an ineffective solution because of their large size, resonance and fixed compensation behavior [19]. Table 1.2 shows the advantages and disadvantages of passive filters [18].

Table 1.2: Advantages and disadvantages of passive filters.

Advantages	Disadvantages
Simple implementation of a given transfer function in terms of the number of required components	Provide no signal gain because of no active elements.
Require no power supplies because they do not have active components	May need to use buffer amplifier to have the desired values of input and output impedances
Work fine at very high frequencies since there are no bandwidth limitations of op amps	May cost a lot because of inductor characteristics such as high accuracy, small physical size and large value.
Work in applications having large current or voltage levels that the active devices cannot handle	Tuning the adjustable inductors to the required values is time-consuming and expensive when producing large quantities of filters.
Generate little noise (compared with active elements).	Can be difficult and time consuming to design complex passive filters (higher than 2nd-order)

1.2.2 Active power filters

Active power filters were introduced to minimize the power quality problems [2]. For some specific conditions of a system, new resonances appear with the application of passive tuned filters [20]. In addition, the number of passive filters often are increased to deal with possible harmonic absorption from the power system. In the last decade, numerous publications have appeared on active power filters (APF) to reduce harmonics in the source currents. Active filters are adjustable with the system conditions in terms of harmonic reduction and reactive power compensation [2]. Unlike passive filters, active filters use amplifying components to synthesize the desired filter characteristics [18]. The concept of an active filter employs power electronics to inject harmonic components to eliminate the harmonic current or voltage components at the source [20]. Table 1.3 shows the advantages and disadvantages of active filters [18].

Table 1.3: Advantages and disadvantages of active filters.

Advantages	Disadvantages
Can have high input impedance, low output impedance, and virtually any arbitrary gain.	Effect on capacitors due to the problem of accuracy and value spacing. Effects here are lesser than for passive filters.
Achieve very good accuracy within the operating frequency.	Limit the performance at high frequencies because of the gain-bandwidth product of the active filter elements (such as amplifiers).
Reduce the number of the inductors.	Generate noise because of the amplifying circuitry which can be minimized by using low-noise amplifiers.

1.2.3 Active power filter topologies

APFs have different topologies based on the desired correction to the voltage, current or both. The common type of APFs are shunt APFs [6], which are utilized to correct the grid/source currents. Three common topologies of APF are shunt, series, hybrid active power filters [6] [20]:

1. Series active power filters:

This type of filter inserts a harmonic voltage in series with a voltage source and acts like a controlled-voltage source capable of compensating voltage source harmonics and voltage imbalance. It utilizes a current-source inverter (CSI) as shown in Figure 1.1.

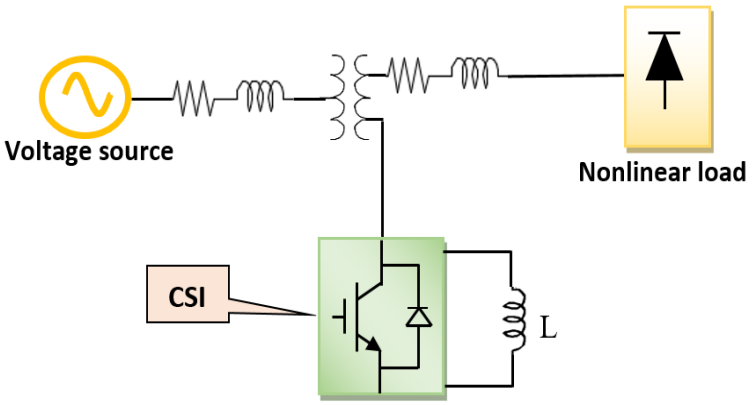

Figure 1.1: Series APF.

2. Shunt active power filters:

Harmonic currents generated by the load are compensated by parallel active filters which inject harmonic currents. It utilizes a voltage-source inverter (VSI) as shown in Figure 1.2.

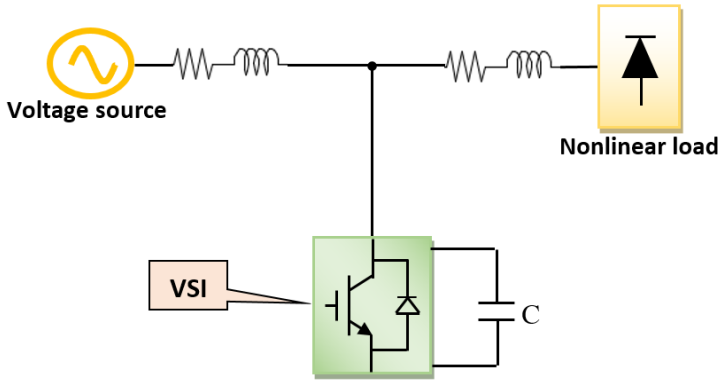

Figure 1.2: shunt APF.

3. Hybrid APF:

Hybrid active filter topologies, shown in Figure 1.3, are composed of both passive and active filters [6]. The role of the passive filters is to reduce the power rating of the APF and to attenuate the switching harmonics.

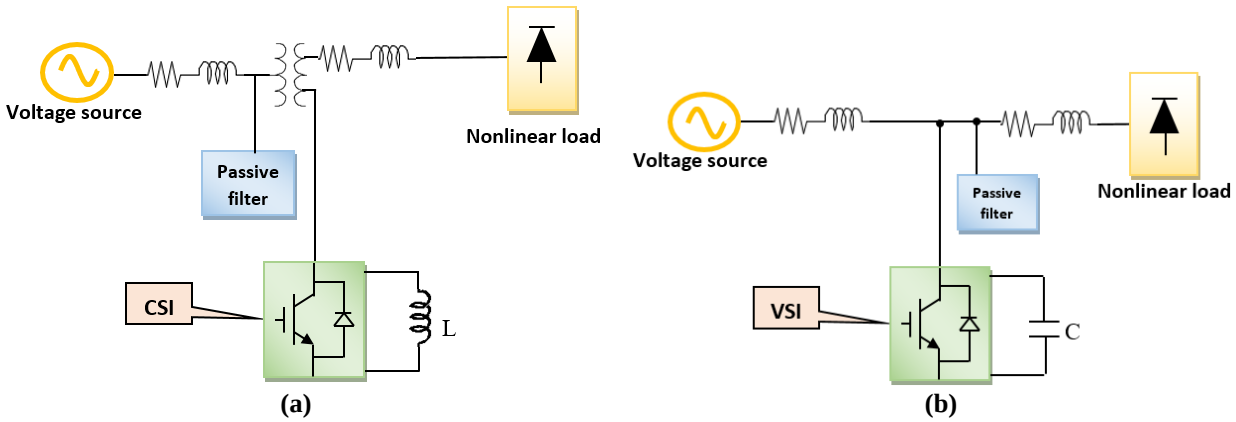

Figure 1.3: (a) Hybrid series APF. (b) Hybrid shunt APF.

1.2.4 Shunt active power filters

Shunt APF's have shown great performance in eliminating power quality problems associated with the source currents [3] [21]. The shunt active filters eliminate the distorted components of the load currents from the grid; therefore, the source currents have low harmonic distortion and are in phase with the source voltages. The shunt APF compensates for the load current harmonics and supplies the load reactive power. Therefore, the source supplies only active power. The shunt APF may compensate for any kind of load and may adjust itself as the load changes. Since the APF is connected in parallel to the AC mains, it does not require a transformer in the system.

The current harmonics and unbalanced currents come from nonlinear and unbalanced loads. The source currents become distorted, unbalanced or both by the nonlinear and unbalanced loads. The shunt active filter is responsible to injects harmonic currents to compensate for reactive power, harmonics, and unbalance. The source currents supply only the fundamental components since the shunt APF injects harmonic components for eliminating the harmonics from the source currents. The injected currents have equal magnitudes of the source current harmonics and opposite phase of the source currents. The shunt APF is mainly located at the load side [22].

1.3 Control of Three-Phase Shunt Active Power Filter

The objective of the APF is to generate a compensation current to eliminate harmonic and reactive power components in the source currents [4] [5]. Complete reactive power compensation achieved by a suitable control system for the shunt APF can yield unity power factor [21]. All control techniques have four stages, which are measuring signals, generating compensating signals, controlling the DC-link voltage, and generating firing (switching) signals for the VSI.

Different control strategies for shunt APF have been presented in the literature [4] [5] [7] [6][22-30]. The performance of the shunt APF depends on the control strategy that is responsible to generate the switching signals in the VSI. These techniques have shown enhancements in the steady state and the dynamic performances and the stability of the filters, which are important features of a control strategy. The performance of a control method can be determined by the amount of reduction in the total harmonic distortion (THD) of the source current and by the dynamic response to changes in the load. Moreover, the control method can be classified as direct or indirect control [31]. In the direct methods, the shunt APF currents are sensed and controlled. While in the indirect methods, the source currents are sensed and controlled. Measuring the voltage and the current on the supply side is common in most control methods. The first step is to measure the voltage signals at the PCC and the load currents. Then, the reference currents can be generated and compared with the measured currents in a current controller to generate the required gate signals.

Some control methods do not operate effectively under unbalanced power systems conditions with or without the presence of harmonics. While others are intended to work in distorted and unbalanced conditions, they do not completely eliminate power quality problems. They could also cause more issues such as phase delay, which degrade the performance of the shunt APF.

1.3.1 Reference current control methods

The control system of the shunt APF mainly depends on the current reference generating methods [4] [5]. Reference current control is responsible for calculating the compensating current signal and can be classified into two categories based on the domain in which the control system is operated [26]. The first category is time domain, which includes notch filters, sliding-mode

controller, and neural network, instantaneous reactive power theory (IRPT), and synchronous reference frame method (SRF). The second category is the frequency domain, which includes fast Fourier transform (FFT) to estimate the harmonics and allow elimination of certain harmonics. The main drawbacks of the FFT method are the poor performance in transients, numerous calculations, the use of considerable memory, and a delay in the extraction of the harmonics. The time-domain methods are less complex than the frequency-domain methods, and the most common time-domain control strategies are SRF and IRPT [6]. Different controls methods are based on modifying the IRPT, including extension IRPT, optimal linear prediction theorem, and dividing frequency theorem. Unlike IRPT, the SRF method uses a Park transformation to transform the measured signals from abc components into rotating frame dq components. The active and reactive powers are calculated in dq coordinates in order to calculate the reference current signals. The above control strategies are all utilized in shunt APFs. However, only IRPT and SRF of the time domain techniques will be discussed hereafter.

1.3.2 Instantaneous reactive power theory (IRPT)

The instantaneous reactive power theory (IRPT) was originated by Akagi [27]. The traditional power flow calculations are based on average power and root-mean-square values of the voltages and the currents. IRPT is based on the instantaneous real and reactive power calculations using a Clark transformation to determine the reference currents of the shunt APF. Although the IRPT method has a good performance and simple implementation, its main drawback is that it is not applicable in unbalanced power system conditions [17]. Figure 1.4 shows the source currents under unbalanced conditions without and with the shunt APF. The source currents with the shunt APF are nearly balanced. But, they are distorted with a THD of about 12%. For that, IRPT is not suitable under unbalanced conditions.

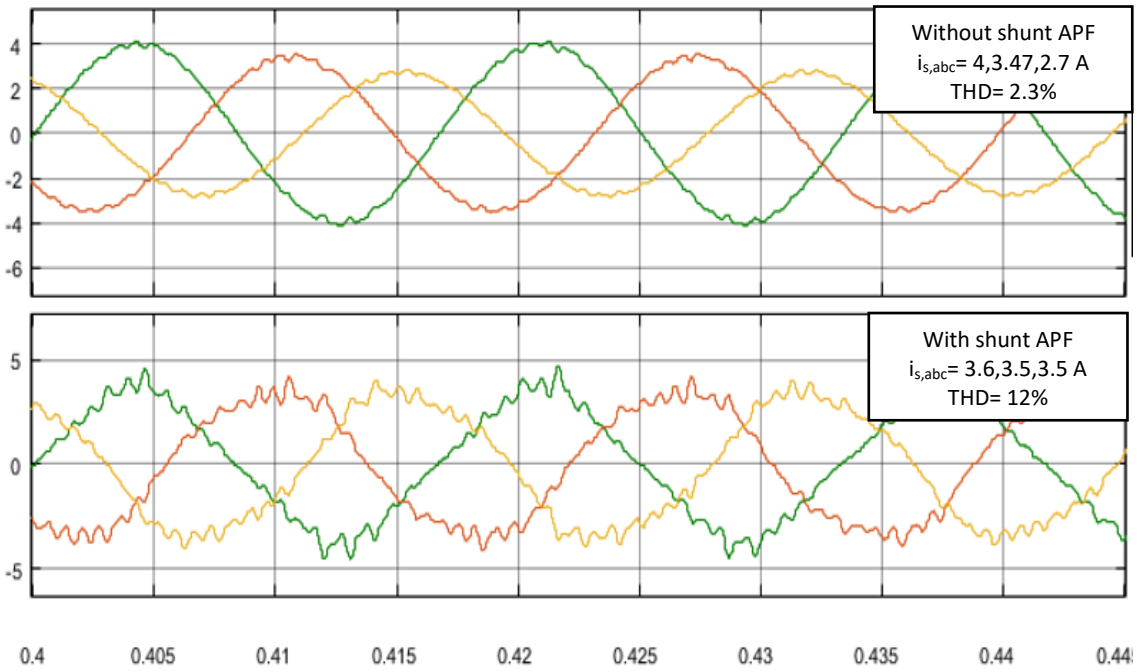

Figure 1.4: Using IRPT, the source currents ($i_{s,abc}$) with and without the shunt APF under unbalanced power system conditions.

1.3.2.1 Clark transformation

The Clark transformation is a mathematical transformation that simplifies the analysis of three-phase circuits [32]. One useful application is the generation of the reference signal used for space vector modulation control of three-phase inverters. The voltage and current equations determine the behavior of three-phase machines [33]. The coefficients of differential equations are varying. Therefore, modeling such a system has a tendency to be complex because the system parameters vary continuously as time varies. For that, a mathematical transformation, such as a Clark transformation, is used to solve equations involving time varying quantities by referring all variables to a common frame of reference. Any three phase quantities can be represented by space vectors. The Clark transformation is a method of space vectors and it can be represented as:

$$\begin{bmatrix} X_\alpha \\ X_\beta \end{bmatrix} = \sqrt{\frac{2}{3}} \begin{bmatrix} 1 & -\frac{1}{2} & \frac{1}{2} \\ 0 & \frac{\sqrt{3}}{2} & -\frac{\sqrt{3}}{2} \end{bmatrix} \begin{bmatrix} X_a \\ X_b \\ X_c \end{bmatrix} \qquad (1.5)$$

The inverse Clark transformation is used to convert back to three phase quantities as:

$$\begin{bmatrix} X_a \\ X_b \\ X_c \end{bmatrix} = \sqrt{\frac{2}{3}} \begin{bmatrix} 1 & 0 \\ -\frac{1}{2} & \frac{\sqrt{3}}{2} \\ -\frac{1}{2} & -\frac{\sqrt{3}}{2} \end{bmatrix} \begin{bmatrix} X_\alpha \\ X_\beta \end{bmatrix} \qquad (1.6)$$

The reason the coefficient $\sqrt{\frac{2}{3}}$ is used is that the standard reference frame uses coefficient $\frac{2}{3}$ where its matrix is not unitary [34]. The active and reactive powers are computed using the above equations in order to preserve the power because the transformation matrix is unitary. For that, the coefficient used to preserve power is $\sqrt{\frac{2}{3}}$.

1.3.2.2 Direct IRPT

The voltages at the PCC and the load currents are measured [17] [27] [35]. The measured signals are then transformed from abc coordinates into two orthogonal rotating vectors called αβ using the Clark transformation in equation (1.5). Then, the instantaneous real and reactive power (P and Q) are calculated as:

$$\begin{bmatrix} p = \bar{p} + \tilde{p} \\ q = \bar{q} + \tilde{q} \end{bmatrix} = \begin{bmatrix} v_\alpha & v_\beta \\ -v_\beta & v_\alpha \end{bmatrix} \begin{bmatrix} i_\alpha \\ i_\beta \end{bmatrix} \qquad (1.7)$$

P and Q have average (DC) components labelled as $\bar{p}$ and $\bar{q}$ and oscillating components labelled as $\tilde{p}$ and $\tilde{q}$. P and Q have only average components for linear loads. The oscillating powers are extracted from P and Q using a low pass filter (LPF) or a high pass filter (HPF), results from the harmonic and reactive currents, and are used to calculate the reference currents as:

$$\begin{bmatrix} i^*_{ref\alpha} \\ i^*_{ref\beta} \end{bmatrix} = \frac{1}{v_\alpha^2 + v_\beta^2} \begin{bmatrix} v_\alpha & -v_\beta \\ v_\beta & v_\alpha \end{bmatrix} \begin{bmatrix} \tilde{p} \\ q \end{bmatrix} \qquad (1.8)$$

The inverse Clark transform (1.6) is applied to the reference currents as:

$$\begin{bmatrix} i^*_{refa} \\ i^*_{refb} \\ i^*_{refc} \end{bmatrix} = \sqrt{\frac{2}{3}} \begin{bmatrix} 1 & 0 \\ -\frac{1}{2} & \frac{\sqrt{3}}{2} \\ -\frac{1}{2} & -\frac{\sqrt{3}}{2} \end{bmatrix} \begin{bmatrix} i^*_{ref\alpha} \\ i^*_{ref\beta} \end{bmatrix} \qquad (1.9)$$

The reference currents are compared with the shunt APF current in a current controller to produce the gating signals. Figure 1.5 shows a block diagram of direct IRPT.

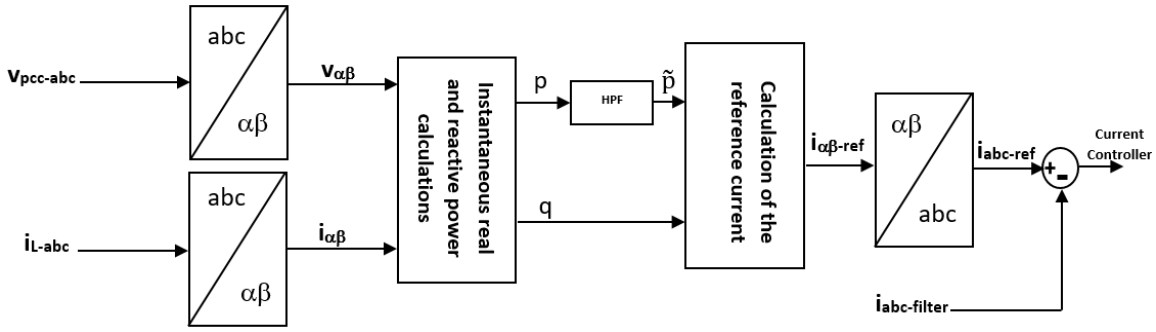

Figure 1.5: Direct IRPT.

1.3.2.3 Indirect IRPT

Unlike the direct IRPT, the indirect IRPT uses the source current for calculating the reference current [17] [35]. The indirect method requires less hardware than the direct method. The PCC voltages and the source currents are transformed from abc coordinates into αβ coordinates. Then, the instantaneous real and reactive power (p and q) are calculated. The average power ($\bar{p}$ and $\bar{q}$) are extracted using an LPF or HPF. The average power is used to calculate the reference currents, which are compared with the source currents in a current controller to produce the gating signals. Figure 1.6 shows a block diagram of direct IRPT.

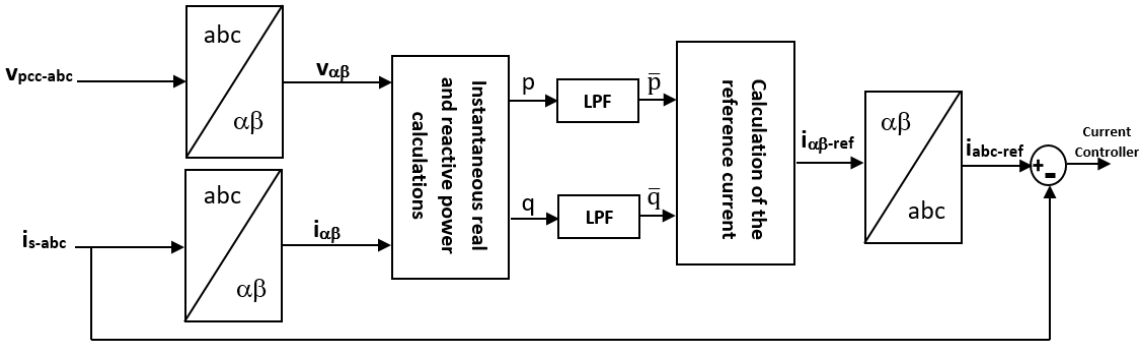

Figure 1.6: Direct IRPT.

1.3.2.4 Elaboration of instantaneous power calculations in αβ coordinates

The power equations are calculated using Clark transformation [36]. The general equation of the complex power in a three-phase system can be calculated as:

$$\bar{S} = 3\bar{V}\bar{I}^{*} \qquad (1.10)$$

where * is used to denote a complex conjugate, $\bar{V}$ is the measured line-to-neutral voltage and $\bar{I}$ is the measured current. The power equation in $\alpha\beta$ coordinates can be expressed as [31]:

$$\bar{S} = p + jq = \bar{v}_{\alpha\beta}\bar{i}^{*}_{\alpha\beta} = \left(v_\alpha + jv_\beta\right)\left(i_\alpha + ji_\beta\right)^{*} = (v_\alpha + jv_\beta)(i_\alpha - ji_\beta)$$

$$= (v_\alpha^{+} + v_\alpha^{-} + jv_\beta^{+} + jv_\beta^{-})(i_\alpha^{+} + i_\alpha^{-} - ji_\beta^{+} + ji_\beta^{-})$$

$$= \left(v_\alpha^{+}i_\alpha^{+} + v_\alpha^{+}i_\alpha^{-} - jv_\alpha^{+}i_\beta^{+} - jv_\alpha^{+}i_\beta^{-}\right) + \left(v_\alpha^{-}i_\alpha^{+} + v_\alpha^{-}i_\alpha^{-} - jv_\alpha^{-}i_\beta^{+} - jv_\alpha^{-}i_\beta^{-}\right)$$

$$+\left(jv_\beta^{+}i_\alpha^{+} + jv_\beta^{+}i_\alpha^{-} + v_\beta^{+}i_\beta^{+} + v_\beta^{+}i_\beta^{-}\right) + \left(jv_\beta^{-}i_\alpha^{+} + jv_\beta^{-}i_\alpha^{-} + v_\beta^{-}i_\beta^{+} + v_\beta^{-}i_\beta^{-}\right) \qquad (1.11)$$

where $^{+}$ indicates positive sequence components and $^{-}$ indicates negative sequence or harmonics components. The instantaneous real power and reactive power are composed of average ($\bar{p}$, $\bar{q}$) and oscillating ($\tilde{p}$, $\tilde{q}$) quantities. The average power is related to the fundamental components of the voltage and the current. Whereas, the oscillating power is related to harmonics or negative sequence components.

$$p = \bar{p} + \tilde{p} = \left(v_\alpha^+ i_\alpha^+ + v_\beta^+ i_\beta^+ + v_\alpha^- i_\alpha^- + v_\beta^- i_\beta^-\right) + \left(v_\alpha^+ i_\alpha^- + v_\beta^+ i_\beta^- + v_\alpha^- i_\alpha^+ + v_\beta^- i_\beta^+\right) \quad (1.12)$$

$$q = \bar{q} + \tilde{q} = \left(-v_\alpha^+ i_\beta^+ + v_\beta^+ i_\alpha^+ - v_\alpha^- i_\beta^- + v_\beta^- i_\alpha^-\right) + \left(-v_\alpha^+ i_\beta^- + v_\beta^+ i_\alpha^- - v_\alpha^- i_\beta^+ + v_\beta^- i_\alpha^+\right) \quad (1.13)$$

1.3.3 Synchronous reference frame (SRF) method

Synchronous reference frame (SRF) is also known as the instantaneous current method [17]. The load currents are transformed into synchronous dq coordinates using the Park transformation as:

$$\begin{bmatrix} i_d \\ i_q \end{bmatrix} = \frac{2}{3}\begin{bmatrix} \cos\theta & \cos(\theta - 120°) & \cos(\theta + 120°) \\ -\sin\theta & -\sin(\theta - 120°) & -\sin(\theta + 120°) \end{bmatrix}\begin{bmatrix} i_a \\ i_b \\ i_c \end{bmatrix} \quad (1.14)$$

where $\theta = wt$ is angular position of the synchronous reference frame determined by a phase locked loop (PLL). The currents i_d and i_q have average components and an oscillating components as follows:

$$i_d = \bar{\imath}_d + \tilde{\imath}_d \quad (1.15)$$

$$i_q = \bar{\imath}_q + \tilde{\imath}_q$$

HPFs are used to extract the oscillating components from i_d and i_q to obtain the reference compensating currents. The shunt APF generates only oscillating components ($\tilde{\imath}_d$ and $\tilde{\imath}_q$) of the load currents to eliminate the unwanted components from the source current. Then, the three reference currents of the shunt APF are transformed into the abc frame using the inverse transformation of (1.14). Figure 1.7 shows a block diagram of the SRF method.

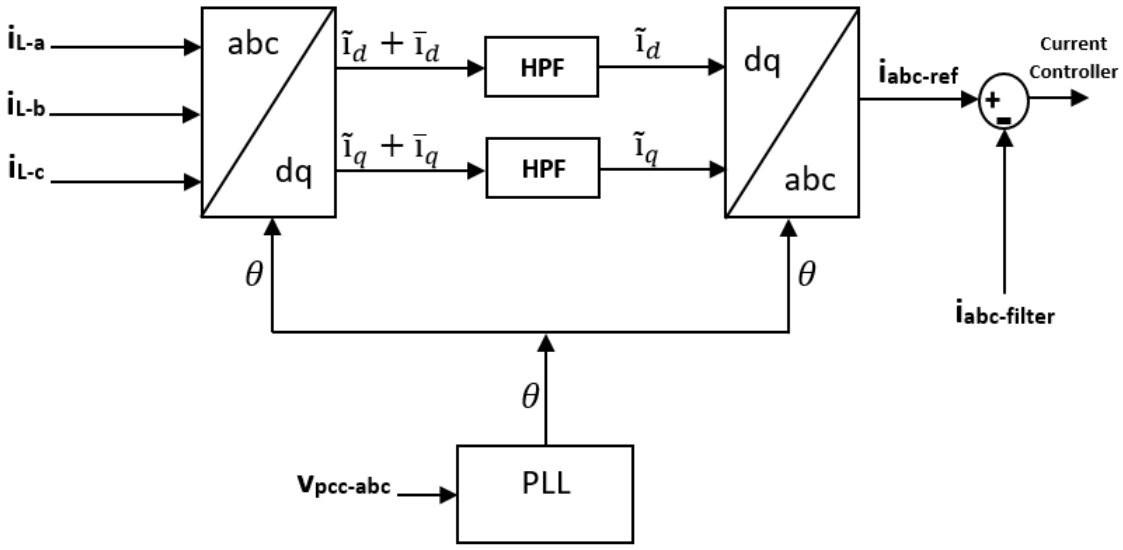

Figure 1.7: A block diagram of SRF method.

The direct and quadrature (d and q) components represent the active and reactive components of the system. This method is stable because it is based mainly on DC quantities. The computation of SRF is instantaneous. A problem of this method is that it experiences time delays in filtering the DC quantities. Additionally, this method is not appropriate for a single-phase system.

1.3.4 Positive sequence extraction methods

The extraction methods of the unwanted components from voltages and currents are a very important characteristic in controlling a shunt APF. IRPT theory and some other control methods have been used to improve the efficiency of the harmonic suppression of the APF [4] [5] [25-28]. But, these theories require detecting the fundamental components and oscillating components. The extraction techniques are classified into frequency-domain techniques and time-domain techniques [17]. The frequency domain techniques utilize a FFT to extract the harmonic components. But, these techniques show poor performance under disturbances and cause a delay that can be at least one period. Examples of time-domain extraction methods are notch and selective band-pass filters. Extraction methods reduce the complexity of the control system. The time-domain methods

are a faster response and require less calculations. However, some of these methods exhibit poor performance under non-ideal power system conditions.

1.3.4.1 Extraction using LPF, HPF and PLL

Traditionally, some control methods employ an LPF or HPF to extract the average or oscillating components [4] [9]. IRPT utilizes LPF and/or HPF in order to obtain the average power components or the oscillating power components (refer to Figures 1.5 and 1.6). The SRF method also employs an LPF and/or HPF to extract the oscillating components of the load currents (refer to Figure 1.7). Although the implementation of LPF and HPF is simple, they cause phase delays at the fundamental frequency that could degrade the performance of the shunt APF. Because of that, other techniques were proposed to overcome the issues from LPF and/or HPF. A PLL can replace the LPF for extracting fundamental components, but it has poor performance under unbalanced or distorted grid voltages [9]. Additionally, a PLL makes the control system more complex.

1.3.4.2 Notch filter

A notch filter can be used to separate the harmonic components from the fundamental components [26] [29]. It operates effectively for unbalanced conditions, simplifies the control system, eliminates the use of a PLL, and is very insensitive to disturbances. It can be modeled to operate similarly as a band-stop filter or band-pass filter because it removes a band of frequencies from a signal. The connection method of the notch filter can determine the type of the filter as shown in Figure 1.8.

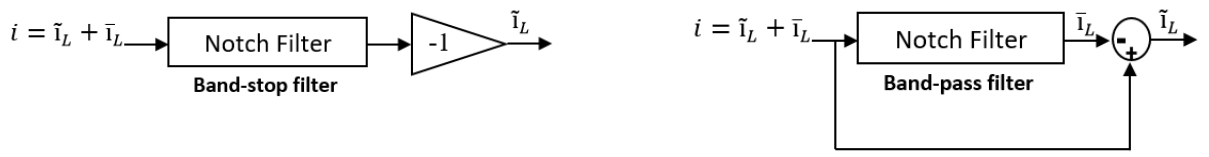

(a) **(b)**

Figure 1.8: (a) Notch filter acting similar to a band-stop filter. (b) Notch filter acting similar to a band-pass filter.

1.3.4.3 Selective band-pass filter

A selective band-pass filter (SBPF), also called a self-tuning filter, is a technique of extracting the positive sequence components and the negative sequence components under non-ideal power system conditions [4] [5] [37] [38]. SBPFs eliminate employing the traditional extraction methods: LPF, HPF and PLL. The output from the filter can be determined from the coupling method as shown in Figure 1.9. The SBPF can be set to extract the fundamental or oscillating components. The transfer function of an SBPF is expressed as follows:

$$H_{SBBF}(s) = \frac{(s + k) + j\omega_c}{(s + k)^2 + j\omega_c^2} \qquad (1.16)$$

The SBPF can be tuned at the nth harmonic frequency by adjusting the system frequency (ω_c) to ω_n in order to compute the dc component at the output of the SBPF. The gain k is very important in designing the SBPF. Each harmonic is amplified by k. Choosing k depends on the frequency response and the total harmonic distortion (THD). A smaller value of k increases the selectivity of the filter. The time constant of the SBPF is equal to 1/k; therefore, the transient response is increased when k is decreased. Moreover, the value of k has an influence on the SBPF harmonic attenuation and on the time constant in the "+" sequence such as when k increases; the time response is faster but the harmonic suppression is less effective. Figure 1.10 shows the response of the filter when $\omega_c = 120\pi$ rad/sec at several values of gain k.

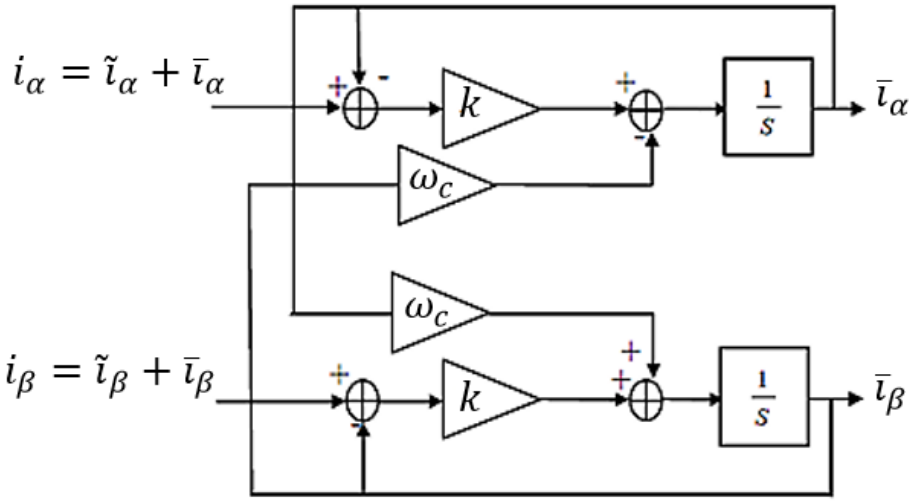

Figure 1. 9: Block diagram of the SBPF.

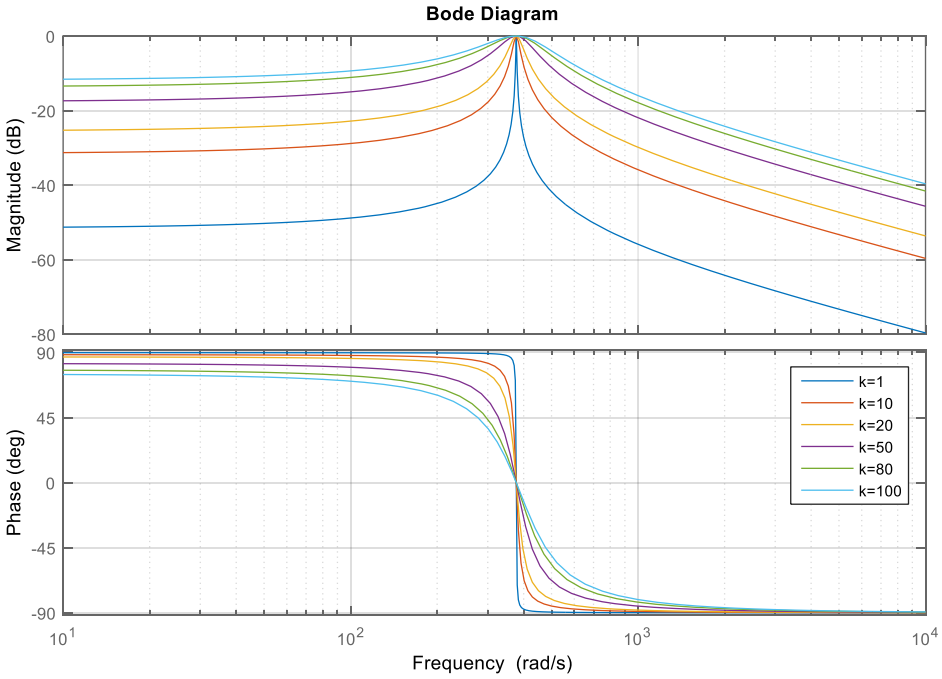

Figure 1.10: Bode diagram for the SBPF versus different values of the parameter k.

1.3.5 DC-link voltage control

The DC input voltage of the inverter in an APF is provided by a capacitor [31]. This DC link voltage can stay constant if there is no active power exchange between the shunt APF and the grid, and if there are no losses in the inverter. Practically, both conditions can be not realized. The

power losses of the inverter can be compensated for by drawing balanced power from the grid to the DC bus. A DC-bus voltage regulator can balance the losses. As a result, the DC-link voltage control is very important in order to stabilize the power exchange, to compensate for the inverter real power losses (p_{dc}), to generate accurate reference currents, and to regulate the DC-link voltage [4] [5] [23]. Several methods for controlling the DC-link voltage are employed in controlling a shunt APF such as a PI controller and a sliding mode controller. An example of DC-link voltage control that can be included in the IRPT method is shown in Figure 1.11.

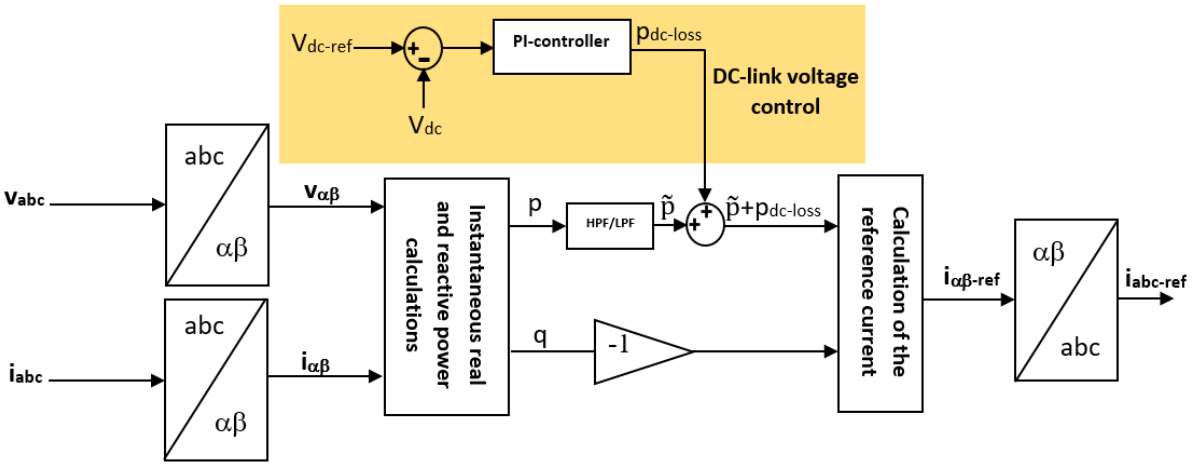

Figure 1.11: DC-link voltage control in IRPT method.

1.3.6 Current control

The current control is the final stage of the shunt APF control system. It is responsible for generating the firing (switching) signals of the inverter [6]. In order to obtain the reference currents, the error signal is calculated as:

$$error = i_{ref} - i_f \qquad (1.17)$$

where i_{ref} is the reference currents and i_f is the actual generated currents from the shunt APF filter. The error signals are input to the current controller. The common current controllers for shunt APFs are sinusoidal pulse-width modulation (PWM) and hysteresis control.

1.3.6.1 Hysteresis control

Hysteresis current control is a well-known method for current control in a shunt APF [6] [11] [17] [26] [31]. It maintains the current in a defined region around the reference current. It has two defined bands: upper and lower. The position of the switches changes as the error signal crosses a certain defined upper band value. And when the error signal crosses a certain defined lower band value, the position of the switches are then changed. Hysteresis control has shown stable performance, fast response to errors, and easy implementation. However, it results in a varying switching frequency [31] [39].

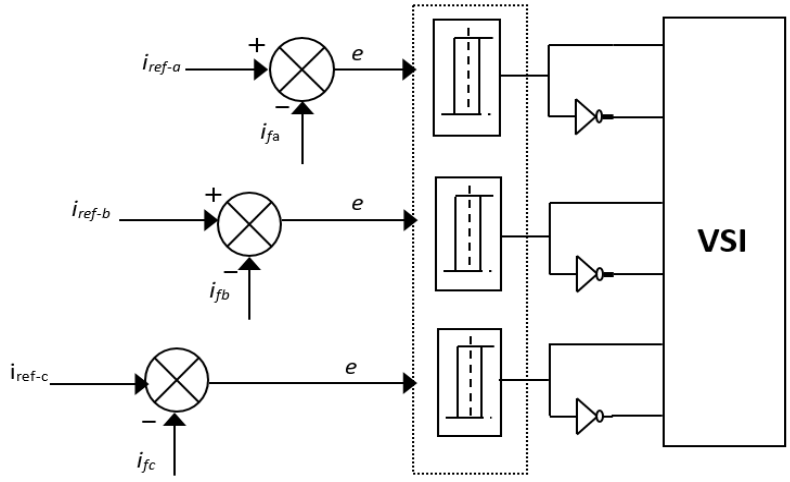

Figure 1.12: Principle hysteresis control block diagram.

1.3.6.2 Sinusoidal pulse-width modulation (SPWM)

Pulse-width modulation (PWM) techniques are employed for current control in a shunt APF [31]. Sinusoidal PWM (SPWM) is one of the most commonly employed current control techniques. Since it utilizes a fixed switching frequency, the cancelation of the switching harmonics is easy. The error signal (1.18) is compared with a triangular carrier signal. The switching frequency is the frequency of the carrier signal. The frequency ratio, that is the frequency of the carrier signal over the reference signal, is very significant. The ratio should be an integer for

synchronizing the carrier signal with the reference signal. An odd integer ratio is preferable to maintain symmetric reference signals. In addition, the ratio should be high to obtain fast switching and to separate the switching harmonics from the injected currents. Figure 1.13 shows the principle of PWM control.

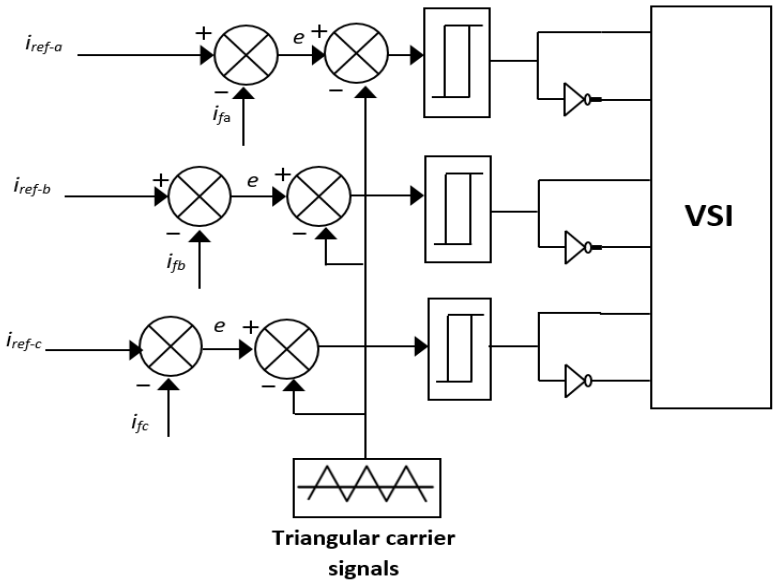

Figure 1.13: Principle of SPWM control method.

1.4 Frequency deviation and detection

The system frequency is a significant variable for power system control. Variations in the system frequency could adversely impact the performance of the APF [35]. Large variations should be corrected to ensure stability and suitable performance. The control techniques for APFs usually consider a constant system frequency. But, the system may become unstable in case of a varying frequency. For such a system, the variations in the system frequency should be accounted for in designing the control system scheme in order to maintain stable and proper system performance.

Adding a frequency detection method to the control scheme of shunt APF would make the control system capable of adapting to changing frequencies. However, the complexity of the

control system increases [40]. Several methods of measuring the system frequency were proposed in [41], [42]. The zero-crossing method measures the frequency by calculating the time between two consecutive zero crossing of a signal. Even though it is the simplest among the other methods, it is not effective with measuring the frequency of distorted signal. To overcome this issue with zero-crossing method, many techniques have been introduced such as orthogonal modified zero-crossing, PLL, peak location, FFT, and period estimation.

1.5 Voltage Sensorless Control

The conventional APF control techniques require the measurements of the voltages and the currents [43] [44]. That means the system is equipped with two types of sensors: voltage sensor and current sensor. Accurate voltage information is critical for performance of the APF [46]. Some methods such as SRF and IRPT need the voltage magnitude and phase to determine the proper reference signals.

However, it is possible to eliminate a number of sensors to implement sensorless control systems [44] [46]. This can offer some advantages such as eliminating sensor offset, resolution limitation and sensor noise, robustness against sensor failures, improving the system reliability and lowering the costs. Because the grid voltage is not sensed directly through sensors or PLL in sensorless control techniques, it is estimated from the other measured variable such as the current and the DC-link voltage [45]. The current sensors and DC-link voltage are important for controlling the VSI and for protecting from short circuit and over-and-under voltage [43]. Several sensorless control techniques were proposed [43] [44]. Among these techniques, there are two known methods, which are voltage oriented control and current shaping. The voltage oriented control method shows poor performance under modeling errors. The current shaping method is simple and has better stable and robust performance.

This dissertation introduces an improved control method based on instantaneous real and reactive power (PQ) theory of three-phase shunt APF that can effectively operate under balanced and unbalanced conditions of the power system and with the presence of the harmonics. The proposed method includes a technique to extract positive sequence and negative sequence components of voltages and currents. It is also employed when the system frequency varies. A frequency detection method is added to the proposed control method. As a result, a frequency adaptive control method is introduced. Moreover, another control strategy that does not require sensing the voltage is proposed. Several simulation and experimental tests have been performed to validate the operation of the proposed control strategies.

1.6 Motivation and Problem Statement

Active power filters have become very common in power applications. Numerous nonlinear loads in the power system cause variations in grid voltages and currents. This project has been focused on the development of a control system that should be capable of working reliably under non-ideal power system conditions.

Figure 1.14 shows a model of a power system with a shunt APF. The source currents could be non-sinusoidal or unbalanced under non-ideal (distorted and unbalanced) conditions of the grid voltages and loads. The distorted conditions come from harmonics generated from the loads, and the unbalanced conditions come from the unbalanced source voltages or loads. The shunt APF is controlled to generate the filter currents which eliminate the unwanted components in the source currents. Therefore, only the fundamental component of the source currents are obtained. In order to achieve to obtain balanced sinusoidal source currents, a control technique is developed to eliminate the current harmonics and balance the source currents. It is also intended to deal with the variations of the network frequency.

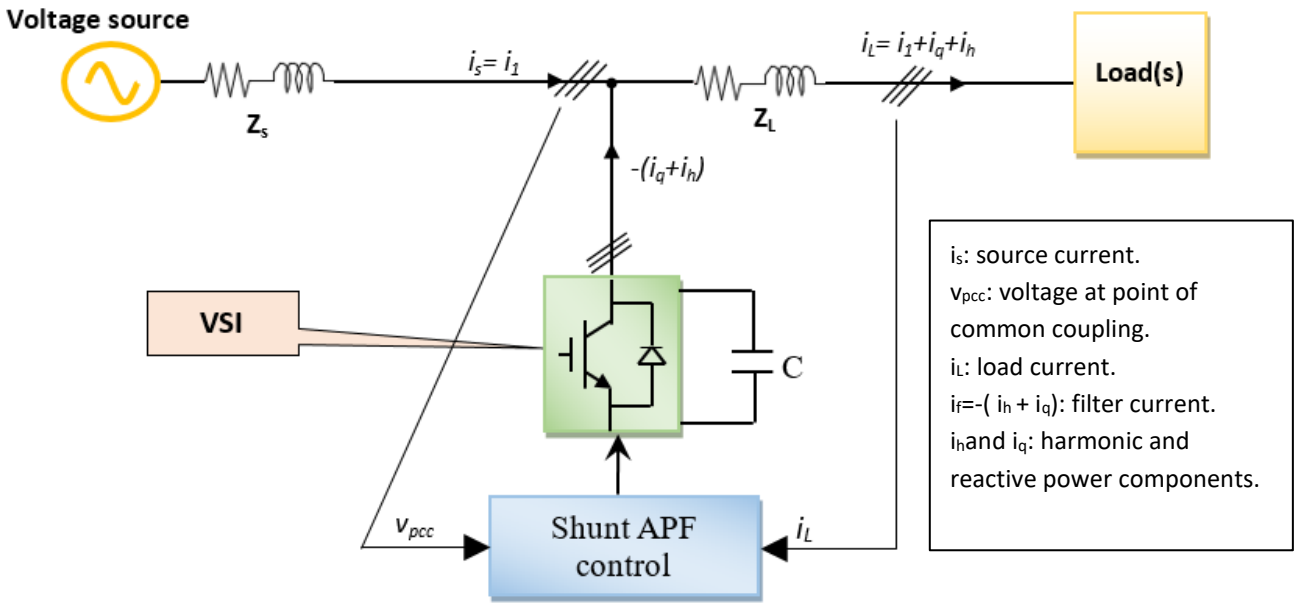

Figure 1.14: A model of basic principle of controlling three-phase shunt APF.

1.7 Objectives and Contributions of Dissertation

The main objectives of this dissertation are as follows:

1. To introduce a novel method of extracting the positive and negative sequence components, and evaluate the performance of this method under ideal and non-ideal power system conditions.
2. To develop a control method for current reference generation for a shunt APF.
3. To describe the modeling of the shunt APF and the power system, and evaluate the performance of the proposed control method under ideal and non-ideal power system conditions.
4. To develop a voltage sensoreless control method, and evaluate the performance of the proposed control method under ideal and non-ideal power system conditions.

5. To develop a frequency adaptive control method based on the original proposed control method, and evaluate the performance of the proposed control method under ideal and non-ideal power system conditions.

The main contributions of this dissertation are listed as follows:

1. A new filtering method of extracting the positive and negative sequence components was investigated and validated. It filters the three-phase quantities in the abc coordinate frame.
2. A control method based on the instantaneous reactive power theory (IRPT or PQ) was developed and evaluated under balanced and unbalanced power system conditions and with and without the presence of the harmonics.
3. The proposed control method was designed based on 60 Hz, and the frequency can be adjusted manually. However, a frequency detecting method was added to the control system allowing operation at any frequency. The simulation and experimental analysis validated the performance of the modified control system.
4. Another control method that does not require a voltage sensor was proposed and investigated under ideal and non-ideal power system conditions. The simulation and experimental results validate the performance of this voltage sensorless control method.

The simulation and experimental evaluations can be summarized in the following points:

- Eliminating the utilization of low pass filters (LPF) and high pass filters (HPF).
- Eliminating the use of a phase locked loop (PLL) as well as the dq transformation.
- Reducing the number of calculations in the control system.
- Providing efficient performance in steady state and in transient.

- Ensuring no phase delay at the fundamental frequency.
- Showing great suppression of negative sequence components.
- Balancing the source currents.
- Performing effectively under small frequency variations.
- Giving almost unity gain at the fundamental frequency.
- Implementing the proposed systems easily in a digital controller.

1.8 Dissertation Outline

This dissertation is organized into five chapters which follow this introductory chapter.

1. Chapter 1 includes an overview of power quality problems including harmonics, unbalance in three phase systems and frequency variations. It also presents a literature review of the active power filter, active power filter topologies, control system of the shunt active power filter, different types of control techniques of shunt APF, control of shunt APF under frequency deviation, an overview of voltage sensorless control techniques.
2. Chapter 2 includes the proposed positive and negative sequence component filter, proposed control strategy, proposed adaptive frequency control technique, proposed voltage sensorless control method. It contains simulation results for the proposed methods.
3. Chapter 3 includes a description of the system, design of the shunt active power filter, design of the measurement circuits, and hardware setup.
4. Chapter 4 includes validation of the proposed filter through experimental results.
5. Chapter 5 includes conclusion and suggestion for future work of this research.

CHAPTER 2: PROPOSED CONTROL STRATEGIES

The proposed control strategies are presented in this chapter. First, the proposed filter is introduced. One of the most important advantages of this filter is the separation of the positive sequence components from the negative sequence components under any power system condition. This filter is then used with instantaneous reactive power theory (IRPT) to obtain a modified version of this theory. The reason for using this filter with the theory is to overcome the problems resulting from the inability of the theory alone to deal with unbalanced systems and to eliminate the problems from using other elements such as low-pass filters, high-pass filters, and a phase-locked loop. The system frequency could encounter variations which could lead to adverse impacts on the power system. For that, a frequency detection method was designed and added to the previous control system. Finally, a voltage sensorless control system is presented. All proposed systems are explained analytically and graphically. Simulation results of these systems are provided.

2.1 Proposed positive and negative sequence components filter

In many control strategies for a shunt active power filter (APF), low-pass filters (LPFs), high-pass filters (HPFs) and phase locked loop (PLL) are employed to separate the fundamental and harmonic quantities and to track the phase angle. However, the use of filters and a PLL can degrade the performance of the control system. The proposed filtering technique eliminates the need for these devices. The proposed filter can provide the following features:

- Production of the positive sequence components, which form a balanced three set of quantities.
- fast detection of the positive and negative sequence components,

- operation under ideal and non-ideal power system conditions,
- excellent performance in both steady state and in transient conditions.

2.1.1 The mathematical relationship between the phase shift and the time

Balanced three-phase quantities have the same amplitude and are displaced by a phase shift of 120°. For a 60 Hz system, balanced three phase signals (f_a, f_b, f_c) can be mathematically expressed as:

$$f_a(t) = f_{max}\cos(120\pi t + \theta)$$

$$f_b(t) = f_{max}\cos(120\pi t + \theta - 120°) \qquad (2.1)$$

$$f_c(t) = f_{max}\cos(120\pi t + \theta + 120°)$$

For positive phase sequence (abc phase sequence), phase A is followed by phase B, and phase B is followed by phase C. For the system of line frequency of 60 Hz, a cycle is 1/60 s (16.667 ms). Moreover, one cycle is 360°. Since the system is balanced, the phasors are displaced equally in each cycle. The amount of displacement in time is one third (1/3) the time of one cycle and in degrees is 120°.

$$1\ cycle\ \rightarrow 360° \qquad \frac{1}{3}\ cycle\ \rightarrow 120°$$

The time shift between the phases is shown in the following equations:

Time of 1 cycle is $t_c = \frac{1}{f}$, where f is the frequency

A cycle is 360° and the time between two consecutive phasors can be calculated as:

$$t_{sh} = \frac{\text{phase shift between two phases in degrees}}{360°} \times t_c \qquad (2.2)$$

A representation of 1 cycle of balanced three phase quantities, for f = 60 Hz, is shown in Figure 2.1.

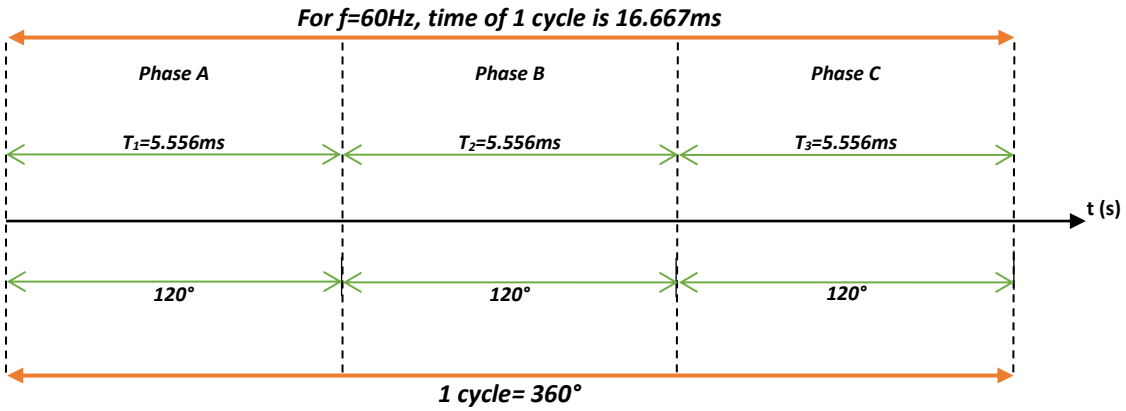

Figure 2. 1: A representation of 1 cycle of balanced three-phase quantities.

2.1.2 Derivation of the positive and negative sequence components

The sequence phase components are defined as:

(1) Positive-sequence components: three phasors have equal magnitude and separated by 120° in phase. They have the same phase sequence as that of the original phasors.

(2) Negative-sequence components: three phasors have equal magnitude and are displaced by 120° from other two phases. They have the opposite phase sequence to that of the original phasors.

(3) Zero-sequence components: three phases have equal magnitudes and are displaced by 0°.

The proposed filtering method is outlined below. The 3-phase quantities in equation (2.1) can be rewritten and expressed as:

$$f_a(t) = |f|e^{j(\omega t+\theta)}$$

$$f_b(t) = |f|e^{j(\omega t+\theta-\frac{2\pi}{3})} \qquad (2.3)$$

$f_c(t) = |f|e^{j(\omega t+\theta-\frac{4\pi}{3})}$

where $\omega = 2\pi f = 120\pi$ radians/second.

Let's calculate the time shift with respect to phase A

$$A \rightarrow B: \quad t_{sh\ a-b} = \frac{120°}{360°} \times \frac{1}{60Hz} = \frac{1}{180}\text{sec} \qquad (2.4)$$

$$A \rightarrow C: \quad t_{sh\ a-c} = \frac{240°}{360°} \times \frac{1}{60Hz} = \frac{1}{90}\text{sec} \qquad (2.5)$$

Based on the calculations of the time shift between a-b and a-c, equation (2.3) can be rewritten as:

$f_a(t) = |f|e^{j(\omega t+\theta)}$

$f_b(t) = |f|e^{j(\omega(t-\frac{1}{180})+\theta)}$ (2.6)

$f_c(t) = |f|e^{j(\omega(t-\frac{1}{90})+\theta)}$

The symmetrical components transformation is utilized to clarify the method of extracting the positive sequence components and negative sequence components.

$$A = \begin{bmatrix} 1 & 1 & 1 \\ 1 & \bar{a}^2 & \bar{a} \\ 1 & \bar{a} & \bar{a}^2 \end{bmatrix}$$

$$A^{-1} = \frac{1}{3}\begin{bmatrix} 1 & 1 & 1 \\ 1 & \bar{a} & \bar{a}^2 \\ 1 & \bar{a}^2 & \bar{a} \end{bmatrix}$$

where $\bar{a} = e^{j\frac{2\pi}{3}}$ and $\bar{a}^2 = e^{j\frac{4\pi}{3}}$. The proposed method is based on the positive phase sequence. With respect to phase a, b lags by 120° ($\frac{j2\pi}{3}$ rad) and c is displaced by 240° ($\frac{j4\pi}{3}$) as shown in Figure 2.2. The phasor $\bar{a}$ and $\bar{a}^2$ can be represented by time as:

$$t_{sh-\bar{a}} = \frac{240°}{360°} \times \frac{1}{60Hz} = \frac{1}{90}\sec \qquad (2.7)$$

$$t_{sh-\bar{a}^2} = \frac{120°}{360°} \times \frac{1}{60Hz} = \frac{1}{180}\sec \qquad (2.8)$$

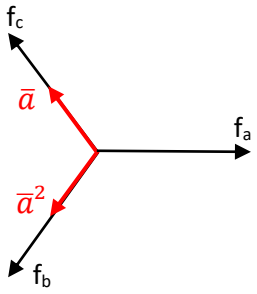

Figure 2.2: Phasors a,b, and c with $\bar{a}$ and $\bar{a}^2$.

The following equations use α and α^2 where α is a delay function of $\frac{1}{90}$ seconds and α^2 is a delay function of $\frac{1}{180}$ seconds. The symmetrical components for 3-phase quantities can be expressed as:

$$\mathbf{f_{012}}(t) = \begin{bmatrix} f^{(0)} \\ f^{(1)} \\ f^{(2)} \end{bmatrix} = A^{-1}\mathbf{f_{abc}}(t) = \frac{1}{3}\begin{bmatrix} (f_a + f_b + f_c) \\ (f_a + \alpha f_b + \alpha^2 f_c) \\ (f_a + \alpha^2 f_b + \alpha f_c) \end{bmatrix} \qquad (2.9)$$

Where $f^{(0)}$ is the zero sequence, $f^{(1)}$ is the positive sequence, and $f^{(2)}$ is the negative sequence.

Based on "012" sequences (equation (2.9)), abc quantities can be written as:

$$\mathbf{f_{abc}}(t) = \begin{bmatrix} f_a \\ f_b \\ f_c \end{bmatrix} = A\mathbf{f_{012}}(t) = \begin{bmatrix} \left(f^{(0)} + f^{(1)} + f^{(2)}\right) \\ \left(f^{(0)} + \alpha^2 f^{(1)} + \alpha f^{(2)}\right) \\ \left(f^{(0)} + \alpha f^{(1)} + \alpha^2 f^{(2)}\right) \end{bmatrix}$$

$$= \begin{bmatrix} f^{(0)} \\ f^{(0)} \\ f^{(0)} \end{bmatrix} + \begin{bmatrix} f^{(1)} \\ \alpha^2 f^{(1)} \\ \alpha f^{(1)} \end{bmatrix} + \begin{bmatrix} f^{(2)} \\ \alpha f^{(2)} \\ \alpha^2 f^{(2)} \end{bmatrix} = \begin{bmatrix} f_a{}^{(0)} \\ f_b{}^{(0)} \\ f_c{}^{(0)} \end{bmatrix} + \begin{bmatrix} f_a{}^{(1)} \\ f_b{}^{(1)} \\ f_c{}^{(1)} \end{bmatrix} + \begin{bmatrix} f_a{}^{(2)} \\ f_b{}^{(2)} \\ f_c{}^{(2)} \end{bmatrix} \qquad (2.10)$$

Positive phase sequence components

Negative phase sequence components

From equation (2.10), phasors a,b and c are composed of zero ($^{(0)}$) components, positive ($^{(1)}$) components and negative ($^{(2)}$) components as:

$$f_a(t) = f_a{}^{(0)}(t) + f_a{}^{(1)}(t) + f_a{}^{(2)}(t) = f^{(0)}(t) + f^{(1)}(t) + f^{(2)}(t)$$

$$f_b(t) = f_b{}^{(0)}(t) + f_b{}^{(1)}(t) + f_b{}^{(2)}(t) = f^{(0)}(t) + \alpha^2 f^{(1)}(t) + \alpha f^{(2)}(t) \quad (2.11)$$

$$f_a(t) = f_c{}^{(0)}(t) + f_c{}^{(1)}(t) + f_c{}^{(2)}(t) = f^{(0)}(t) + \alpha f^{(1)}(t) + \alpha^2 f^{(2)}(t)$$

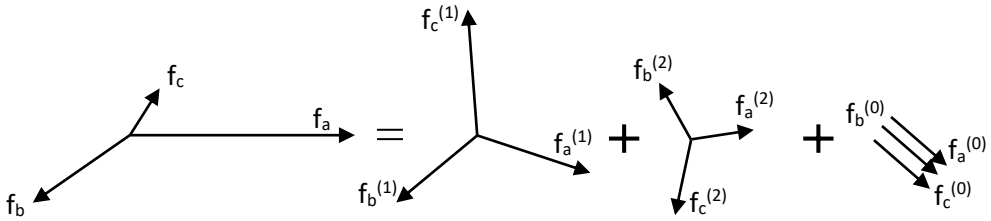

Figure 2.3: Phasor relationship between phase sequence components.

$$f^{(0)}(t) = \frac{1}{3}(f_a(t) + f_b(t) + f_c(t))$$

$$f^{(1)}(t) = \frac{1}{3}(f_a(t) + \alpha f_b(t) + \alpha^2 f_c(t)) \quad (2.12)$$

$$f^{(2)}(t) = \frac{1}{3}(f_a(t) + \alpha^2 f_b(t) + \alpha f_c(t))$$

The proposed method extracts the positive-sequence components as:

$$f_a{}^{(1)}(t) = f^{(1)}(t) = \left|f^{(1)}\right| e^{j(\omega t + \theta_{f_1})}$$

$$f_b{}^{(1)}(t) = \alpha^2 f^{(1)}(t) = \left|f^{(1)}\right| e^{j(\omega t + \theta_{f_1} - 120°)} \quad (2.13)$$

$$f_c{}^{(1)}(t) = \alpha f^{(1)}(t) = \left|f^{(1)}\right| e^{j(\omega t + \theta_{f_1} + 120°)}$$

where θ_{f_1} is the phase angle of $f^{(1)}(t)$. All phasors have equal magnitude, and they are displaced by 120° in phase. $f_b{}^{(1)}(t)$ is shifted by 120° from $f_a{}^{(1)}(t)$. $f_c{}^{(1)}(t)$ is also shifted from $f_a{}^{(1)}(t)$ by

240°. Based on based on equations (2.7) and (2.8), the phase shift can be translated in time with respect to the phase of $f_a{}^{(1)}(t)$ as following:

$$f^{(1)}(t) = \frac{1}{3}\left(f_a(t) + \alpha f_b(t) + \alpha^2 f_c(t)\right) = \frac{1}{3}\left(f_a(t) + f_b\left(t - \frac{1}{90}\right) + f_c\left(t - \frac{1}{180}\right)\right) \qquad (2.14)$$

$$f_a{}^{(1)}(t) = f^{(1)}(t) = \left|f^{(1)}\right| e^{j(\omega t + \theta_{f_1})}$$

$$f_b{}^{(1)}(t) = \alpha^2 f^{(1)}(t) = f^{(1)}\left(t - \frac{1}{180}\right) = \left|f^{(1)}\right| e^{j\left(\omega\left(t - \frac{1}{180}\right) + \theta_{f_1}\right)} \qquad (2.15)$$

$$f_c{}^{(1)}(t) = \alpha f^{(1)}(t) = f^{(1)}\left(t - \frac{1}{90}\right) = \left|f^{(1)}\right| e^{j(\omega(t - \frac{1}{90}) + \theta_{f_1})}$$

The negative sequence components can be also represented as:

$$f^{(2)}(t) = \frac{1}{3}\left(f_a(t) + \alpha^2 f_b(t) + \alpha f_c(t)\right) = \frac{1}{3}\left(f_a(t) + f_b\left(t - \frac{1}{180}\right) + f_c\left(t - \frac{1}{90}\right)\right)$$

$$f_a{}^{(2)}(t) = f^{(2)}(t) = \left|f^{(2)}\right| e^{j(\omega t + \theta_{f_1})}$$

$$f_b{}^{(2)}(t) = \alpha f^{(2)}(t) = f^{(2)}\left(t - \frac{1}{90}\right) = \left|f^{(2)}\right| e^{j(\omega(t - \frac{1}{90}) + \theta_{f_1})} \qquad (2.16)$$

$$f_c{}^{(2)}(t) = \alpha^2 f^{(2)}(t) = f^{(2)}\left(t - \frac{1}{180}\right) = \left|f^{(2)}\right| e^{j(\omega(t - \frac{1}{180}) + \theta_{f_1})}$$

The zero sequence is zero in a balanced system, in an ungrounded system, or in a delta-connected systems. However, the zero components of a grounded system can be represented as:

$$f^{(0)}(t) = \tfrac{1}{3}(f_a(t) + f_b(t) + f_c(t)) \qquad (2.17)$$

For an ungrounded system, the negative sequence components can be found as:

$$\mathbf{f_{abc}{}^{(0)}(t) = 0}$$

$$\mathbf{f_{abc}(t) = f_{abc}^{(1)}(t) + f_{abc}^{(2)}(t) + f_{abc}^{(0)}(t)}$$

$$\mathbf{f_{abc}^{(2)}(t) = f_{abc}(t) - f_{abc}^{(1)}(t)}$$

where $\mathbf{f_{abc}} = \begin{bmatrix} f_a \\ f_b \\ f_c \end{bmatrix}$.

The proposed algorithm maintains constant magnitude and phase angle relative to the input signals. The proposed sequence component filter eliminates the use low-pass filters (LPFs) and/or high-pass filters (HPFs). It is intended to extract the positive components from the positive sequence producing 3-phase balanced sinusoidal signals. The coupling method of this filter determines the extraction type whether negative sequence components or positive sequence components as shown in Figure 2.4. In the case of distorted signals, a passband filter is utilized with the proposed filter.

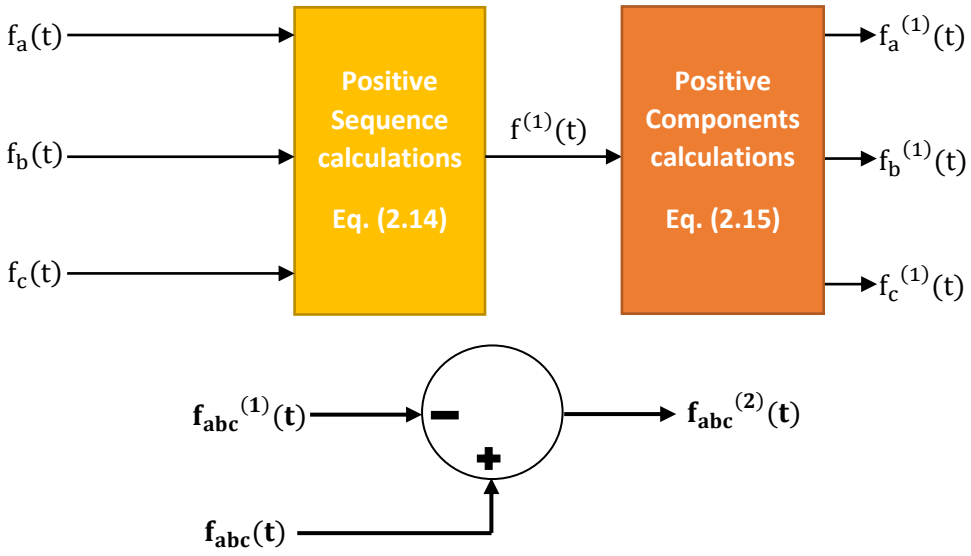

Figure 2.4: Block diagram of the proposed filter algorithm.

2.1.3 Simulation verification of the proposed filter

The simulation results were obtained using Matlab by computing equation (2.13) which represents the main method based on a frequency-domain approach and the modified method (equations (2.14) and (2.15)) which represent the proposed method based on a time-domain approach. The results are shown in Figure 2.5, 2.6 and 2.7 for balanced and unbalanced three-phase quantities.

Balanced 3-phase quantities:

$$f_a(t) = 100e^{j(\omega t)} \qquad f_b(t) = 100e^{j(\omega t - 120°)} \qquad f_c(t) = 100e^{j(\omega t + 120°)}$$

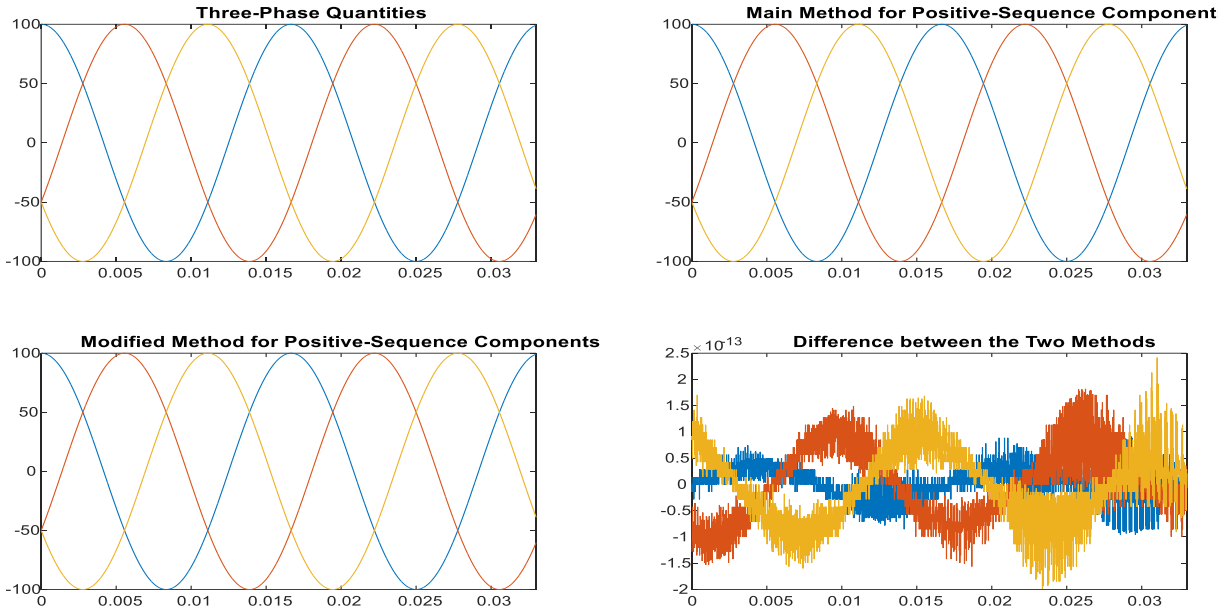

Figure 2.5: The outputs from the main method and modified method under balanced conditions.

Unbalanced magnitudes:

$$f_a(t) = 100e^{j(\omega t)} \qquad f_b(t) = 85e^{j(\omega t - 120°)} \qquad f_c(t) = 92e^{j(\omega t + 120°)}$$

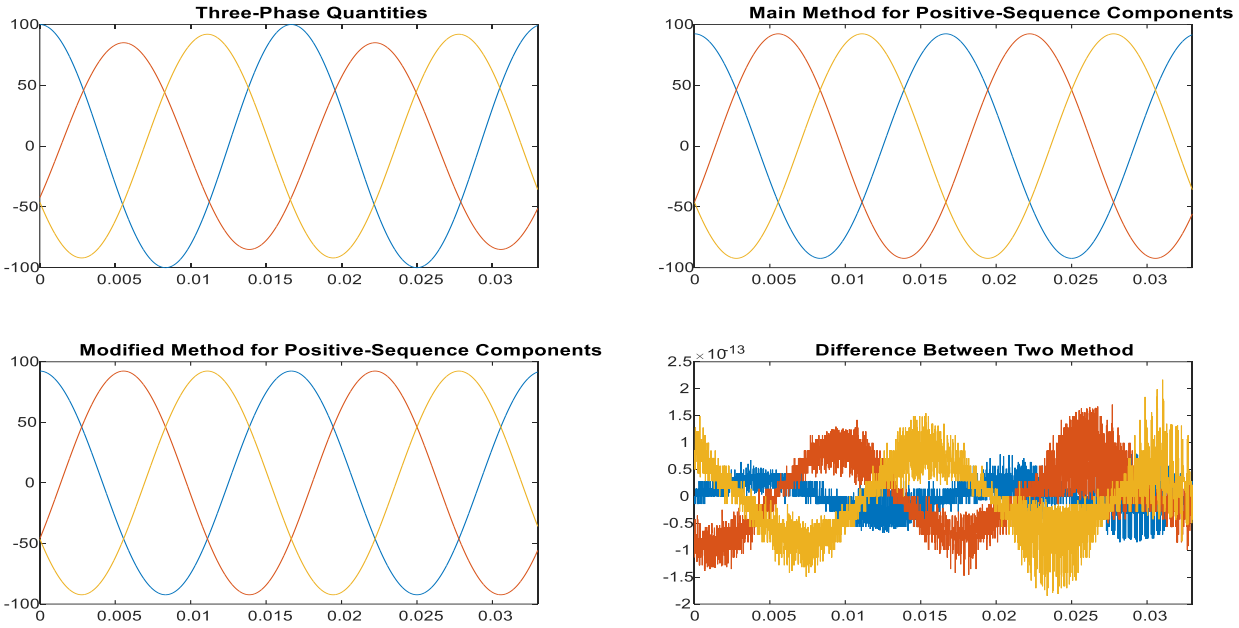

Figure 2.6: The outputs from the main method and modified method for unbalanced magnitudes.

Unbalanced magnitudes and phases:

$$f_a(t) = 100e^{j(\omega t)} \qquad f_b(t) = 90e^{j(\omega t - 110°)} \qquad f_c(t) = 80e^{j(\omega t + 100°)}$$

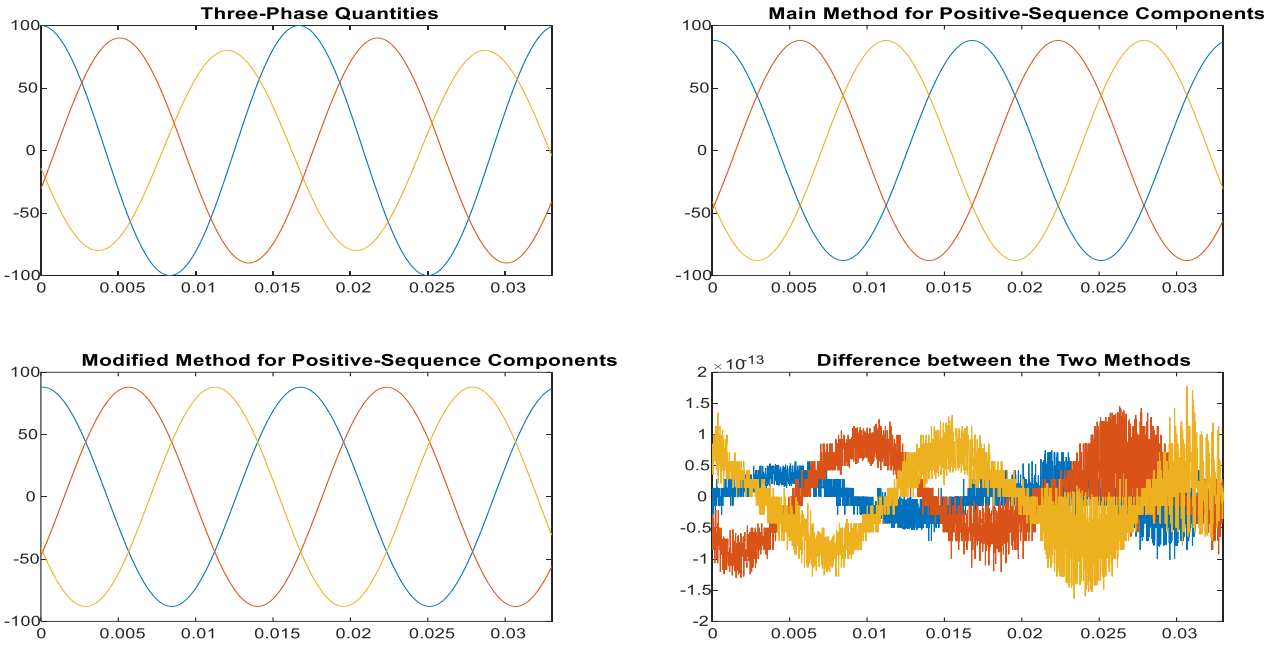

Figure 2.7: The outputs from the main method and modified method for unbalanced magnitudes and phases.

The simulation results show that the main method and the modified method yield similar results. The proposed filter maintains balanced signals under balanced and unbalanced three phase quantities. The figures show that the difference between the methods is almost zero.

2.2 Proposed Control Method

The purpose of the control of shunt APF is to maintain sinusoidal source currents under ideal and non-ideal conditions of the grid voltages and load(s). The proposed control method is based on a modified IRPT method. The voltages at the point of the common coupling (v_{pcc}), the load currents (i_L) and the actual shunt APF currents (i_f) are sensed as shown in Figure 2.8. The load currents can be expressed as:

$$i_L = i_1 + i_h + i_q \qquad (2.18)$$

where i_L is the load current, i_1 is the fundamental current, i_h is the harmonic current, and i_q is the reactive current. The shunt APF can be modeled as a current source in parallel with the system load. The VSI is controlled to generate a current that has an equal magnitude to that of the harmonic and reactive load current and has the opposite phase angle as:

$$i_f = -(i_h + i_q) \qquad (2.19)$$

The source current (i_S) is a combination of the load current and the ShAPF current (i_f). The resulting current of the combination is the fundamental load current that is sinusoidal as:

$$i_S = i_L + i_f = i_1 \qquad (2.20)$$

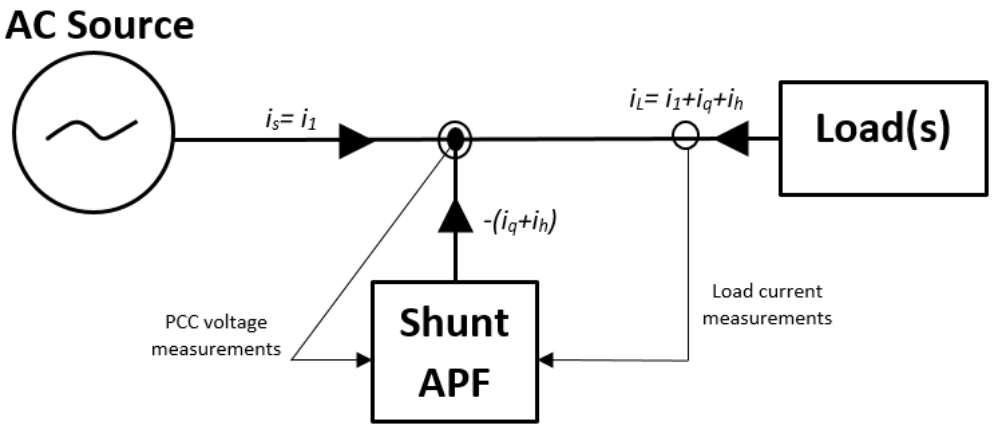

Figure 2.8: A single line diagram of a shunt APF in a power system.

The quantities v_{pcc} and i_L are composed of positive sequence components and negative sequence components. Both v_{pcc} and i_L are filtered using the proposed filter. The filter is set to generate the fundamental components of v_{pcc} and the harmonic and reactive components of i_L. The filtered signals are then transformed from abc coordinates into αβ coordinates. Then, the instantaneous real and reactive power ($\tilde{p}_n$ and $\tilde{q}_n$), related to the harmonic and reactive load currents, are calculated as:

$$\tilde{p}_n = v_\alpha^+ i_\alpha^- + v_\beta^+ i_\beta^- \qquad \tilde{q}_n = -v_\alpha^+ i_\beta^- + v_\beta^+ i_\alpha^-$$

If the VSI is powered by a DC power source, p_{dc} is not needed since the error signal from the PI controller is equal to zero. The reference currents are then calculated as:

$$\begin{bmatrix} i_{ref\alpha} \\ i_{ref\beta} \end{bmatrix} = \frac{1}{v_\alpha^{+2} + v_\alpha^{+2}} \begin{bmatrix} v_\alpha^+ & v_\beta^+ \\ v_\beta^+ & -v_\alpha^+ \end{bmatrix} \begin{bmatrix} \tilde{p}_n \\ \tilde{q}_n \end{bmatrix}$$

The inverse Clark transformation is applied to the reference currents to transform them into abc coordinates as:

$$\begin{bmatrix} i_{ref,a} \\ i_{ref,b} \\ i_{ref,c} \end{bmatrix} = \sqrt{\frac{2}{3}} \begin{bmatrix} 1 & 0 \\ -\frac{1}{2} & \frac{\sqrt{3}}{2} \\ -\frac{1}{2} & -\frac{\sqrt{3}}{2} \end{bmatrix} \begin{bmatrix} i_{ref\alpha} \\ i_{ref\beta} \end{bmatrix}$$

The reference compensation currents are compared with the actual filter currents (i_f). PWM generates the switching function and controls the inverter switches from the error signals. Figure 2.9 shows the block diagram of the proposed control method.

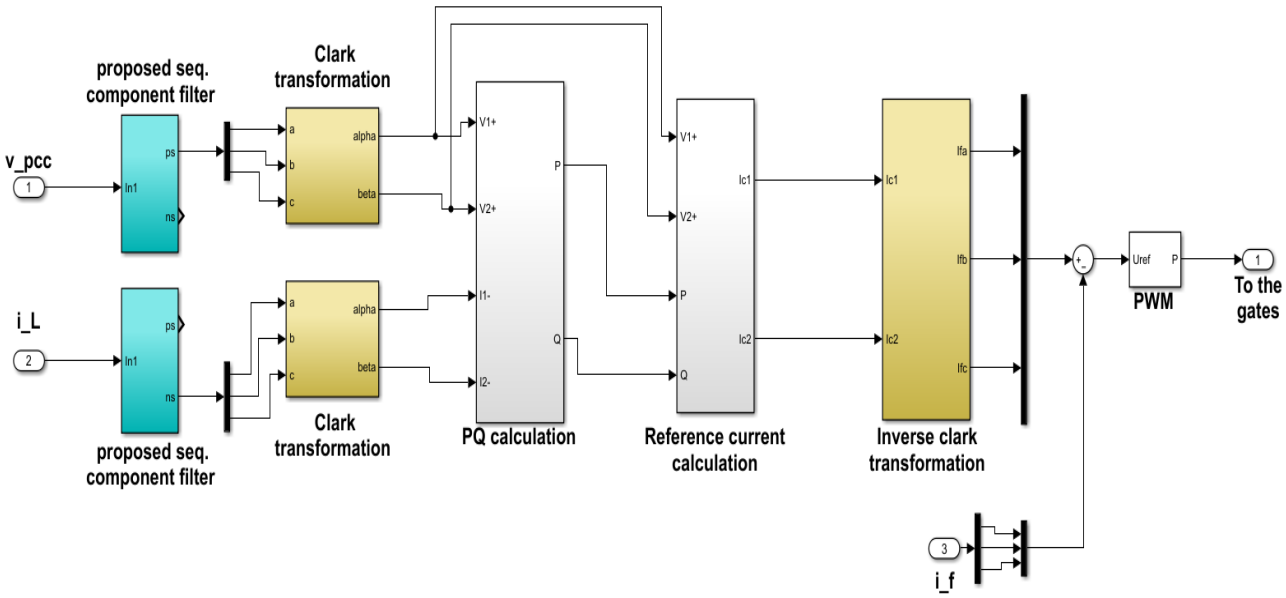

Figure 2.9: Proposed modified PQ based control system.

2.2.1 Simulation verification of the proposed control method

The software program utilized to design, model and simulate the system is Simulink using the *powerscape* library. The model of the proposed system is shown in Figure 2.10. The parameters of the test system are shown in Table 2.1. The model consists of a three-phase programmable voltage source, grid impedances, line impedances, five load sets, two measurement blocks, a three-phase PWM inverter with LCL filter, DC power source, and the control system. The system was

evaluated under different source and load conditions in steady state and transient. The simulation was performed on a 2-second time frame that is divided into different time segments as following:

- 0 - 0.4 sec: nonlinear load (NL)
- 0.4 – 0.8 sec: NL and balanced linear load (BLL)
- 0.8 – 1.2 sec: NL and unbalanced linear load (ULL)
- 1.2 – 1.6 sec: BLL
- 1.6 – 2 sec: ULL

The control system consists of the current reference control and PWM controller. It uses the measurements of the pcc voltages and load currents to calculate the reference current. The filter currents are utilized with the PWM controller to generate the switching signals. The switching frequency is set to be 10 kHz, and the sampling time is 50 μs. The results are obtained via scopes and the FFT analysis tool.

The results are listed in tables and shown in figures in the following sections and were analyzed based on three aspects: the amount of harmonic elimination based on the total harmonic distortion (THD), the ability to balance the magnitudes of the source currents, and the ability to obtain unity power factor. The unbalance in the signals can be determined from the magnitudes of the source currents.

Table 2.1: System parameters.

Frequencies	Grid f_0= 60 Hz, switching f_{sw}= 10 kHz
Grid voltages	$\overline{V}_{an} = 14\lfloor 0° \text{ V}, \overline{V}_{bn} = 14\lfloor -120° \text{ V}, \overline{V}_{cn} = 14\lfloor 120° \text{ V}$
DC Voltage	36V
Grid impedance	$L = 300\ \mu H$
Line impedance	$R = 0.06\ \Omega \quad , \quad L = 1\ mH$
R load for rectifier	$R = 5\ \Omega$
Linear loads	Balanced: $R = 4{,}4{,}4\ \Omega$, Unbalanced: $R = 2{,}4{,}6\ \Omega$
LCL Filter	$L_i = 4\ mH, C_f = 10\ \mu F, R_d = 2\Omega, L_g = 300\ \mu H$

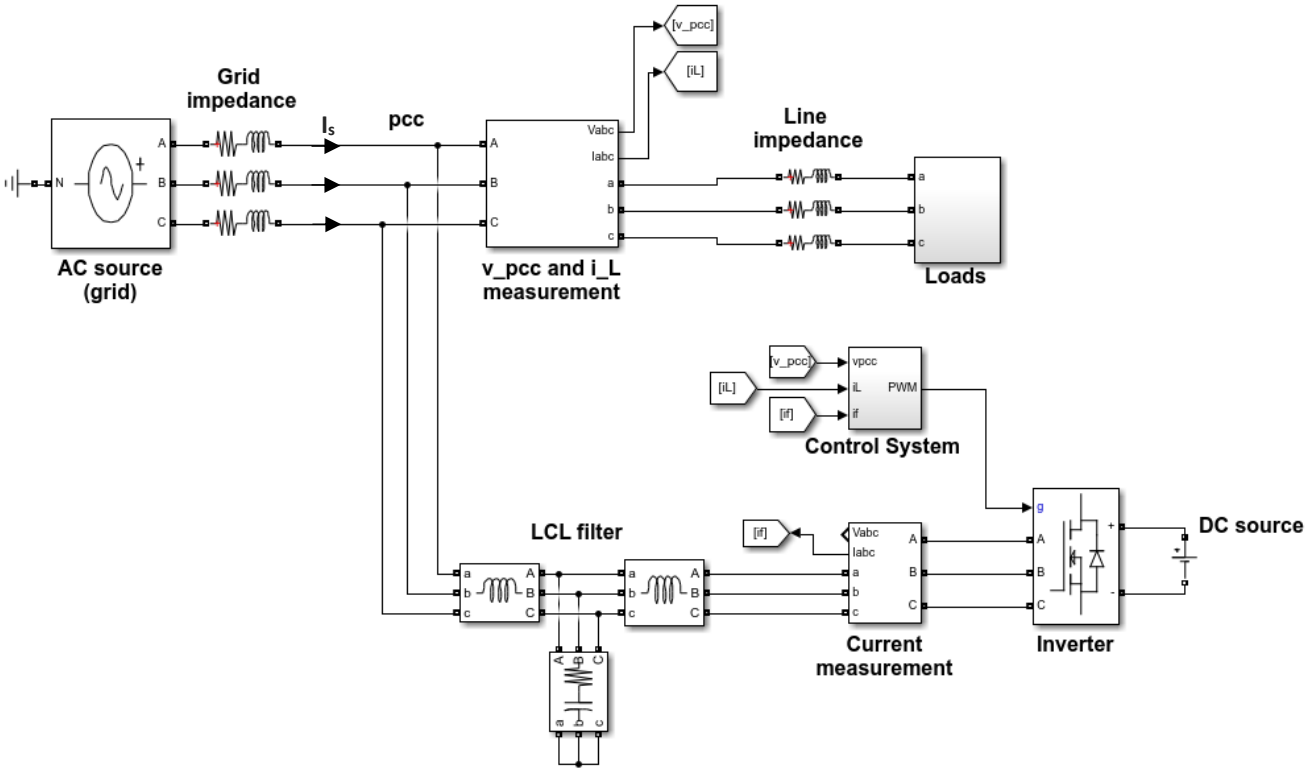

Figure 2.10: Simulink model of the system.

Case 1: Balanced source:

This case presents the evaluation of the system under balanced source voltages. Table 2.2 presents the THD of the source currents with and without the shunt APF. The THD of the three phase source currents could be equal or different based on the system conditions. The THD represented by one value is shared by all phases, while two values of THD represent the lowest and highest THD among the three phase source currents. The THD of the source current is relatively small. Table 2.3 shows the magnitudes of the source currents with and without the shunt APF. The magnitudes of the source currents with the shunt APF are almost equal which indicates balanced three phase quantities. Figures 2.11 and 2.12 show that the source currents are pure sinusoidal waves.

Table 2.2: THD of I_s without and with the shunt APF.

	THD of I_s w/o the shunt APF	THD of I_s w/ the shunt APF
NL	21.96%	3%
NL+BLL	10.96%	1.2%, 1.33%
NL+ULL	8.51%, 11.72%	1.07%, 1.3%
BLL	0.65%	2.16%, 2.22%
ULL	0.55%, 0.7%	1.95%, 2.19%

Table 2.3: The magnitudes of I_s without and with the shunt APF.

	$\|I_{sa}\|,\|I_{sb}\|,\|I_{sc}\|$ (A) w/o the shunt APF	$\|I_{sa}\|,\|I_{sb}\|,\|I_{sc}\|$ (A) w/ the shunt APF
NL	4.37, 4.37, 4.37	4.46, 4.47, 4.47
NL+BLL	7.43, 7.43, 7.43	7.50, 7.51, 7.51
NL+ULL	7.62, 6.94, 8.56	7.77, 7.75, 7.51
BLL	3.42, 3.42, 3.42	3.49, 3.50, 3.50
ULL	2.79, 3.95, 4.61	3.80, 3.78, 3.81

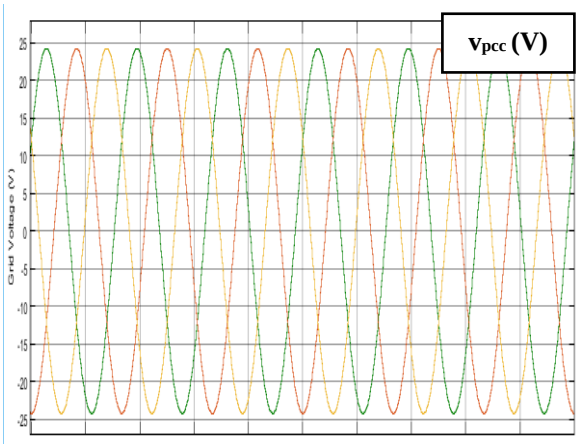

(a) Balanced source voltages.

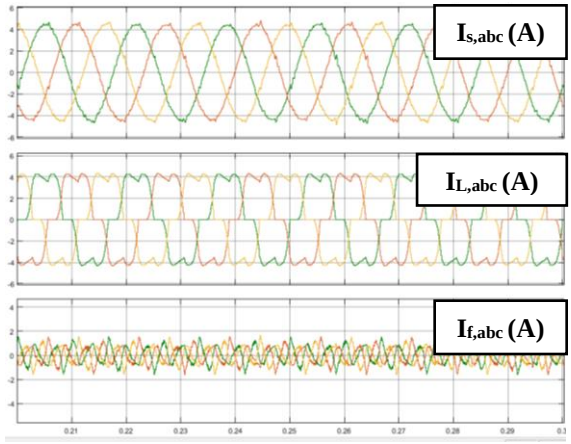

(b) I_s, I_L and I_f with NL.

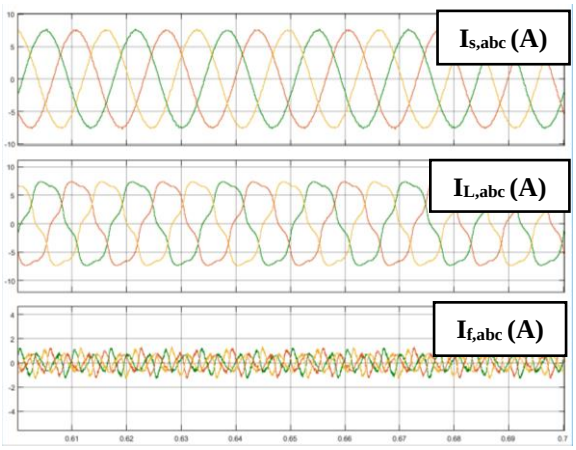

(c) I_s, I_L and I_f with NL & BLL.

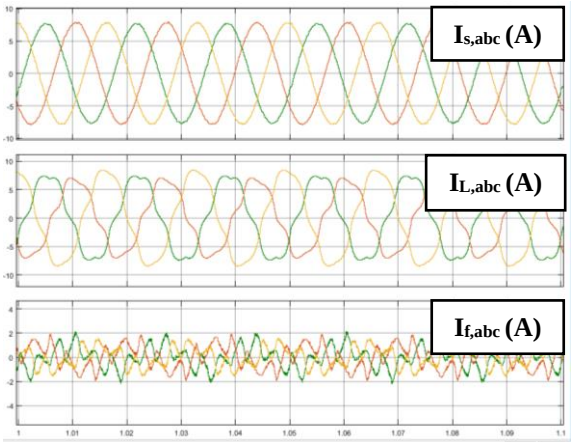

(d) I_s, I_L and I_f with NL & ULL.

Figure 2.11: For nonlinear load, I_s, I_L and I_f with the shunt APF when the source voltages are balanced.

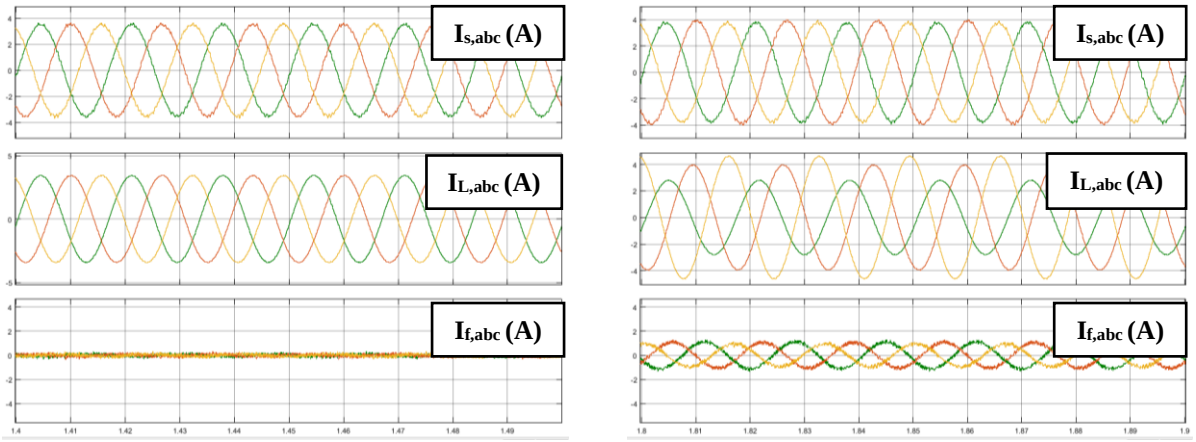

(a) I_s, I_L and I_f with BLL. **(b) I_s, I_L and I_f with ULL.**

Figure 2.12: For linear load, I_s, I_L and I_f with the shunt APF when the source voltages are balanced.

Case 2: Unbalanced magnitudes of the source voltages:

The source voltages are unbalanced where the magnitudes of phases B and C are 80% of phase A magnitude. Table 2.4 shows the THD of the source currents with and without the shunt APF. The THD is relatively small with amount less than 5%. Table 2.5 shows the magnitudes of the source currents, which are considered balanced three phase quantities since the difference between the magnitudes is very small. Figure 2.13 shows that the source currents are balanced sinusoidal waveforms.

Table 2.4: THD of I_s without and with the shunt APF.

	THD of I_s w/o the shunt APF	THD of I_s w/ the shunt APF
NL	20.07%, 24.33%	2.74%, 2.99%
NL+BLL	10.18%, 12.24%	1.34%, 1.42%
NL+ULL	7.96%, 12.42%	1.14%, 1.22%
BLL	0.61%, 0.66%	2.40%, 2.64%
ULL	0.49%, 0.77%	2.18%, 2.37%

Table 2.5: The magnitudes of I_s without and with the shunt APF.

	$\|I_{sa}\|$,$\|I_{sb}\|$,$\|I_{sc}\|$ (A) w/o the shunt APF	$\|I_{sa}\|$,$\|I_{sb}\|$,$\|I_{sc}\|$ (A) w/ the shunt APF
NL	3.89, 4.20, 4.34	4.22, 4.20, 4.22
NL+BLL	6.64, 7.20, 7.32	7.12, 7.11, 7.12
NL+ULL	6.81, 6.77, 8.39	7.35, 7.34, 7.35
BLL	3.08, 3.34, 3.35	3.33, 3.33, 3.35
ULL	2.52, 3.91, 4.54	3.64, 3.63, 3.66

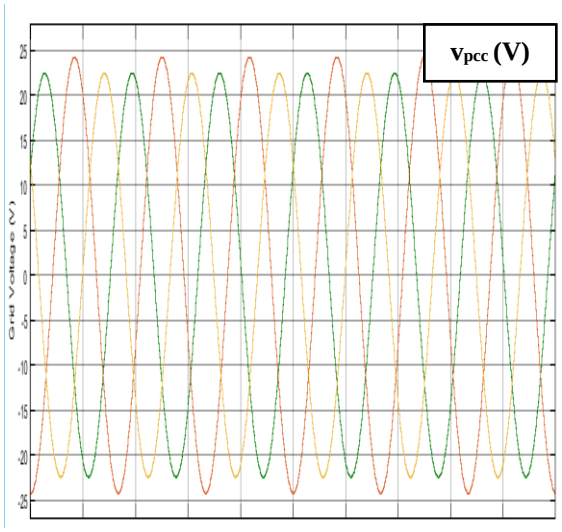

(a) Unbalanced source voltages.

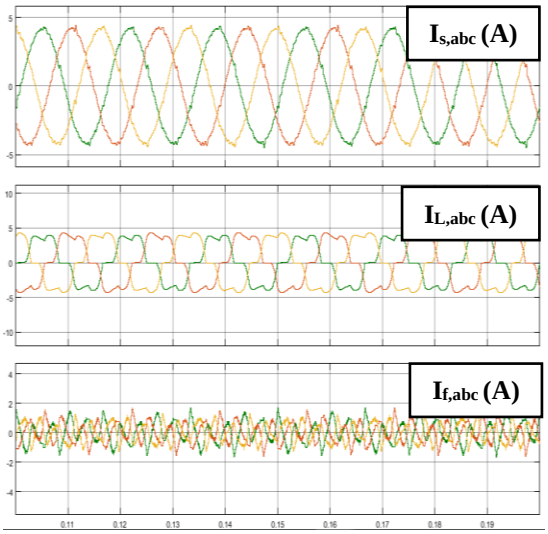

(b) I_s, I_L and I_f with NL.

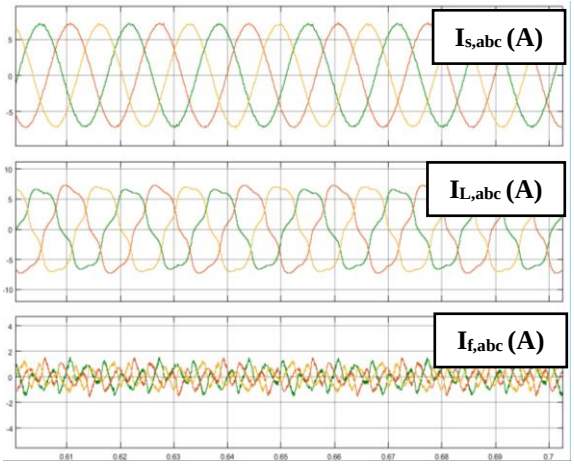

(c) I_s, I_L and I_f with NL & BLL.

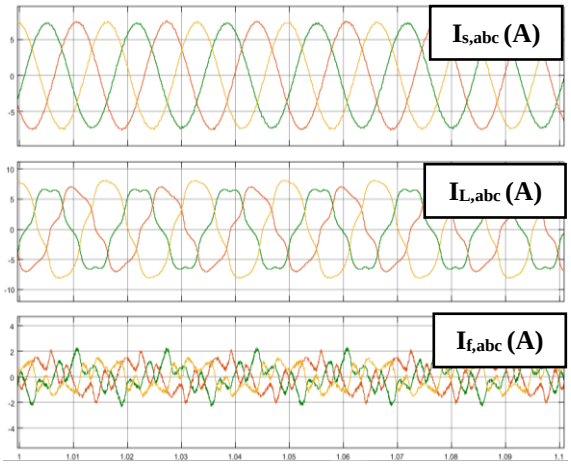

(d) I_s, I_L and I_f with NL & ULL.

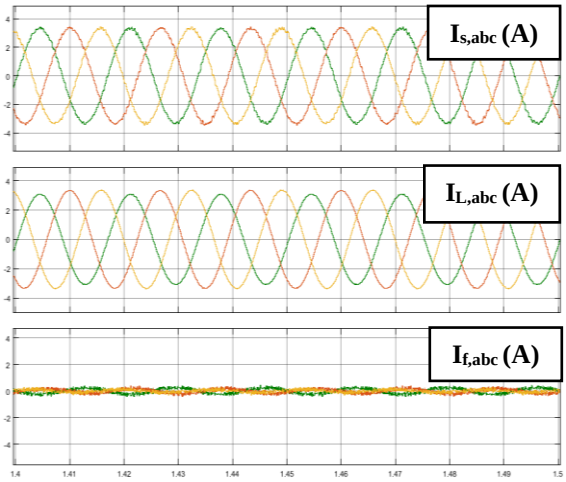

(e) I_s, I_L and I_f with BLL.

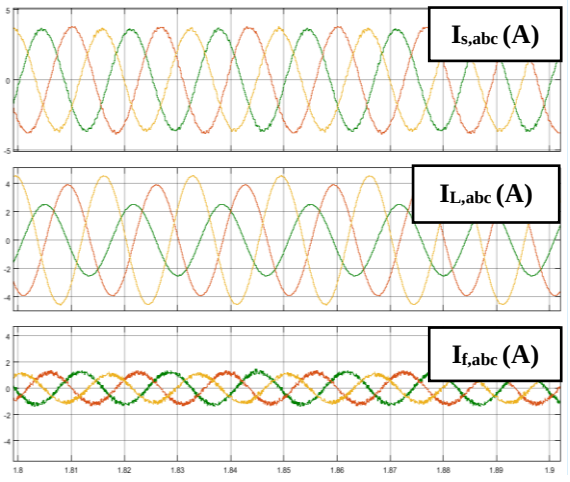

(f) I_s, I_L and I_f with ULL.

Figure 2.13: I_s, I_L and I_f with the shunt APF when the source voltages are unbalanced.

Case 3: Distorted source voltage

In this case, the source voltages are distorted where the THD is about 19%. Table 2.6 shows the lowest and the highest THD of the source currents with and without the shunt APF. The THD of the source current is under 5%. Table 2.7 shows that the magnitudes of the source currents with the shunt APF are balanced. The source currents are balanced and sinusoidal quantities as shown in Figure 2.14.

Table 2.6: THD of I_s without and with the shunt APF.

	THD of I_s w/o the shunt APF	THD of I_s w/ the shunt APF
NL	21.17%	4.88%, 4.91%
NL+BLL	15.29%	2.73%, 2.79%
NL+ULL	12.90%, 15.93%	2.83%, 3.08%
BLL	11.46%	2.54%, 2.68%
ULL	10.38%, 12.21%	2.42%, 2.47%

Table 2.7: The magnitudes of I_s without and with the shunt APF.

	$\|I_{sa}\|,\|I_{sb}\|,\|I_{sc}\|$ (A) w/o the shunt APF	$\|I_{sa}\|,\|I_{sb}\|,\|I_{sc}\|$ (A) w/ the shunt APF
NL	4.21, 4.21, 4.21	4.30, 4.31, 4.31
NL+BLL	7.23, 7.23, 7.23	7.33, 7.33, 7.33
NL+ULL	7.50, 6.72, 8.23	7.63, 7.57, 7.57
BLL	3.42, 3.42, 3.42	3.51, 3.52, 3.52
ULL	2.79, 3.95, 4.61	3.80, 3.79, 3.81

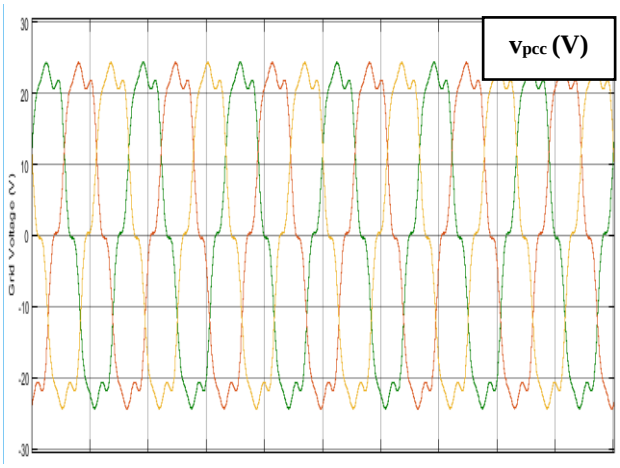

(a) Distorted source voltages.

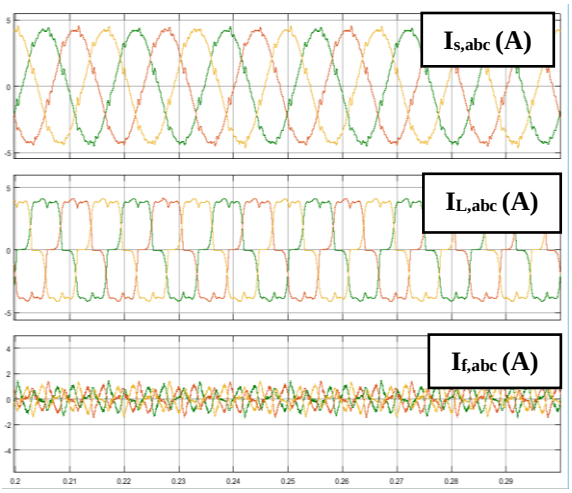

(b) I_s, I_L and I_f with NL.

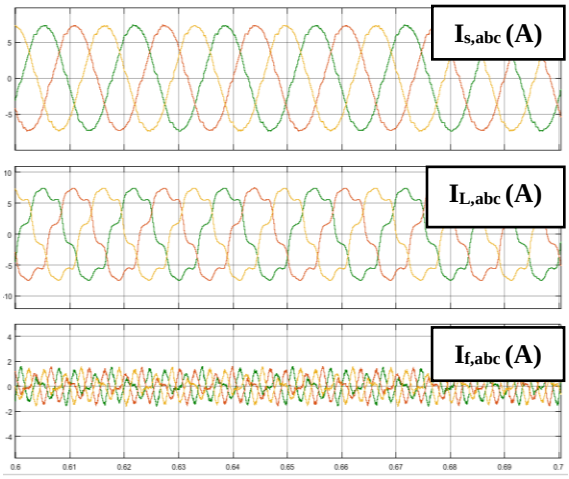

(c) I_s, I_L and I_f with NL & BLL.

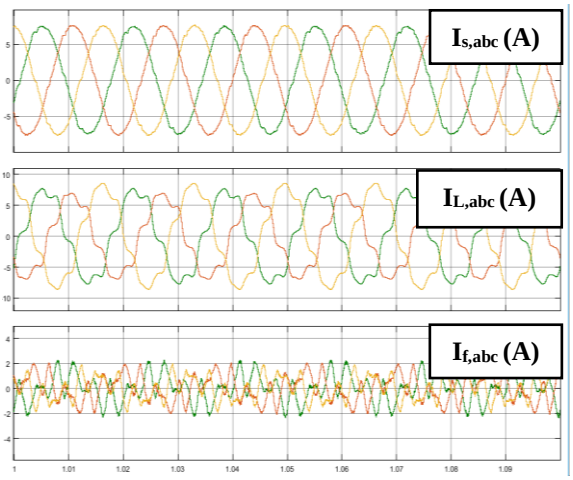

(d) I_s, I_L and I_f with NL & ULL.

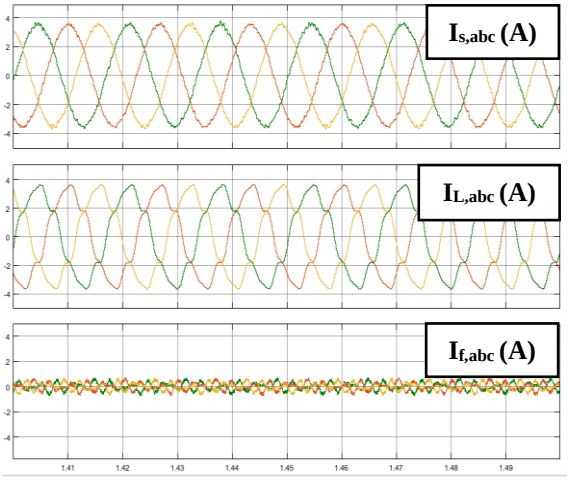

(e) I_s, I_L and I_f with BLL.

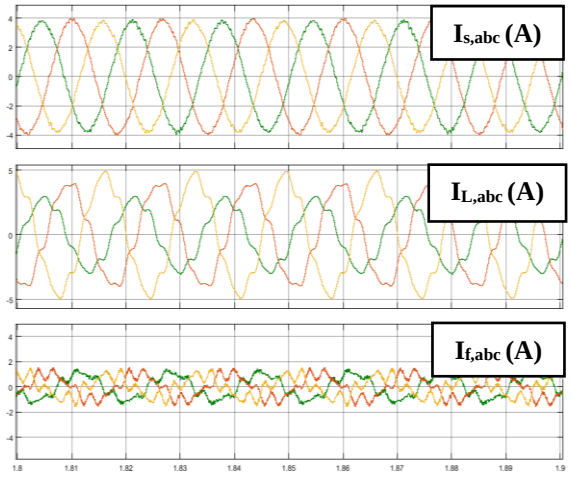

(f) I_s, I_L and I_f with ULL.

Figure 2.14: I_s, I_L and I_f with the shunt APF when the source voltages are distorted.

The results confirmed that the proposed control system was able to inject the desired currents required to eliminate the unwanted components from the source currents. The source currents were also balanced where the difference between the magnitudes is zero or very small. Because the source currents had the same shape as the grid voltages and in phase with the grid voltages, almost unity power factor has been achieved for all conditions except when the source voltages were distorted. Therefore, the proposed control system was able to achieve its purposes under different conditions of the grid voltages and loads.

2.3 Proposed Frequency Adaptive Control

A proposed frequency detection method uses zero-crossing detection [47]. It utilizes the proposed filter to obtain accurate measurement and can be set to count rising or falling edges as shown in Figure 2.15. The frequency is calculated from the period between two consecutive rising or falling edges. It is modified by rounding the output. The proposed frequency detection method was evaluated in software using a three-phase AC source with the frequency initially set to 40 Hz. Then, the frequency was increased by 10 Hz until it reaches 70 Hz. The simulation is executed in 4 seconds where the frequency increases 10 Hz each second. The simulation result is show in Figure 2.16. It can be seen from the results that the proposed detection method works properly in tracking the system frequency. The response time of this method to the frequency change is about 0.2 sec.

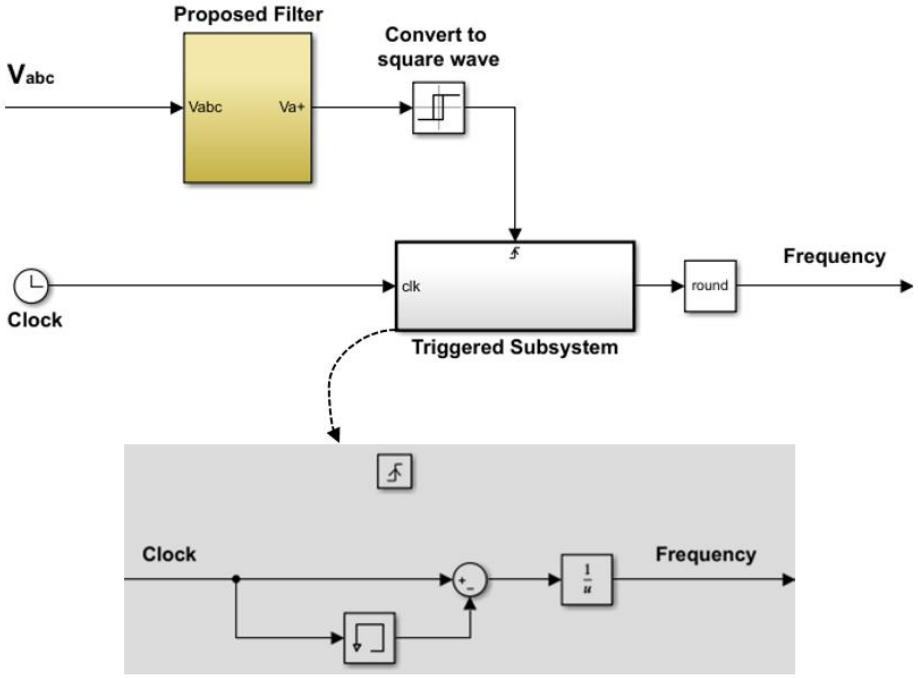

Figure 2.15: Frequency detector.

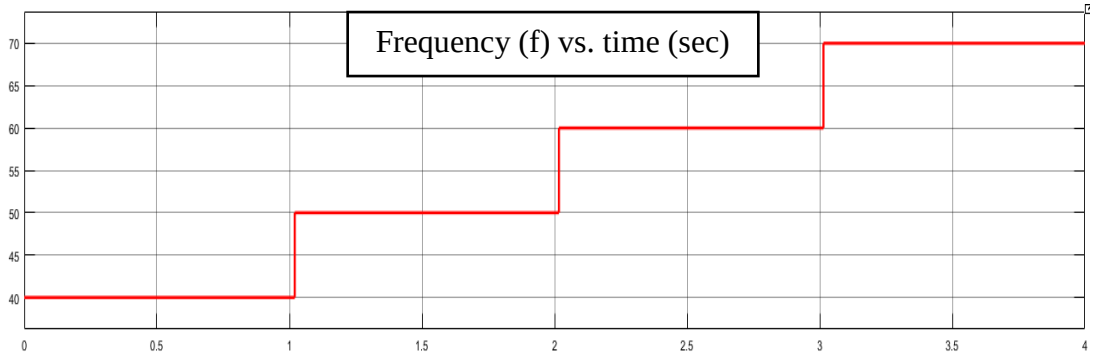

Figure 2.16: Simulation result of measuring the system frequency using the proposed frequency detection method.

The proposed control system in the previous section is modified to adapt the system frequency. The frequency (f) is determined from one of the voltage phases. Then, the proposed filter uses the measured frequency in order to generate the positive sequence components and negative sequence components. The positive sequence components are calculated as:

$$f^{(1)}(t) = \frac{1}{3}\left(f_a(t) + f_b\left(t - \frac{2}{3f}\right) + f_c\left(t - \frac{1}{3f}\right)\right)$$

$$f_a^{(1)}(t) = f^{(1)}(t)$$

$$f_b^{(1)}(t) = \alpha^2 f^{(1)}(t) = f^{(1)}\left(t - \frac{1}{3f}\right)$$

$$f_c^{(1)}(t) = \alpha f^{(1)}(t) = f^{(1)}\left(t - \frac{2}{3f}\right)$$

The negative sequence and negative sequence components are calculated as:

$$f^{(2)}(t) = \frac{1}{3}\left(f_a(t) + f_b\left(t - \frac{1}{3f}\right) + f_c\left(t - \frac{2}{3f}\right)\right)$$

$$f_a^{(2)}(t) = f^{(2)}(t)$$

$$f_b^{(2)}(t) = \alpha f^{(2)}(t) = f^{(2)}\left(t - \frac{2}{3f}\right)$$

$$f_c^{(2)}(t) = \alpha^2 f^{(2)}(t) = f^{(2)}\left(t - \frac{1}{3f}\right)$$

The negative sequence components can also be determined from:

$$\begin{bmatrix} f_a^{(2)} \\ f_b^{(2)} \\ f_c^{(2)} \end{bmatrix} = \begin{bmatrix} f_a \\ f_b \\ f_c \end{bmatrix} - \begin{bmatrix} f_a^{(1)} \\ f_b^{(1)} \\ f_c^{(1)} \end{bmatrix}$$

The reference current signals are calculated from the calculations of the instantaneous real and reactive powers as shown previously:

$$\tilde{p}_n = v_\alpha^+ i_\alpha^- + v_\beta^+ i_\beta^- \qquad \tilde{q}_n = -v_\alpha^+ i_\beta^- + v_\beta^+ i_\alpha^-$$

The DC-link voltage is not sensed because a DC voltage source is used, which means that DC power losses from the inverter are supplied by the DC power source with a fixed value.

$$\begin{bmatrix} i_{ref\alpha} \\ i_{ref\beta} \end{bmatrix} = \frac{1}{v_\alpha^{+2} + v_\alpha^{+2}} \begin{bmatrix} v_\alpha^+ & v_\beta^+ \\ v_\beta^+ & -v_\alpha^+ \end{bmatrix} \begin{bmatrix} \tilde{p}_n \\ \tilde{q}_n \end{bmatrix}$$

The inverse Clark transformation is applied on the reference current to transform into abc coordinates as:

$$\begin{bmatrix} i_{ref,a} \\ i_{ref,b} \\ i_{ref,c} \end{bmatrix} = \sqrt{\frac{2}{3}} \begin{bmatrix} 1 & 0 \\ -\frac{1}{2} & \frac{\sqrt{3}}{2} \\ -\frac{1}{2} & -\frac{\sqrt{3}}{2} \end{bmatrix} \begin{bmatrix} i_{ref\alpha} \\ i_{ref\beta} \end{bmatrix}$$

These signals should have the same frequency as that of the system frequency. The reference current signals and the filter currents are then compared through a PWM controller to produce the gating signals. The block diagram of this method is shown in Figure 2.17.

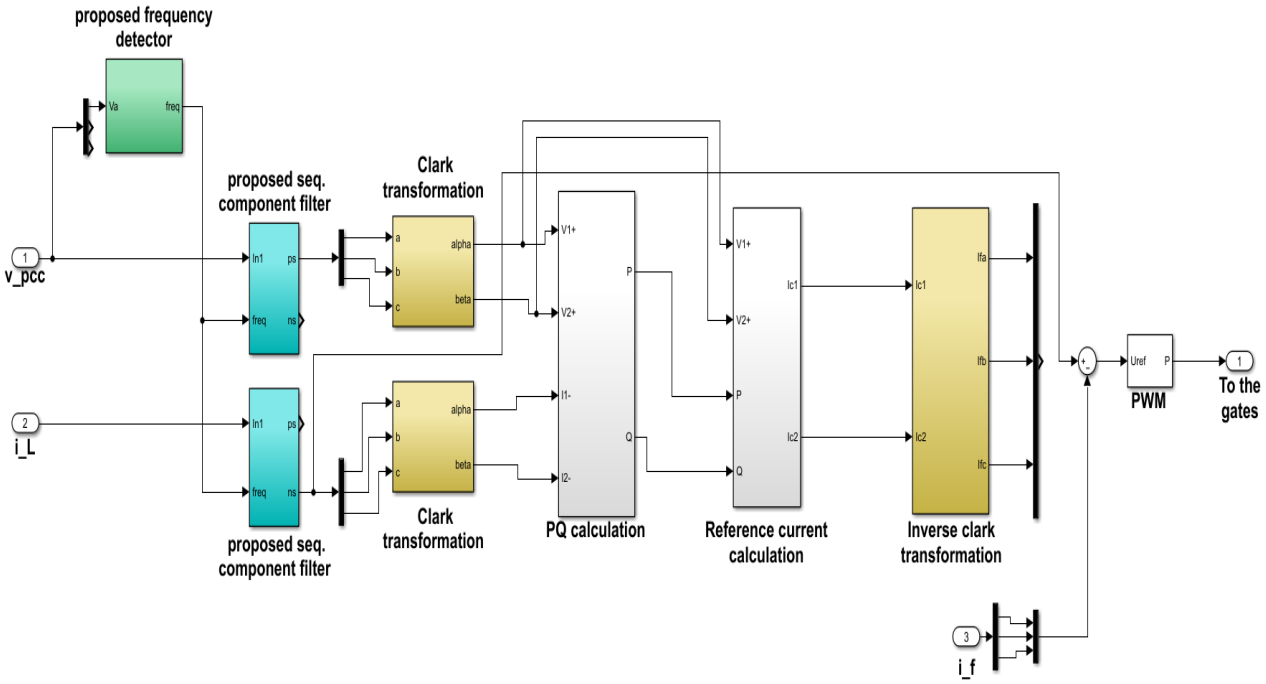

Figure 2.17: Block diagram of the proposed adaptive frequency modified IRPT method.

2.3.1 Simulation results of the proposed control method under frequency deviation

The results were obtained with and without the shunt APF to detect the response of the proposed control system under the frequency deviation. The simulation results are shown in Tables 2.8 and 2.9 and Figures 2.18, 2.19, 2.20, 2.21, and 2.22.

Table 2.8: Simulation results from changing the frequency without the shunt APF.

System condition	Without the shunt APF		
	f (Hz)	$\|I_{sa}\|,\|I_{sb}\|,\|I_{sc}\|$ (A)	THD%
Balanced system	58	3.38, 3.38, 3.38	0.14, 0.22, 0.2
	59	3.38, 3.38, 3.38	0.02, 0.02, 0.02
	60	3.38, 3.38, 3.38	0, 0, 0
	61	3.38, 3.38, 3.38	0.18, 0.12, 0.18
	62	3.38, 3.38, 3.38	0.11, 0.13, 0.08
Unbalanced system	58	4, 3.43, 2.75	0.23, 0.2, 0.17
	59	4, 3.43, 2.75	0.02, 0.02, 0.02
	60	4, 3.43, 2.75	0.1, 0.1, 0.17
	61	4, 3.43, 2.75	0.19, 016, 0.15
	62	4, 3.43, 2.75	0.1, 0.1, 0.13

Table 2.9: Simulation results from changing the frequency with the shunt APF.

System condition	With the shunt APF		
	f (Hz)	$\|I_{sa}\|,\|I_{sb}\|,\|I_{sc}\|$ (A)	THD%
Balanced system	58	3.54, 3.35, 3.35	2.36, 2.56, 2.33
	59	3.5, 3.41, 3.51	2.44, 2.43, 2.41
	60	3.46, 3.46, 3.46	2.4, 2.38, 2.33
	61	3.4, 3.5, 3.4	2.6, 2.5, 2.65
	62	3.37, 3.52, 3.31	2.71, 2.53, 2.7
Unbalanced system	58	3.5, 3.36, 3.56	2.3, 2.68, 2.38
	59	3.49, 3.41, 3.51	2.3, 2.63, 2.66
	60	3.45, 3.46, 3.46	2.4, 2.6, 2.7
	61	3.35, 3.47, 3.37	2.4, 2.4, 2.44
	62	3.3, 3.48, 3.27	2.42, 2.55, 2.73

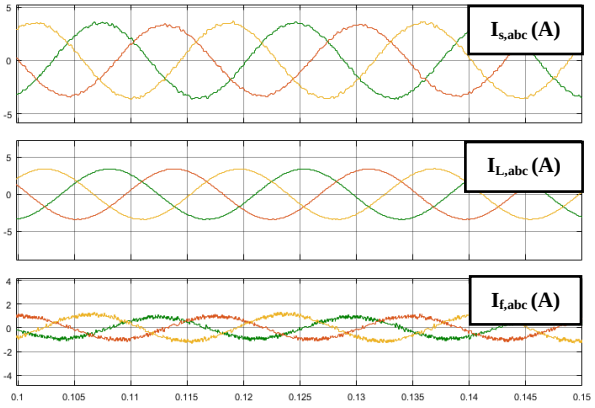

For balanced system: from the top, i_s, i_L and i_f.

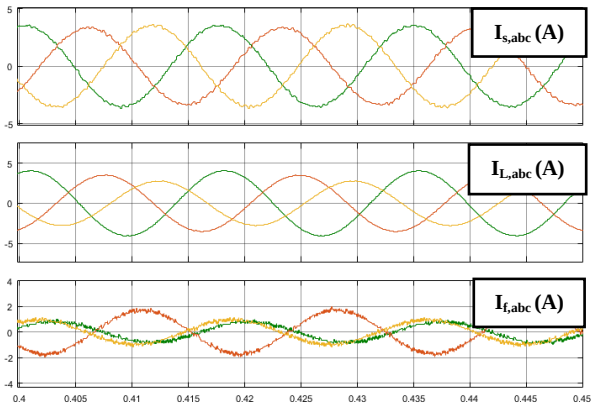

For unbalanced system: from the top, i_s, i_L and i_f.

Figure 2.18: i_s, i_L and i_f when f= 58 Hz.

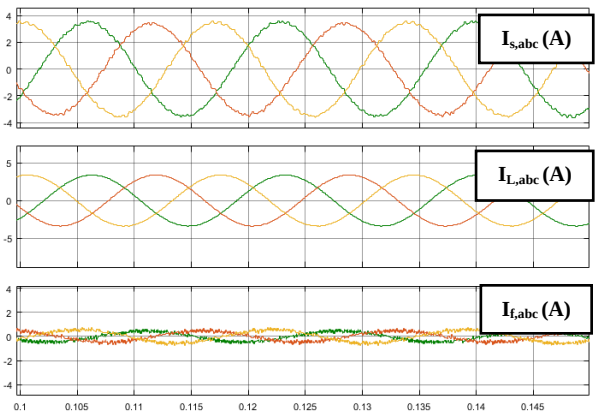

For balanced system: from the top, i_s, i_L and i_f when f= 59 Hz.

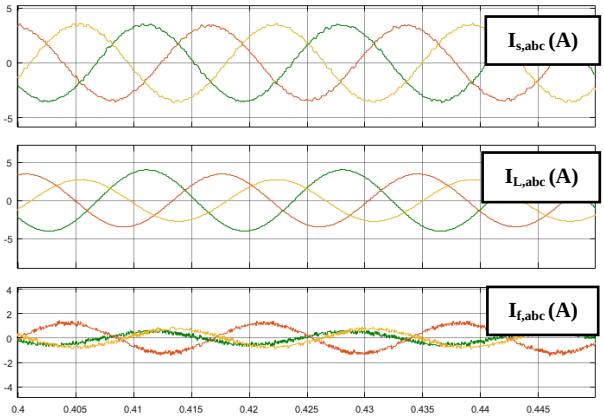

For unbalanced system: from the top, i_s, i_L and i_f when f= 58 Hz.

Figure 2.19: i_s, i_L and i_f when f= 59 Hz.

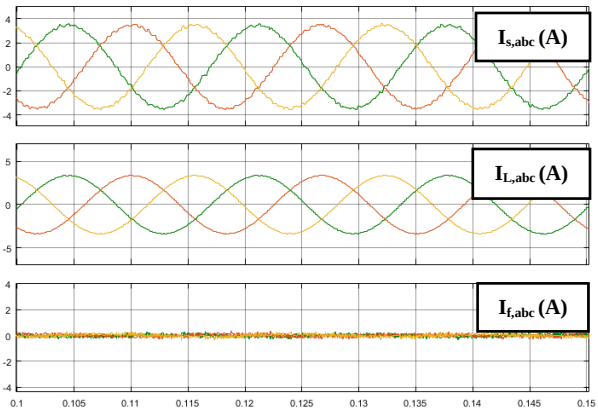

For balanced system: from the top, i_s, i_L and i_f.

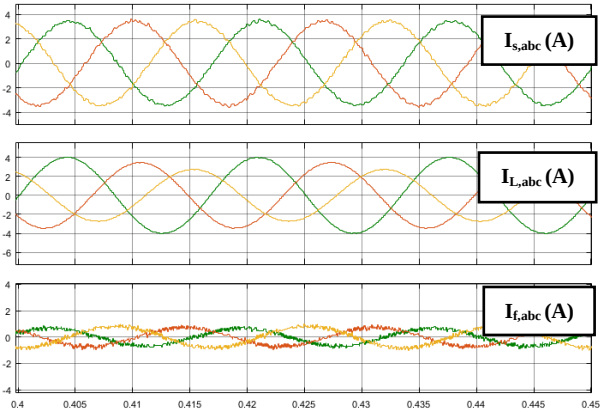

For unbalanced system: from the top, i_s, i_L and i_f.

Figure 2.20: i_s, i_L and i_f when f= 60 Hz.

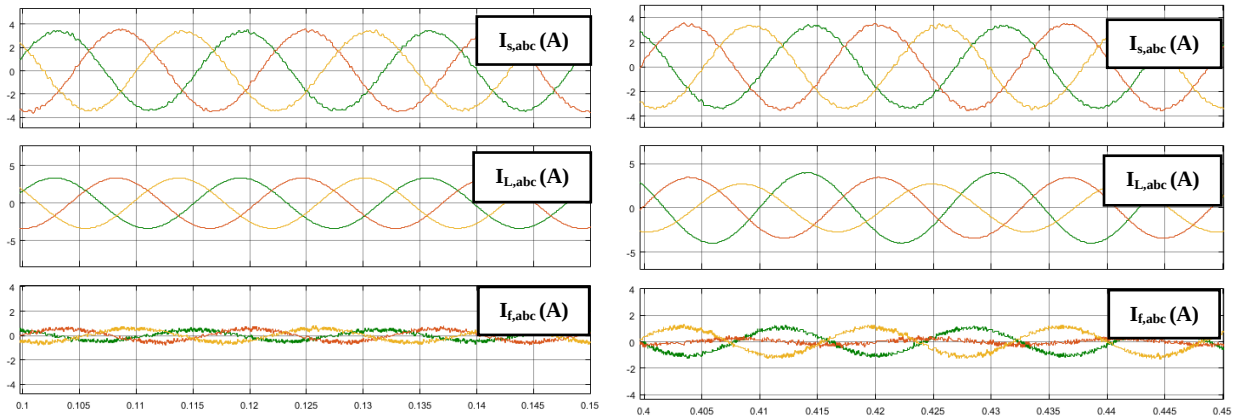

For balanced system: from the top, i_s, i_L and i_f. **For unbalanced system: from the top, i_s, i_L and i_f.**

Figure 2.21: i_s, i_L and i_f when f= 61 Hz.

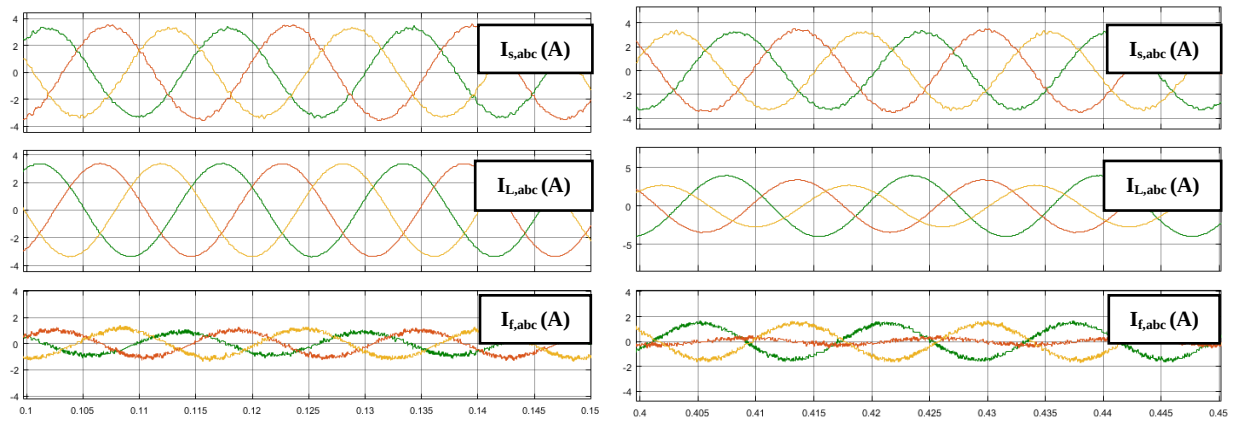

For balanced system: from the top, i_s, i_L and i_f. **For unbalanced system: from the top, i_s, i_L and i_f.**

Figure 2.22: i_s, i_L and i_f when f= 62 Hz.

The simulation results show that the shunt APF with the proposed control method maintained sinusoidal currents as the frequency changes. Ideally, the filter currents are very small for the balanced system as seen in the simulation results. But, the filter currents were increased as the frequency deviation increases. The source currents were almost balanced source currents under balanced and unbalanced power system conditions. However, the differences between the magnitudes of the source currents were enlarged as the frequency deviation increased. Moreover, the simulation THDs increased as the frequency deviation increases. Based on the above results, the shunt APF shows acceptable performance under frequency variations, but it does not change the system frequency to the desired frequency of 60 Hz.

2.3.2 Simulation results of the proposed frequency adaptive control method

The performance of the proposed frequency adaptive control method with the shunt APF can be determined from the simulation results. This control method was evaluated under balanced and unbalanced conditions. The simulation results are shown in Table 2.10 and Figures 2.23, 2.24, 2.25, 2.26, and 2.27.

Table 2.10: Simulation results for the magnitude and the THD of the source currents.

	f (Hz)	$\|I_{sa}\|,\|I_{sb}\|,\|I_{sc}\|$ (A)	THD%
Balanced system	58	3.47, 3.47, 3.47	2.5, 2.5, 2.5
	59	3.47, 3.47, 3.47	2.4, 2.4, 2.4
	60	3.47, 3.47, 3.47	2.4, 2.4, 2.4
	61	3.47, 3.47, 3.47	2.6, 2.6, 2.6
	62	3.47, 3.47, 3.47	2.4, 2.4, 2.4
Unbalanced system	58	3.44, 3.46, 3.45	2.3, 2.3, 2.3
	59	3.44, 3.46, 3.45	2.3, 2.5, 2.75
	60	3.43, 3.45, 3.44	2.4, 2.7, 2.5
	61	3.43, 3.46, 3.45	2.5, 2.5, 2.5
	62	3.42, 3.44, 3.44	2.3, 2.5, 2.6

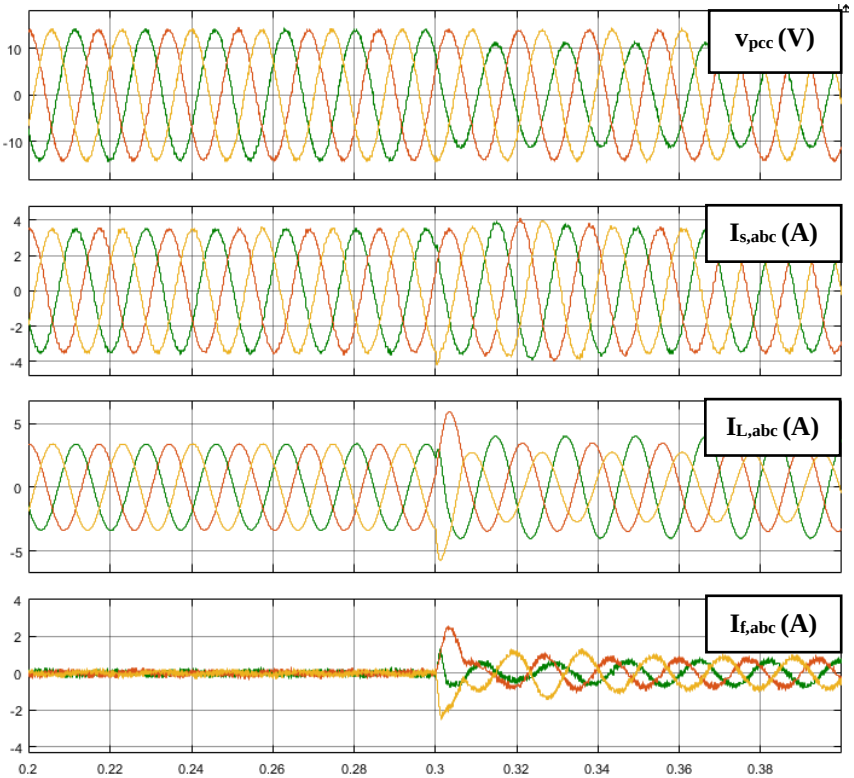

Figure 2.23: For balanced and unbalanced conditions: from the top, v_{pcc}, i_s, i_L, and i_f when f= 58 Hz.

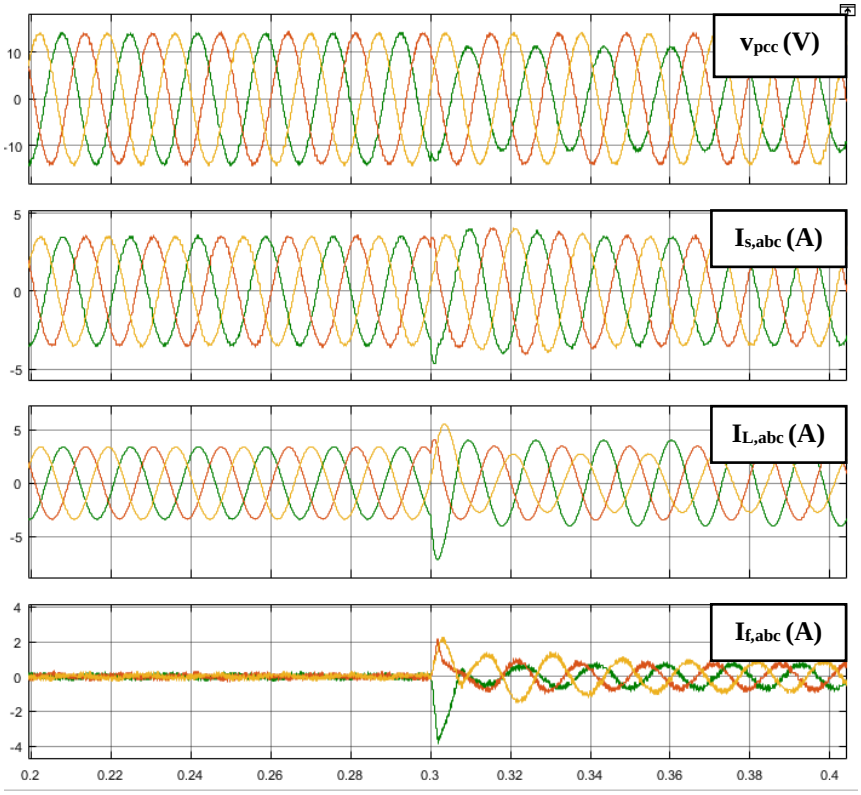

Figure 2.24: For balanced and unbalanced conditions: from the top, v_{pcc}, i_s, i_L, and i_f when f= 59 Hz.

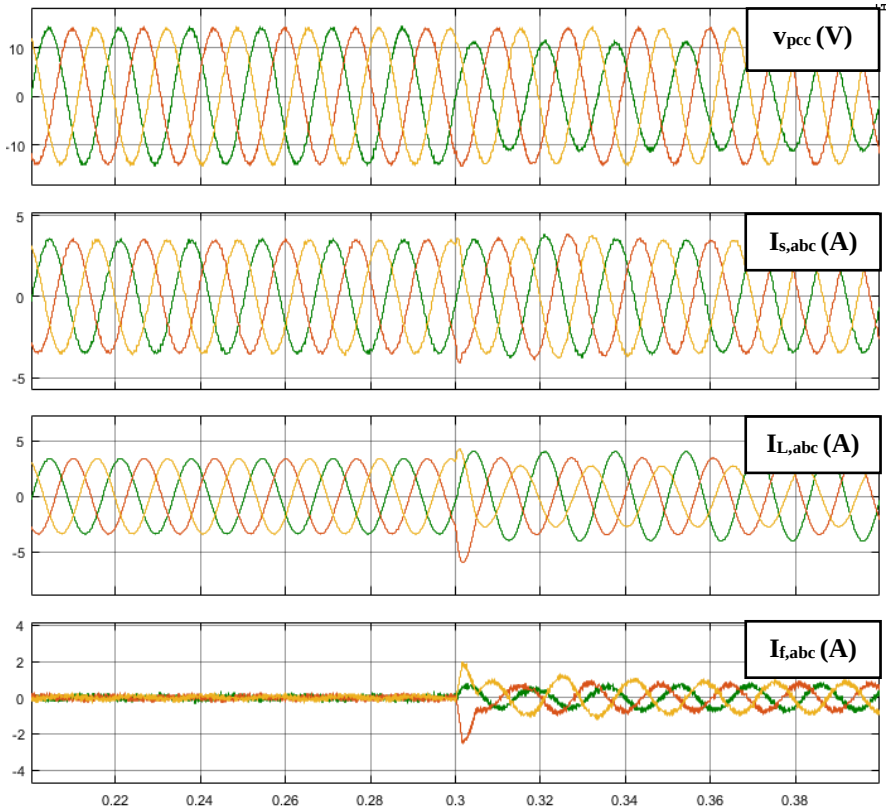

Figure 2.25: For balanced and unbalanced conditions: from the top, v_{pcc}, i_s, i_L, and i_f when f= 60 Hz.

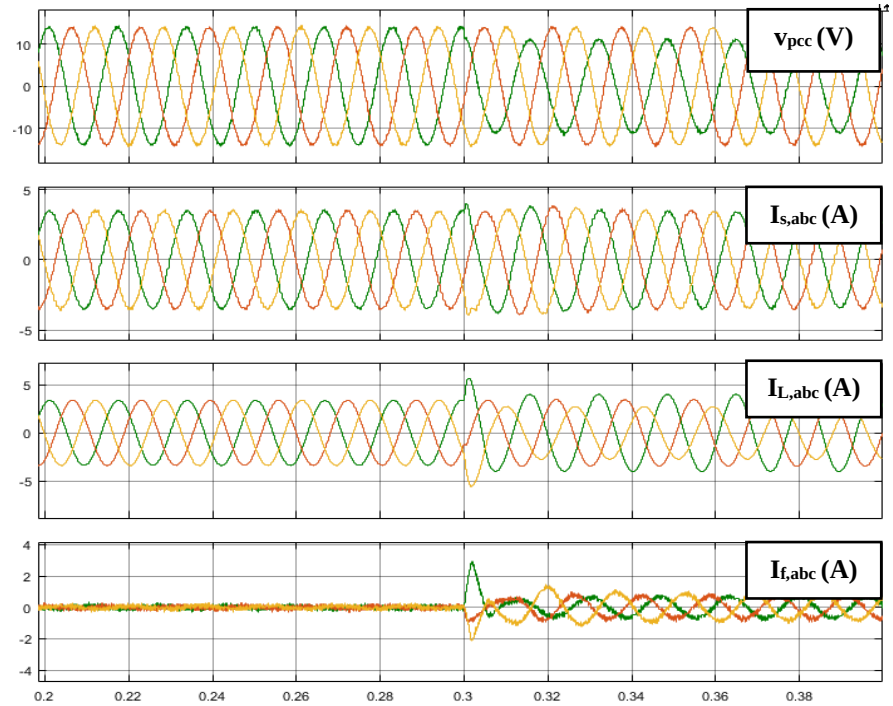

Figure 2.26: For balanced and unbalanced conditions: from the top, v_{pcc}, i_s, i_L, and i_f when f= 61 Hz.

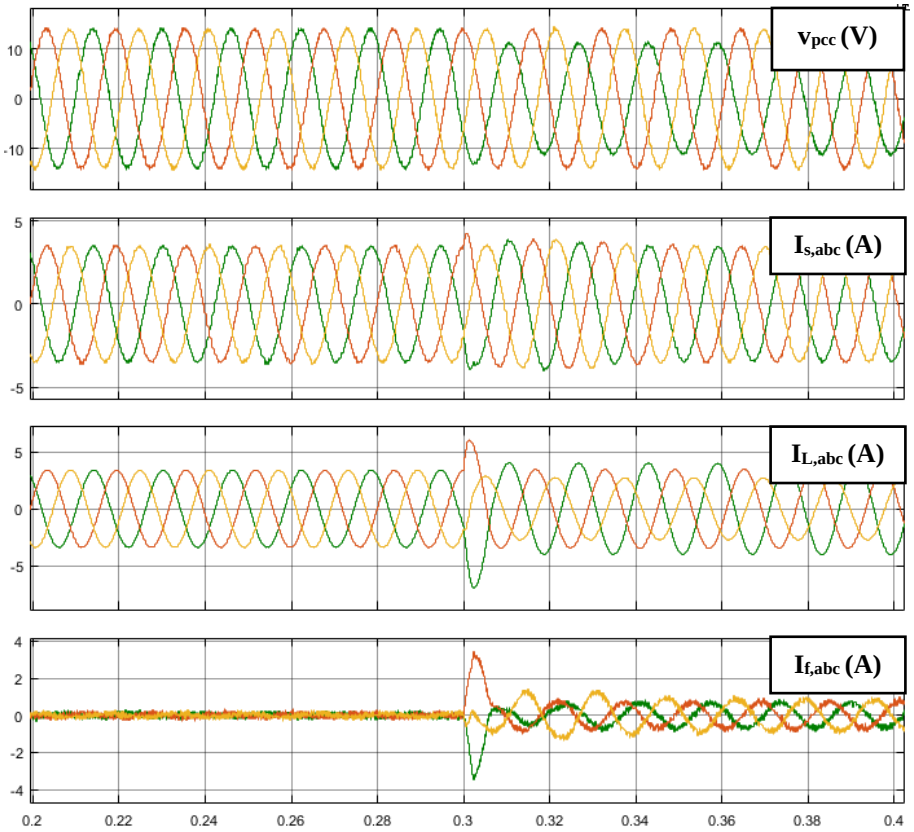

Figure 2.27: For balanced and unbalanced conditions: from the top, v_{pcc}, i_s, i_L, and i_f when f= 61 Hz.

The simulation results show that the shunt APF injected currents that eliminate the negative sequence components from the currents as the frequency changes. For balanced conditions, the filter currents were very small when the system frequency deviates as seen in the simulation results. Additionally, the source currents were almost balanced under balanced and unbalanced power system conditions. The THDs were very low for all cases. The shunt APF shows suitable performance under frequency variations where the source current has the same frequency as the grid voltage frequency.

2.4 Proposed PCC Voltage Sensorless Control Method

The proposed voltage sensorless control method generates the reference current signals without sensing the grid voltages. The proposed positive and negative sequence filter generates the reference signals. The load currents are measured. The measured currents are then filtered to obtain the negative sequence components which are the reference signals as the following:

$$\begin{bmatrix} i_{ref,a} \\ i_{ref,b} \\ i_{ref,c} \end{bmatrix} = \begin{bmatrix} i_a{}^{(2)} \\ i_b{}^{(2)} \\ i_c{}^{(2)} \end{bmatrix}$$

The reference signals are then compared with the filter currents. The compared signals are controlled by a PWM controller to generate the switching signals. The error signal could be scaled to estimate the proper voltage. This method does not require any transformation of the measured signals, and it has fewer calculations and steps. The sensorless control system can be seen in Figure 2.28.

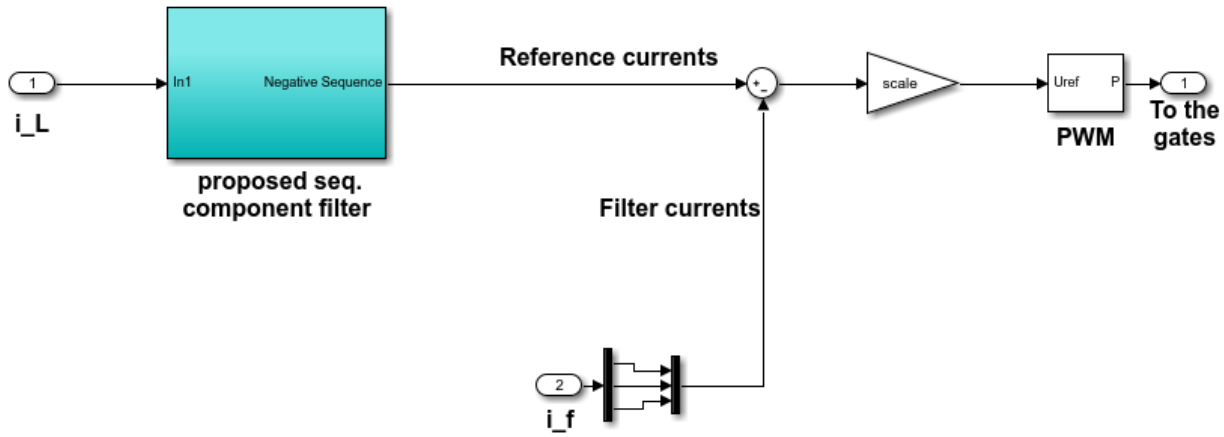

Figure 2.28: Block diagram of the proposed voltage sensorless control method.

2.4.1 Simulation study of the proposed voltage sensorless control method

The system parameters of the simulated system are presented in Table 2.1. The results are shown in the tables and figures below. The results were analyzed based on three aspects: the THD, the ability to balance the magnitudes of the source current, and the power factor. Different source and load conditions were tested in steady state and transient. The simulation was performed on a 2-second time frame that is divided into five time segments based on the load conditions which are NL, NL and BLL, NL and ULL, BLL, and ULL.

Balanced grid voltages:

The shunt APF with the proposed voltage sensorless control method was evaluated under balanced source voltages. Table 2.11 presents the THD of the source currents with and without the shunt APF. The THD of the three phase source currents could be either equal or unequal based on the system conditions. The THDs of source current with the shunt APF are small and do not exceed 3%. Table 2.12 shows the magnitudes of the source currents with and without the shunt APF. The magnitudes of the source currents with the shunt APF are almost similar which indicates balanced

three phase quantities. Figures 2.29 and 2.30 show that the source currents are pure sinusoidal waves.

Table 2.11: THD of I_s without and with the shunt APF.

	THD of I_s w/o the shunt APF	THD of I_s w/ the shunt APF
NL	21.8%, 21.8%, 21.8%	3, 2.83,2.7
NL+BLL	10.81%, 10.81%, 10.81%	1.35,1.29,1.25
NL+ULL	8.39%, 11%, 11.52%	1.24,1.26,1.35
BLL	0.65%, 0.65%, 0.65%	2.42,2.46,2.45
ULL	0.5%, 0.64%, 0.74%	2.28,2.44,2.33

Table 2.12: The magnitudes of I_s without and with the shunt APF.

	$\|I_{sa}\|,\|I_{sb}\|,\|I_{sc}\|$ (A) w/o the shunt APF	$\|I_{sa}\|,\|I_{sb}\|,\|I_{sc}\|$ (A) w/ the shunt APF
NL	4.3, 4.3, 4.3	4.38, 4.383, 4.384
NL+BLL	7.25, 7.25, 7.25	7.31, 7.31, 7.317
NL+ULL	8.33,7.43,6.78	7.546, 7.559, 7.549
BLL	3.38, 3.38, 3.38	3.464, 3.47, 3.463
ULL	4.613,3.71,2.88	3.735, 3.758, 3.739

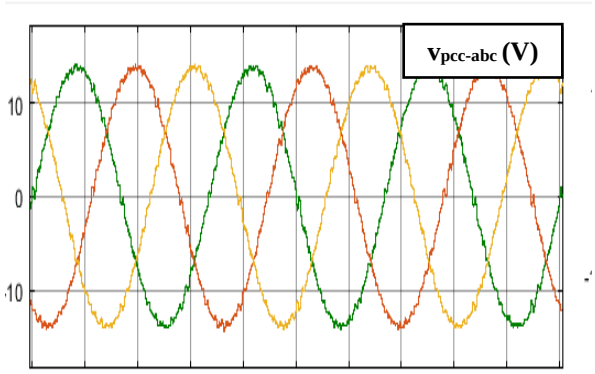

(a) PCC voltages.

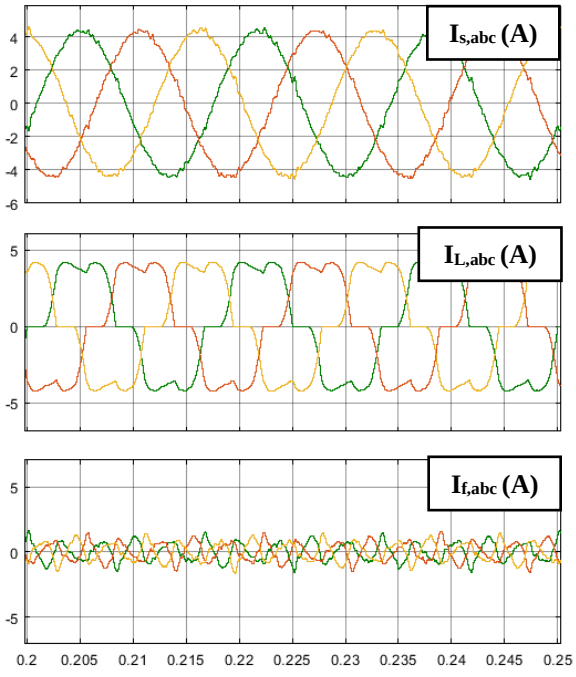

(b) I_s, I_L and I_f with NL.

Figure 2.29: With nonlinear load, I_s, I_L and I_f with the shunt APF when the source voltages are balanced.

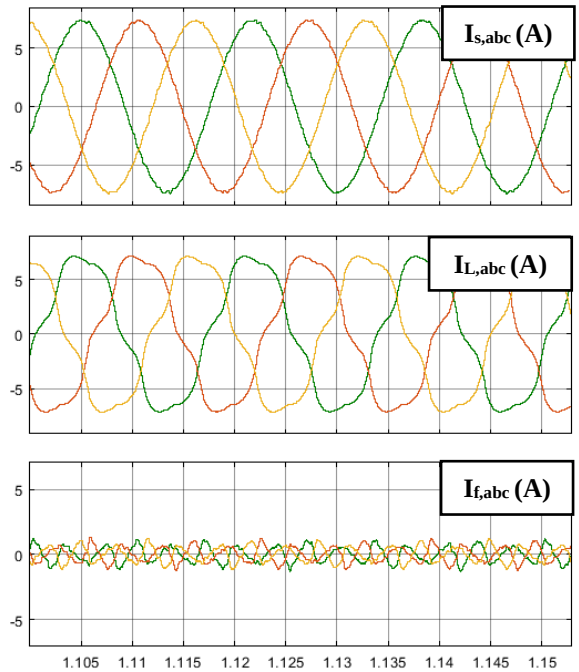

(a) I_s, I_L and I_f with NL & BLL.

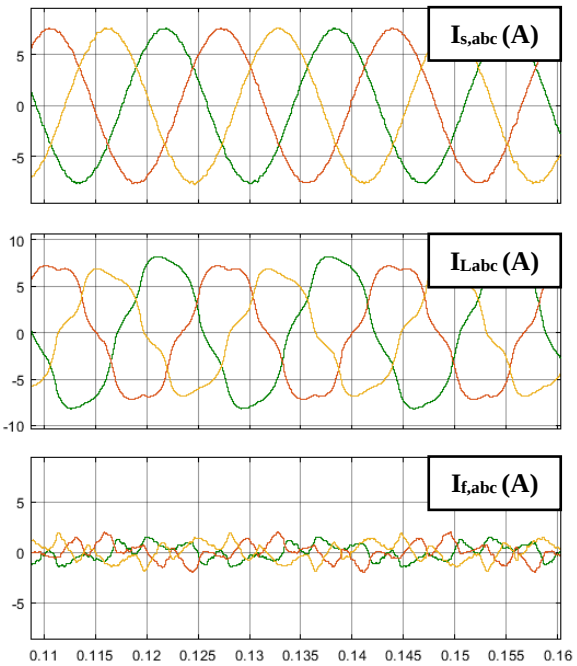

(b) I_s, I_L and I_f with NL & ULL.

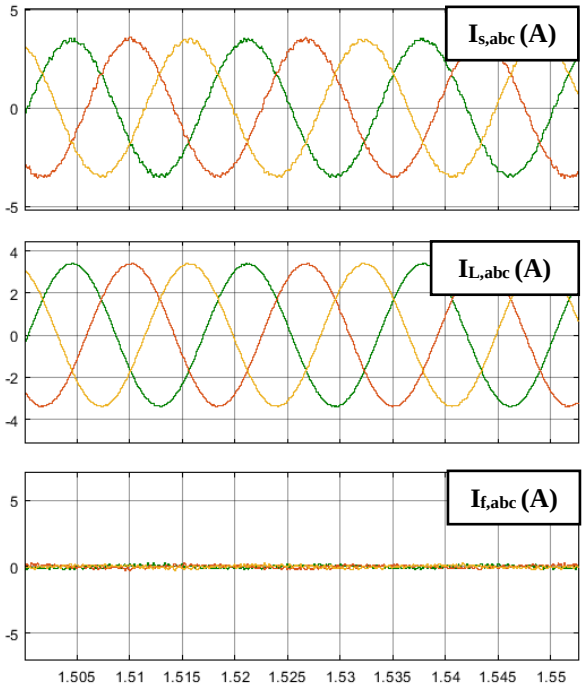

(c) I_s, I_L and I_f with BLL.

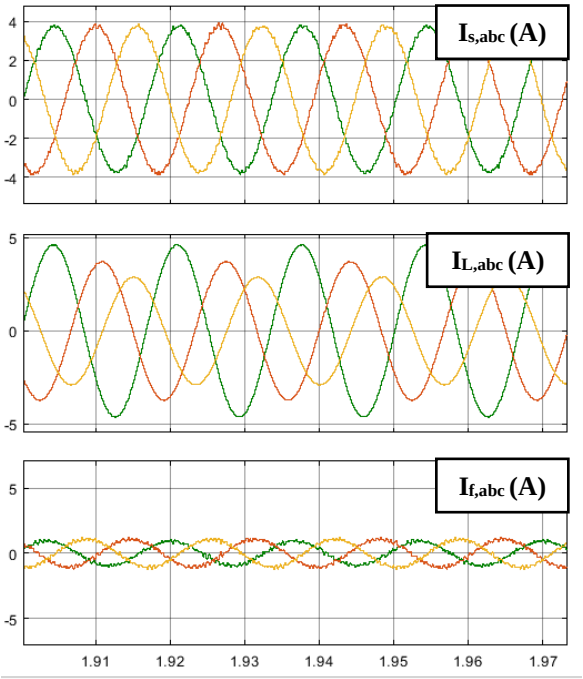

(d) I_s, I_L and I_f with ULL.

Figure 2.30: I_s, I_L and I_f with the shunt APF when the source voltages are balanced.

Unbalanced magnitudes of the source (magnitude of phase A is 80% of the magnitudes of phases B and C):

The source voltages are unbalanced where the magnitudes of phases B and C are 80% of the phase A magnitude. Table 2.13 shows the THD of the source currents with and without the shunt APF. The THDs with the shunt APF were low indicating the source currents were sinusoidal. Table 2.14 shows the magnitudes of the source currents. The source currents are considered balanced three phase quantities since the magnitudes are almost similar. Figures 2.31 and 2.32 show that the source currents are balanced sinusoidal waveforms.

Table 2.13: THD of I_s without and with the shunt APF.

	THD of I_s w/o the shunt APF	THD of I_s w/ the shunt APF
NL	25.14% ,21.6% , 19.3%	3.13%, 2.9%, 2.98%
NL+BLL	12.6%, 10.45%, 9.72%	1.48%, 1.4%, 1.45%
NL+ULL	9.9%, 10.83%, 10.34%	1.31%, 1.4%, 1.45%
BLL	0.77%, 0.67%, 0.7%	2.79%, 2.72%, 2.85%
ULL	0.58%, 0.68%, 0.82%	2.49%, 2.69%, 2.69%

Table 2.14: The magnitudes of I_s without and with the shunt APF.

	$\|I_{sa}\|,\|I_{sb}\|,\|I_{sc}\|$ (A) w/o the shunt APF	$\|I_{sa}\|,\|I_{sb}\|,\|I_{sc}\|$ (A) w/ the shunt APF
NL	3.67, 4.08, 4.26	4.066, 4.066, 4.078
NL+BLL	6.21, 6.96, 7.11	6.811, 6.809, 6.823
NL+ULL	7.16, 7.03, 6.59	6.983, 6.995, 6.997
BLL	2.93, 3.27, 3.28	3.233, 3.233, 3.24
ULL	4.01, 3.46, 2.73	3.426, 3.445, 3.441

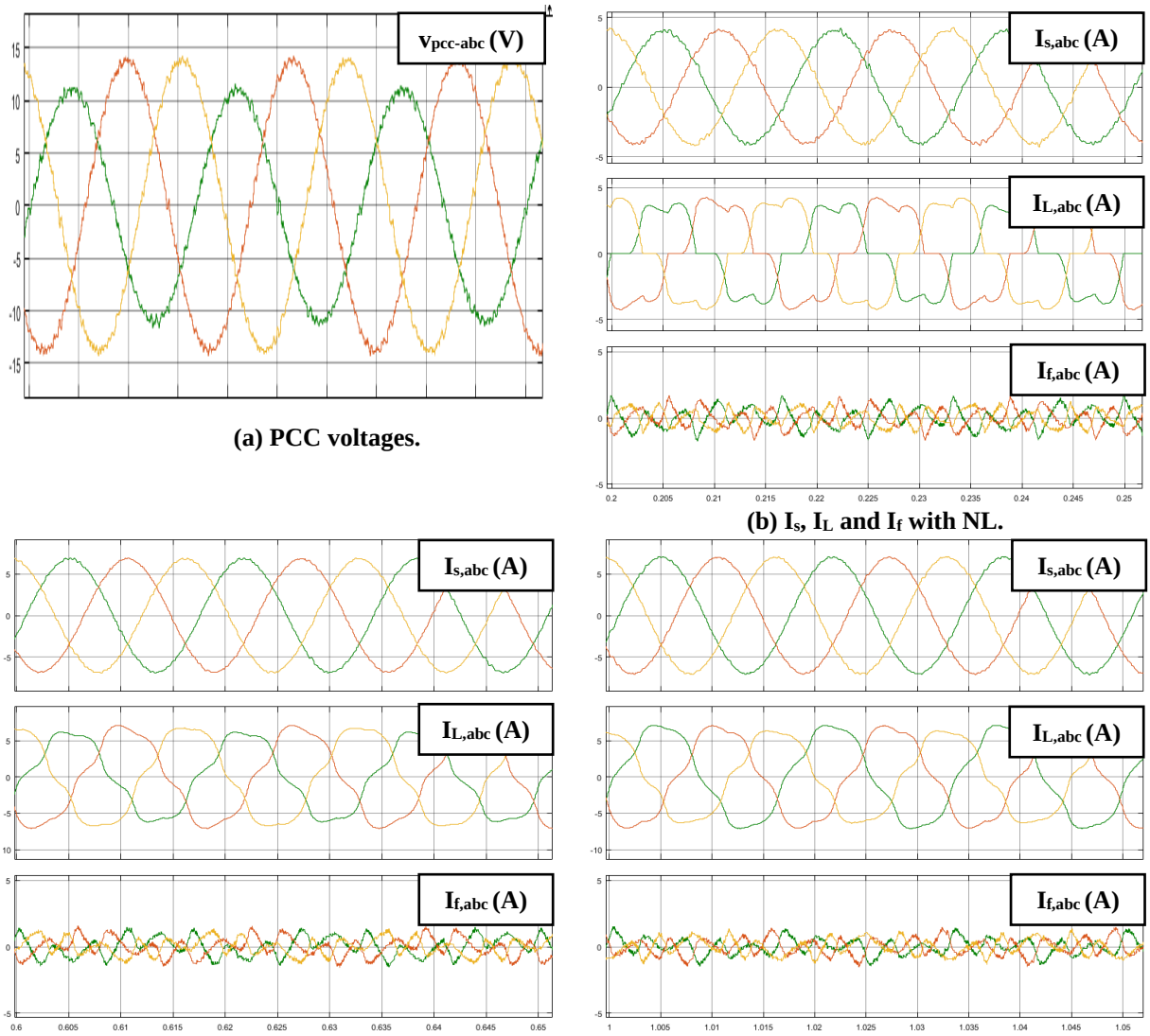

(a) PCC voltages.

(b) I_s, I_L and I_f with NL.

(c) I_s, I_L and I_f with NL & BLL.

(d) I_s, I_L and I_f with NL & ULL.

Figure 2.31: With nonlinear load: I_s, I_L and I_f with the shunt APF when the source voltages are unbalanced.

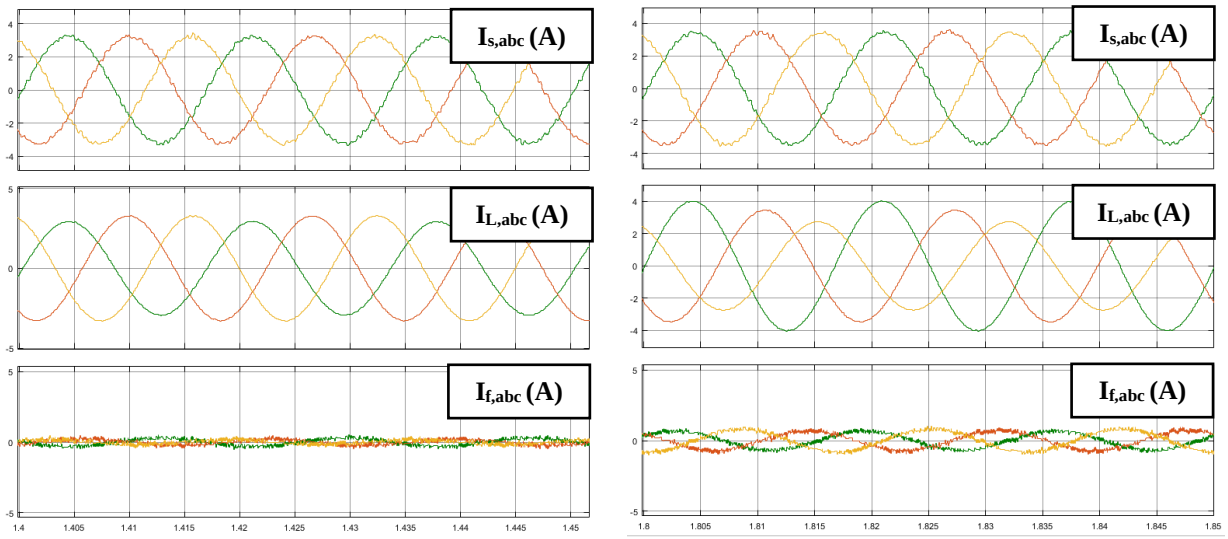

(a) I_s, I_L and I_f with BLL. **(b) I_s, I_L and I_f with ULL.**

Figure 2.32: I_s, I_L and I_f with the shunt APF when the source voltages are unbalanced.

Distorted source:

In this case, the source voltage is distorted where the THD is about 16%. Table 2.15 shows the THD of the source currents with and without the shunt APF. The THD of the source currents with the shunt APF are less than 5%. Table 2.16 shows that the magnitudes of the source currents with the shunt APF are balanced. The source currents are balanced and sinusoidal quantities as shown in Figures 2.33 and 2.34.

Table 2.15: THD of I_s without and with the shunt APF.

	THD of I_s w/o the shunt APF	THD of I_s w/ the shunt APF
NL	18.6%, 18.6%, 18.6%	3.23%, 3.23%, 3.23%
NL+BLL	16.4%, 16.4%, 16.4%	1.63%, 1.63%, 1.63%
NL+ULL	14.39%, 17.37%, 16.5%	1.76%, 1.78%, 1.56%
BLL	14.4%, 14.4%, 14.4%	2.46%, 2.46%, 2.46%
ULL	12.88%, 15.19%, 13.38%	2.54%, 2.71%, 2.46%

Table 2.16: The magnitudes of I_s without and with the shunt APF.

	$\|I_{sa}\|,\|I_{sb}\|,\|I_{sc}\|$ (A) w/o the shunt APF	$\|I_{sa}\|,\|I_{sb}\|,\|I_{sc}\|$ (A) w/ the shunt APF
NL	4.11, 4.11, 4.11	4.18, 4.18, 4.18
NL+BLL	7, 7, 7	7.07, 7.07, 7.07
NL+ULL	8.04,7.23,6.53	7.3, 7.33, 7.3
BLL	3.38, 3.38, 3.38	3.48, 3.48, 3.48
ULL	4.61, 3.71, 2.88	3.75, 3.76, 3.75

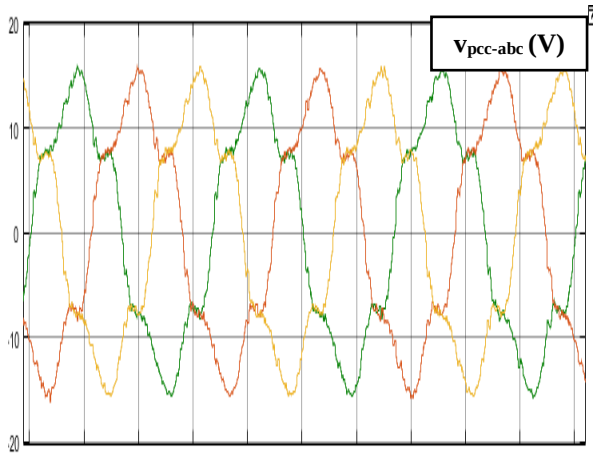

(a) The PCC grid voltages.

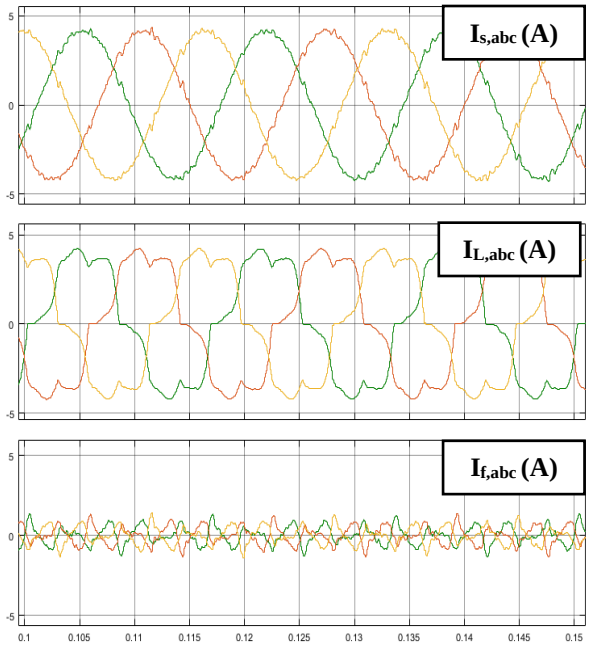

(b) I_s, I_L and I_f with NL.

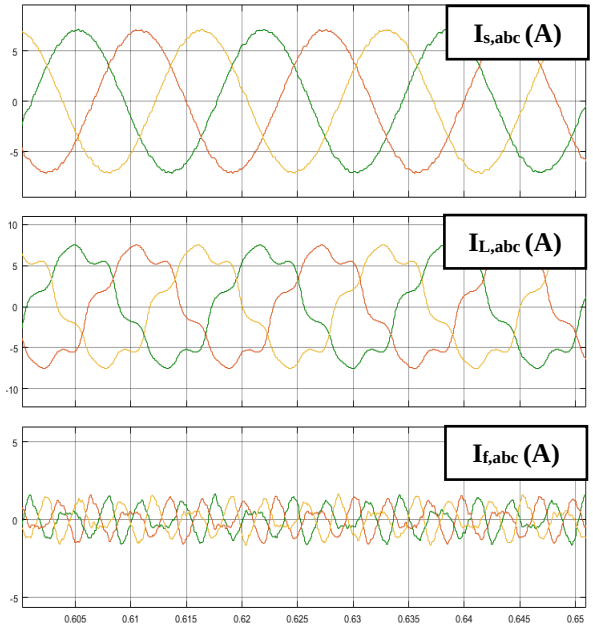

(c) I_s, I_L and I_f with NL & BLL.

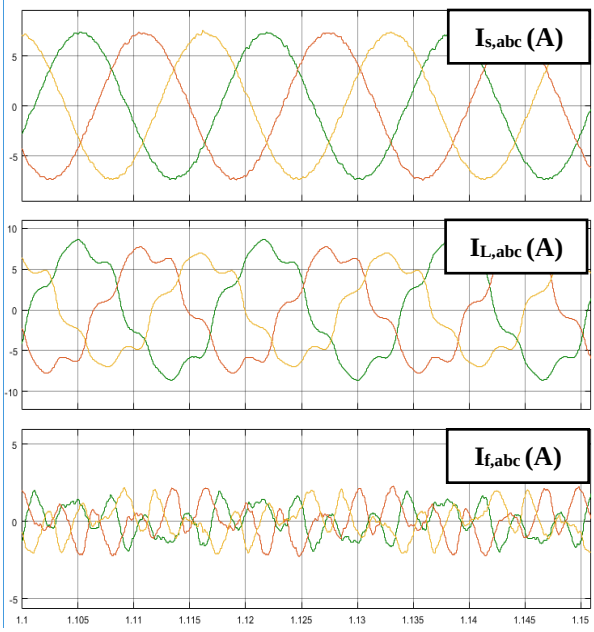

(d) I_s, I_L and I_f with NL & ULL.

Figure 2.33: With nonlinear load: I_s, I_L and I_f with the shunt APF when the source voltages are distorted.

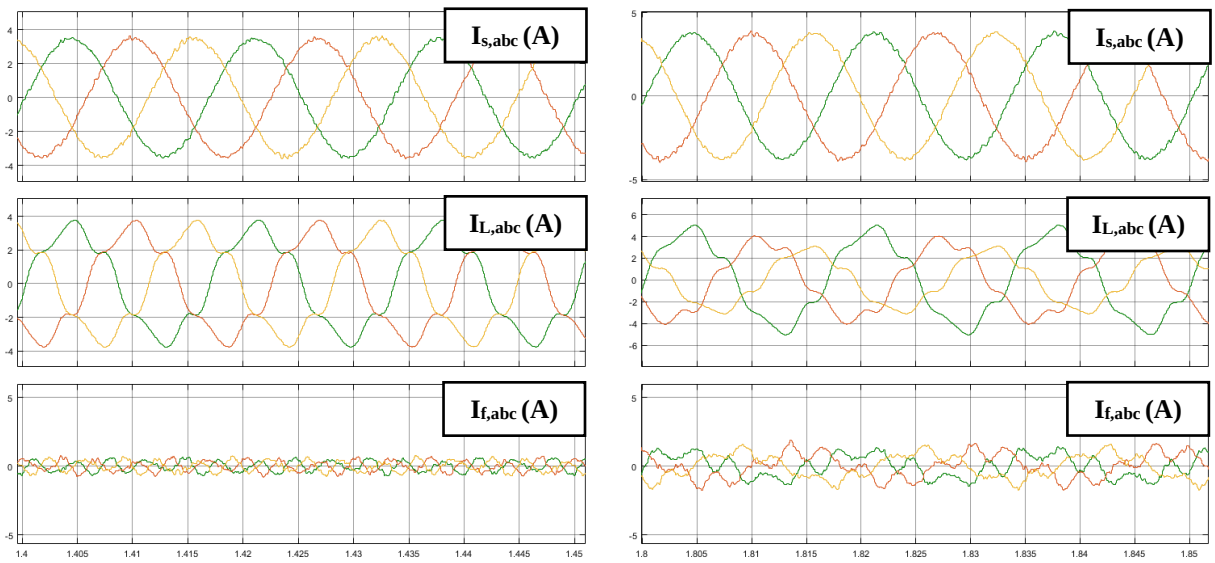

(a) I_s, I_L and I_f with BLL. **(b) I_s, I_L and I_f with ULL.**

Figure 2.34: I_s, I_L and I_f with the shunt APF when the source voltages are distorted.

The simulation results demonstrate that the shunt APF with the proposed sensorless control system was able to eliminate the undesirable components from the source current. For all conditions, the THD of the source current was acceptable with a THD less than 5%. The source currents were balanced with very small difference between the source current magnitudes under unbalanced conditions. Since the source currents had the same waveform shape as the grid voltages and in phase with the grid voltages, almost unity power factor has been achieved for all conditions except when the source voltage is distorted. Therefore, the proposed sensorless control system performs effectively under different conditions of the grid voltages and loads.

CHAPTER 3: SYSTEM MODELING AND DESCRIPTIO

The power circuit of the shunt APF is composed of a three-phase voltage-source inverter (VSI), DC power supply and the control unit as shown in Figure 3.1. A passive filter couples the shunt APF to the grid network. A three-phase power supply with Z_g represents the grid voltages and impedances. The loads are connected to the power supply through a line impedance. The loads may be nonlinear, balanced linear, or unbalanced linear. Three parameters are measured: the pcc voltages, the load currents and the filter currents. The shunt APF is designed to maintain balanced three-phase source currents under ideal and non-ideal power system conditions.

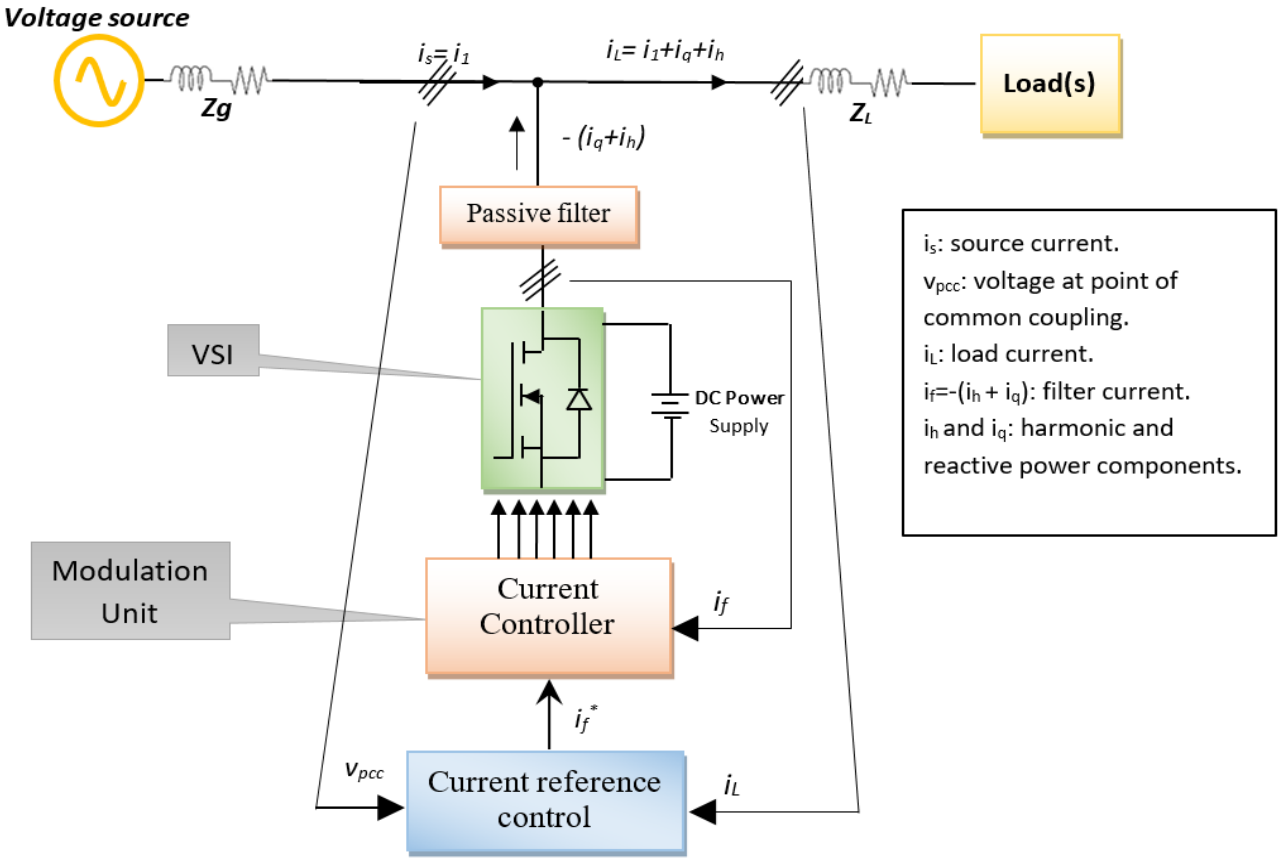

Figure 3.1: A line diagram of the shunt APF connected to the power system.

3.1 Design of the System

The design of the system is important in order to achieve suitable operation of the shunt APF. In this chapter, design of the three parts of the system is demonstrated and was validated through simulation and experimental tests.

3.1.1 Design of the shunt APF circuit

The shunt APF consists of a VSI, a DC power source and a passive filter. The VSI is connected in parallel with the three-phase supply via a passive filter. The DC power supply provides a fixed DC voltage to compensate for the inverter's losses [11].

3.1.1.1 Design of the DC-link voltage

The selection of the DC bus voltage is very important in order to accurately inject harmonic current into the grid [4] [5] [11] [35]. The value of the DC bus voltage should be greater than the peak value of the grid voltage ($V_{pcc-max}$). If it is smaller than the grid voltage, the system will experience voltage variations. By assuming the linear modulation mode of PWM (0<m<1), the DC bus voltage can be expressed as:

$$V_{dc} \geq 2\sqrt{2}V_{pcc-max} \qquad (3.1)$$

3.1.1.2 Design of the coupling filter

This filter couples the grid and the VSI. An L filter is usually used as smoothing coupler between the grid and the shunt APF. A large inductor is needed in order to reduce the harmonics around the switching frequency of the VSI. But, large inductors are very expensive and big in size. For that reason, LCL filters are used because of better performance at high power levels [48] [49]. The LCL filter can achieve higher harmonic attenuation which allows the use of a lower switching frequency as well as reducing the switching frequency harmonics. In addition, it minimizes the

amount of the distortion in the injected current to the grid to improve the power quality of the system. An LCL filter is often utilized because it uses small values of inductance and capacitance. Figure 3.2 shows a single phase representation of the LCL filter with VSI modeled as an AC voltage source where L_g is inductance of the grid side, L_i is inductance of the inverter side, C_f is the filter capacitor, V_i is voltage of the inverter, I_i is LCL filter inverter-side current, and I_g is the LCL filter grid-side current.

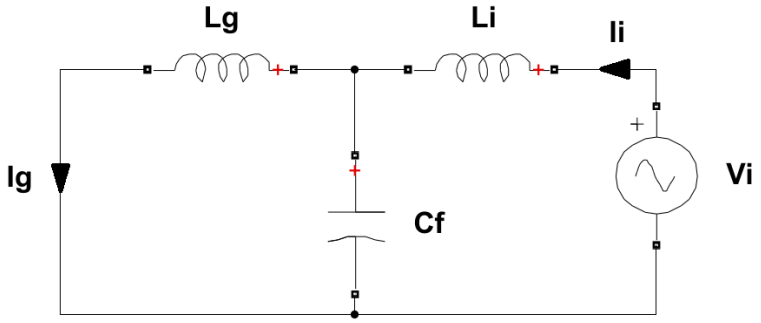

Figure 3.2: A single phase representation of the LCL filter with VSI.

The transfer function of the LCL is of the following form:

$$H_{LCL}(s) = K\frac{1}{s(s^2 + 2\zeta\omega_{res}s + \omega_{res}^2)} \tag{3.2}$$

$$H_{LCL}(s) = \frac{I_g(s)}{V_i(s)} = \frac{1}{L_iL_gC_fs^3 + (L_i+L_g)s} = \frac{1}{L_iL_gC_f}\frac{1}{s\left(s^2 + \frac{L_i+L_g}{L_iL_gC_f}\right)} \tag{3.3}$$

$$\omega_{res} = \sqrt{\frac{L_i+L_g}{L_iL_gC_f}} \tag{3.4}$$

where ω_{res} is the resonant frequency and ζ is the damping ratio. In order to find the magnitude equation and phase angle equation, let $s = jh\omega$ (h is the number of harmonic). The transfer function can be expressed as:

$$H_{LCL}(jh\omega) = \frac{I_g(jh\omega)}{V_i(jh\omega)} = \frac{-j}{-h^3\omega^3 L_i L_g C_f + h\omega(L_i + L_g)} = \frac{-j}{h\omega[-h^2\omega^2 L_i L_g C_f + (L_i + L_g)]}$$

$$|H_{LCL}(jh\omega)| = \frac{1}{-h^3\omega^3 L_i L_g C_f + h\omega(L_i + L_g)} \qquad (3.5)$$

$$\angle H_{LCL}(jh\omega) = -\pi - \angle\left(j\omega h + \frac{L_i L_g C_f}{L_i + L_g}(j\omega h)^3\right) \qquad (3.6)$$

Several LCL filter designs have been reported in the literature [48 – 53]. The proposed design combines the virtues of these previous designs and tries to avoid their negatives. The following definitions and parameters were used in the design:

E is the grid line-to-line voltage magnitude; Z_b, C_b, and L_b are the base impedance, capacitance and inductance; P_n is the rated load power; r is the relationship index between L_i and L_g; fc is the grid frequency; f_{res} is the resonant frequency of the LCL filter; and f_{sw} is the switching frequency of the inverter.

The proposed LCL filter is designed based on several conditions and constraints that are:

1. ΔI (ripple) is limited by up to 10%.

2. 5% voltage drop on L_i.

3. per unit of (L_i+ L_g) is less than 10% of L_b to limit voltage drop.

4. acceptable x (maximum power factor variation) is 5%.

5. L_g must satisfy the desirable attenuation rate (k_a); typical k_a is 20%.

6. $10f_c \leq f_{res} \leq f_{sw}/2$.

7. Reasonable value of R_d (damping resistance).

The above quantities can be calculated as shown below which are taken from [48-53].

$$Z_b = \frac{E^2}{\mathrm{P_n}} \tag{3.7}$$

$$C_b = \frac{1}{\omega_c * Z_b} \tag{3.8}$$

$$L_b = \frac{Z_b}{\omega_c} \tag{3.9}$$

$$r = \left|\frac{I_g(jh\omega)}{I_i(jh\omega)}\right|$$

$$\mathrm{k_a} = \frac{1}{\left|1 + r\left(1 - \mathrm{L_i}{\omega_{\mathrm{res}}}^2\,\mathrm{C_b}x\right)\right|}$$

$$\Delta \mathrm{I_{max}} = 0.1\frac{\mathrm{P_n}\sqrt{2}}{\sqrt{3}E} \tag{3.10}$$

$$\mathrm{L_i} \le \frac{0.025\,E}{\mathrm{f_{sw}}\,\Delta \mathrm{I_{max}}}$$

$$\mathrm{L_i} = \frac{\mathrm{V_{dc}}}{6\,\mathrm{f_{sw}}\,\Delta \mathrm{I_{max}}} \tag{3.11}$$

$$\mathrm{C_f} \le 0.05\mathrm{C_b} \tag{3.12}$$

$$\frac{1}{10}\mathrm{X_{Lg}} \le \mathrm{X_{Cf}} \le \frac{1}{5}\mathrm{X_{Lg}}$$

$$\mathrm{L_g} = \frac{\sqrt{\frac{1}{{\mathrm{k_a}}^2} + 1}}{{\omega_{\mathrm{res}}}^2\,\mathrm{C_f}} \tag{3.13}$$

$$\mathrm{R_d} = \frac{1}{3\omega_{\mathrm{res}}\mathrm{C_f}} \tag{3.14}$$

Based on the above equations, the element values for the LCL filter were calculated and rounded to the following values:

$$L_i = 4\,mH \;;\; L_g = 300\,uH;\; C_f = 10\,uF$$

This design was simulated and experimentally tested in order to investigate its performance. The experimental results were obtained using an AP Instruments Inc. model 300. Both simulation and experimental results show that they have the same attenuation rate and the same phase response as shown in Figure 3.3. The resonant frequencies were 3 kHz from simulation and 2.67 kHz from the experiment. The difference between the frequencies is about 300 Hz, but it is not significant because the device used to test the filter has its own components that could affect the frequency.

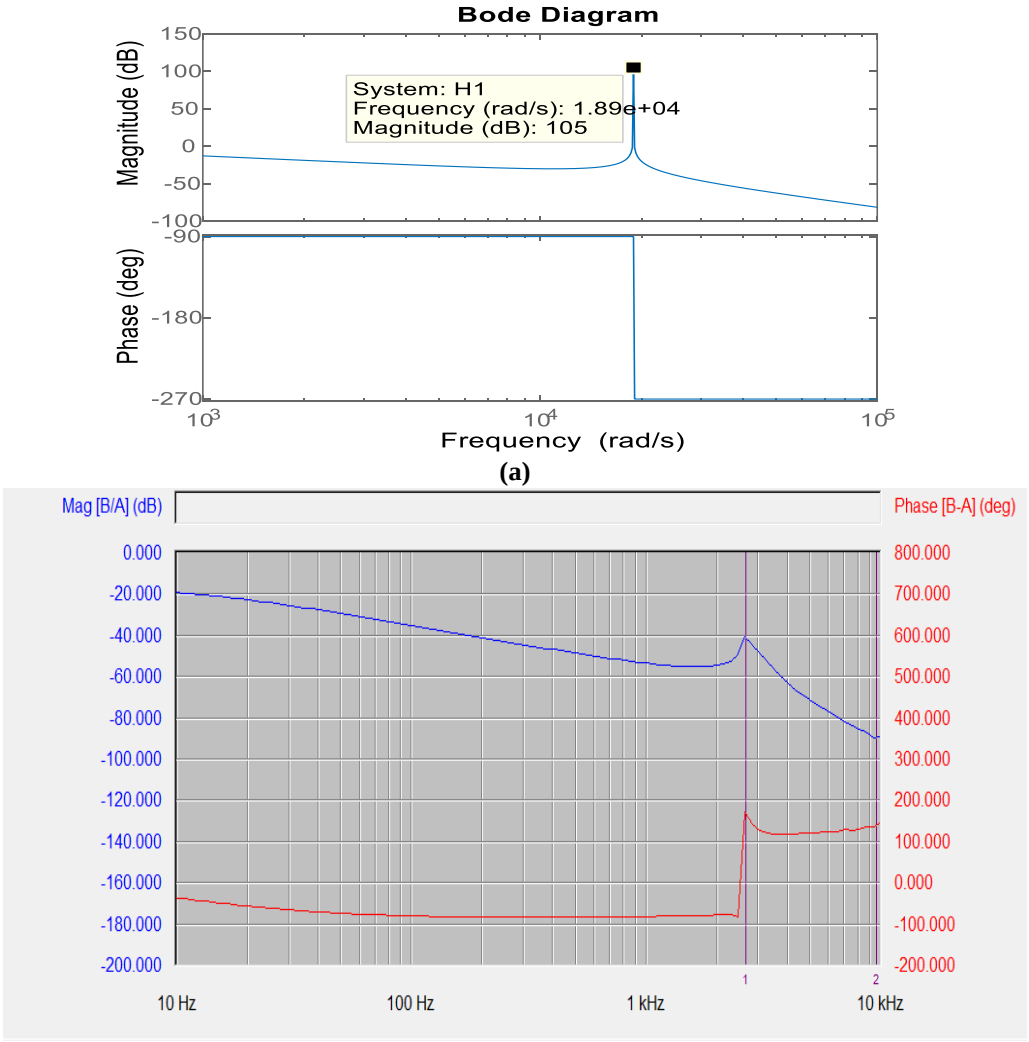

Figure 3.3: (a) Simulation and (b) experimental magnitude and phase responses of the designed LCL filter.

3.1.2 Design of the measurement circuits

Two circuits were designed for measuring the voltages and the currents. Multisim was used for testing the measurement designs and for designing the measurement board. For certain limitations of the hardware devices, the maximum and the minimum tolerable output voltages are ± 10V. The two designs have common parts:

- DC offset filter at the input and the output sides of the op-amp.
- Low-pass filters (LPF) at the output.

➢ Design of the DC offset filter

From the input side, the cut-off frequency is 1.592 Hz; which was calculated as:

$$f_c = \frac{1}{2\pi RC} \qquad (3.15)$$

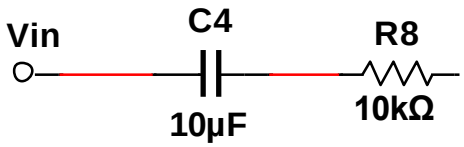

Figure 3.4: DC offset filter of the input side.

Figures 3.5 and 3.6 show the dc offset filter at the output side of the measurement circuits. The cut-off frequency for the voltage circuit was 0.884 Hz. For the current measurement circuit, the cut-off frequency was 0.707 Hz.

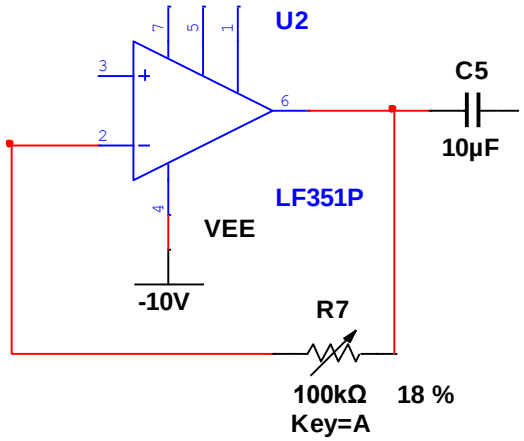

Figure 3.5: DC offset filter at the output side for the voltage measurement circuit.

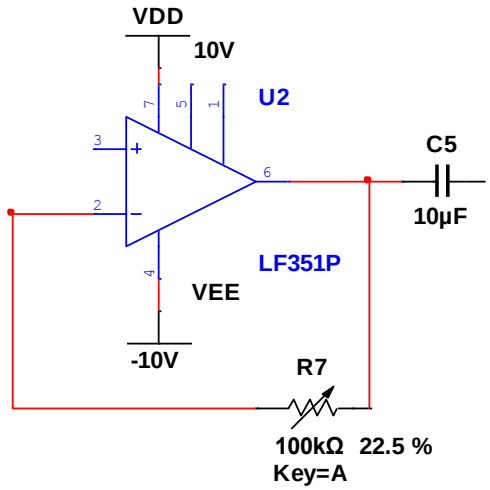

Figure 3.6: DC offset filter at the output side for the current measurement circuit.

- Low pass filter design

The LPF for the measuring circuits is shown in Figure 3.7. The gain and phase shift of the LPF can be calculated as following.

$$H(j\omega) = \frac{V_{o1}}{V_o} = \frac{1}{1 + j\omega RC} \qquad (3.16)$$

The filter gain can be calculated as:

$$|H(j\omega)| = \left|\frac{V_{o1}}{V_o}\right| = \sqrt{\frac{1}{1+(\omega RC)^2}} = 0.8756$$

where R= 1kΩ and C= 1μF. The phase angle of the filter is calculated as:

$$\angle H(j\omega) = -\tan^{-1}\omega RC = -20.656°$$

The cut-off frequency and the time response are calculated as:

$$f_c = \frac{1}{2\pi RC} = 159.155\ Hz$$

$$\tau = RC = 1\ ms$$

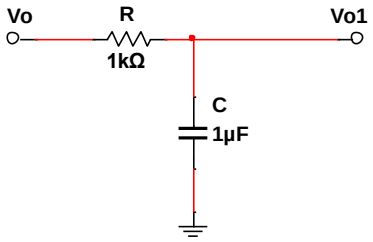

Figure 3.7: Low-pass filter for the measuring circuits.

This filter causes a phase shift between the input and the output. Therefore, a phase compensator is added latter to the control system to overcome this issue as following.

$$H_c(s) = \frac{1+aTs}{1+Ts} \qquad (3.17)$$

where: a= 9.251 and T=ωRC

Voltage measurement circuit design

The op-amp used in this design was an LF351P. The gain can be calculated from Figure 3.8 as following.

$$G_{op-amp} = G_1 = \frac{V_o}{V_{in}} = \frac{-18k}{110k} = -0.16364$$

The non-inverting of the op-amp is grounded through a resistance of value 10 kΩ.

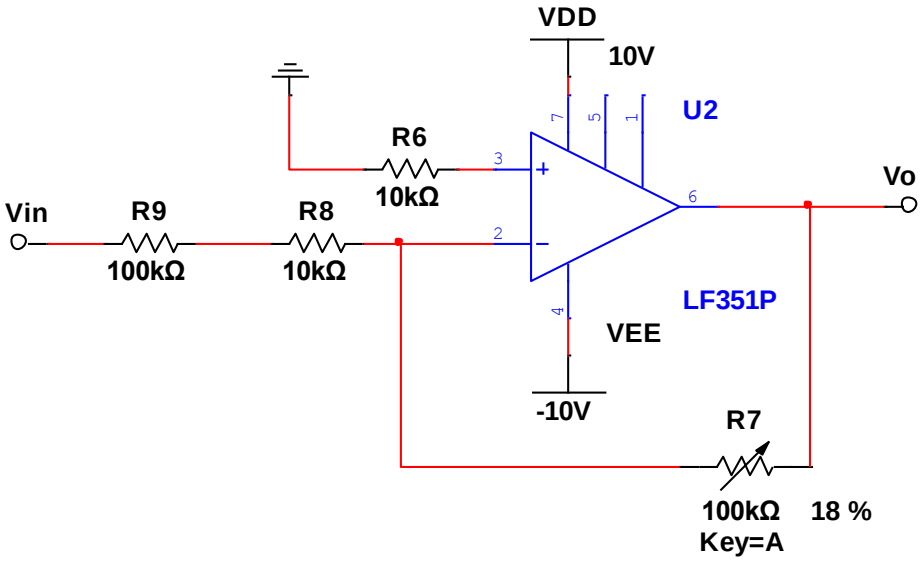

Figure 3.8: Op-amp design of the voltage circuit.

Figure 3.9 shows the complete design of the voltage measuring circuit. The voltage gain of the measuring circuit can be expressed as:

$$|V_o| = |V_{in} \times G_1 \times G_{LPF}| \qquad (3.18)$$

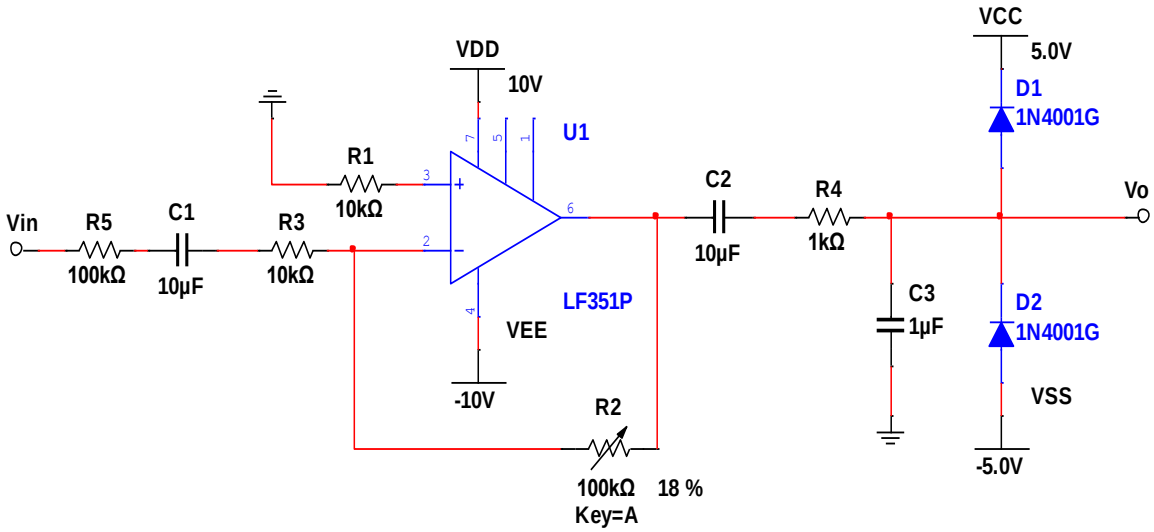

Figure 3.9: Voltage Measurement Circuit.

Current measurement circuit design

The gain of the op-amp can be calculated from Figure 3.10 as following.

$$G_{op-amp} = G_2 = \frac{V_o}{V_{in}} = \frac{-22.5k}{10k} = -2.25$$

The non-inverting of the op-amp is grounded through a resistance of value 10 kΩ.

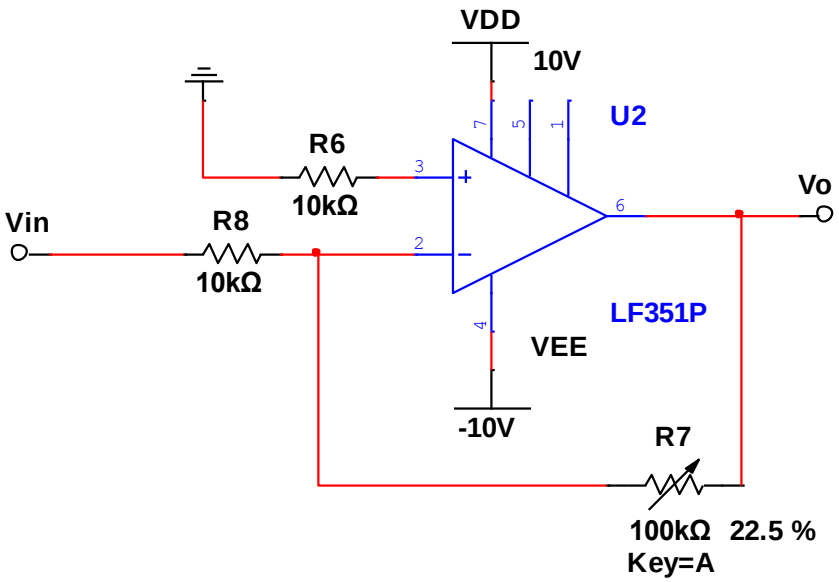

Figure 3.10: Op-amp design of the current circuit.

A current sensor is employed, which can sense up to 9A as maximum current. The output of this sensor is calculated as:

$$V_{out} = I \times 0.282$$

where I is the measured current and 0.282 is the gain of the current sensor. Figure 3.11 shows the complete design of the current measuring circuit. The equation that represent the current measuring circuit can be expressed as:

$$|V_o| = |I_{in} \times 0.282 \times G_2 \times G_{LPF}| \qquad (3.19)$$

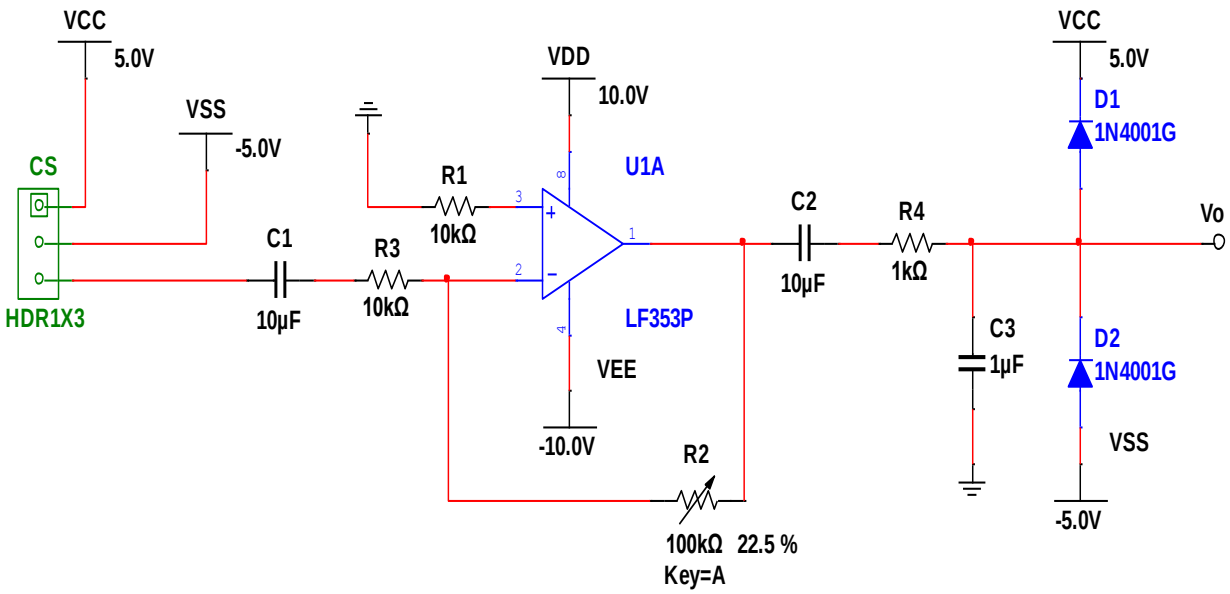

Figure 3.11: Current Measurement Circuit.

Simulation and experimental validation of the measurement designs:

An AC source of 17.78 V_{rms} and a resistive load of 10Ω with a power rating of 225W were used to examine the proposed measurement designs. The simulation and experimental output voltages from the voltage measurement circuit (V_{o-VR}) and the current measurement circuit (V_{o-I}) are nearly equal as shown in Table 3.1. Figures 3.12 and 3.13 show the simulation and experimental results.

Table 3.1: Simulation and experimental results from the measurements.

Parameter	Simulation	Experimental
V_{in} (V_{rms})	17.8	17.8
I (A_{rms})	1.78	1.7
V_{o-VR} (V_{rms})	2.55	2.46
V_{o-I} (V_{rms})	0.988	0.999

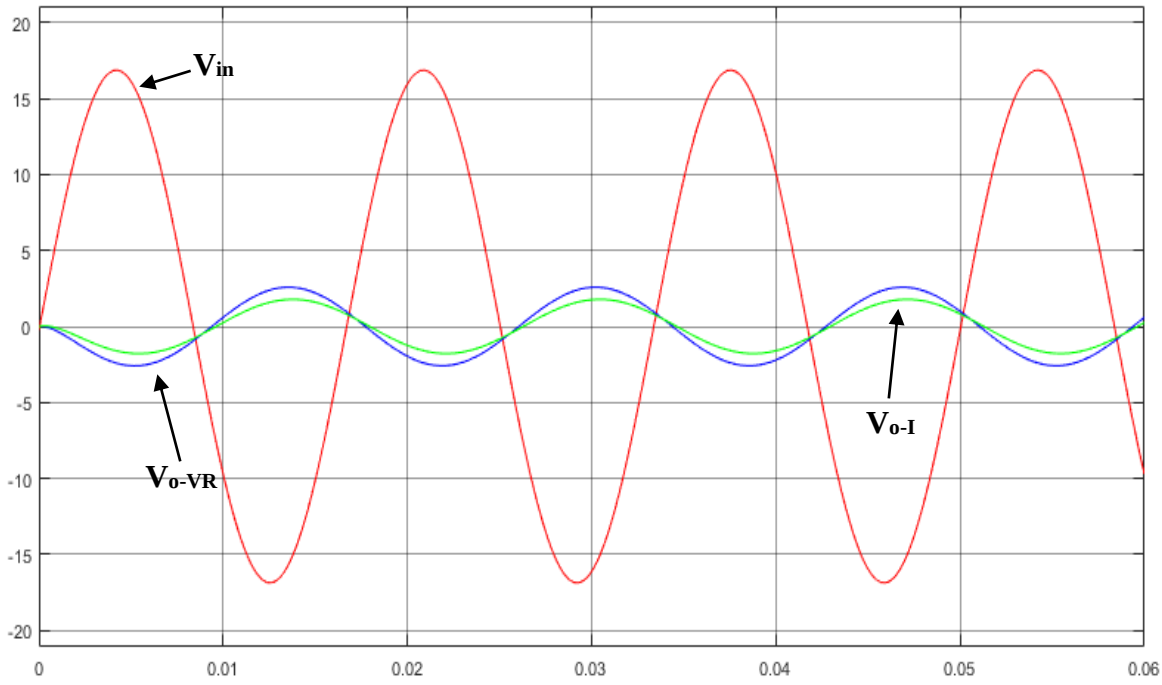

(a)

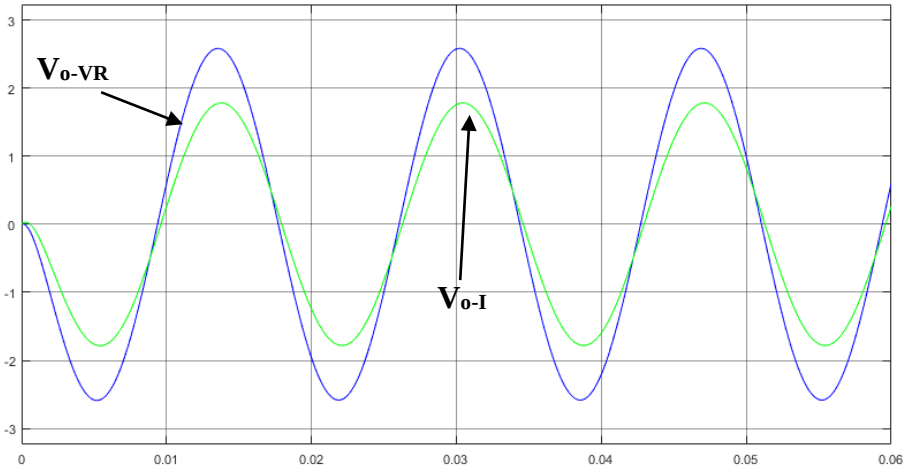

(b)

Figure 3.12: The simulation outputs of the measurement circuit (a) V_{in}, V_{o-VR} and V_{o-I}. (b) V_{o-VR} and V_{o-I}

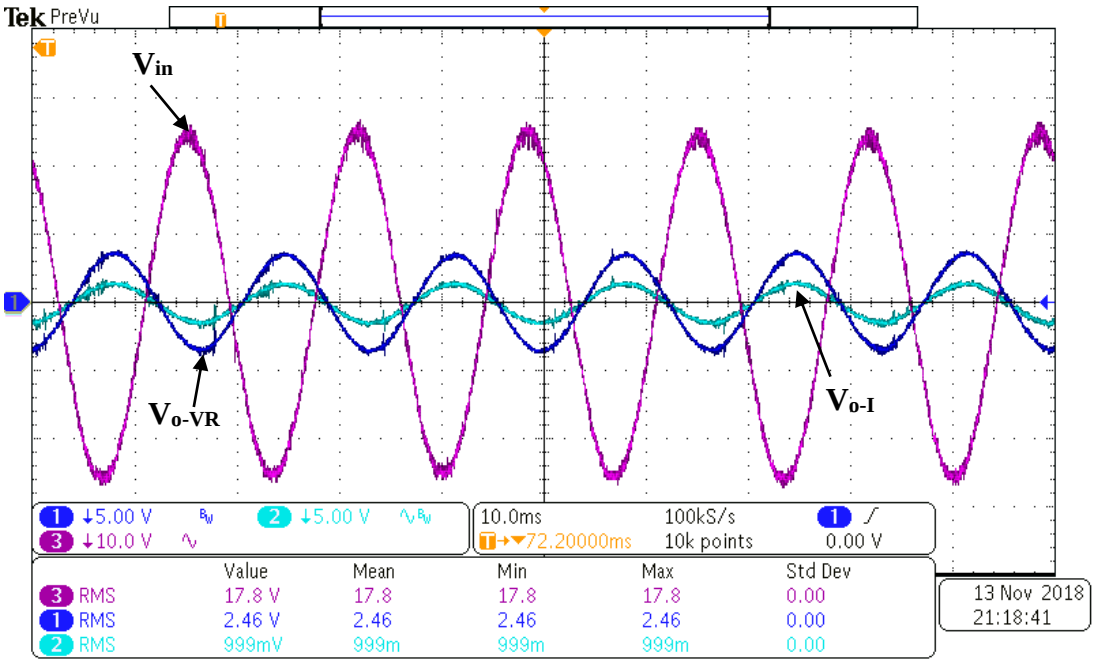

Figure 3.13: The experimental outputs of the measurement circuit for V_{in} (C4), V_{o-VR} (C2) and V_{o-I} (C3).

3.2 Hardware Setup

The experimental setup of the DSP-based APF is presented in Figure 3.14. Six main components were used to perform all the experimental tests. They are as follows: 1)NHR 9410 grid simulator was used as a grid voltage generator, 2) HiRel power electronics drive board as the inverter board, 3) DSP based dSpace DS1104 R&D controller card and CP 1104 I/O, 4) DC power sources, 5) Matlab Simulink and dSpace control-desk, and 6) measurement boards for measuring the voltages and currents.

The three-phase source acts as the grid voltages. The network includes adjustable grid impedances and fixed line impedances. Different loads are used including a nonlinear resistive load, balanced linear loads, and unbalanced linear loads. A three-phase MOSFET inverter is used as the converter. A DC power source is used as a DC-bus voltage to feed the inverter. The inverter output is connected to the grid via coupling component(s) represented by an L filter and an LCL filter. Measurement boards were designed to measure the PCC voltages, the source currents, the

load currents and the inverter output (filter) currents. The DSP controller board controls the shunt APF and generates the switching signals. The DSP board contains a built-in signal conditioning system. Two power supplies are used to power the measurement boards.

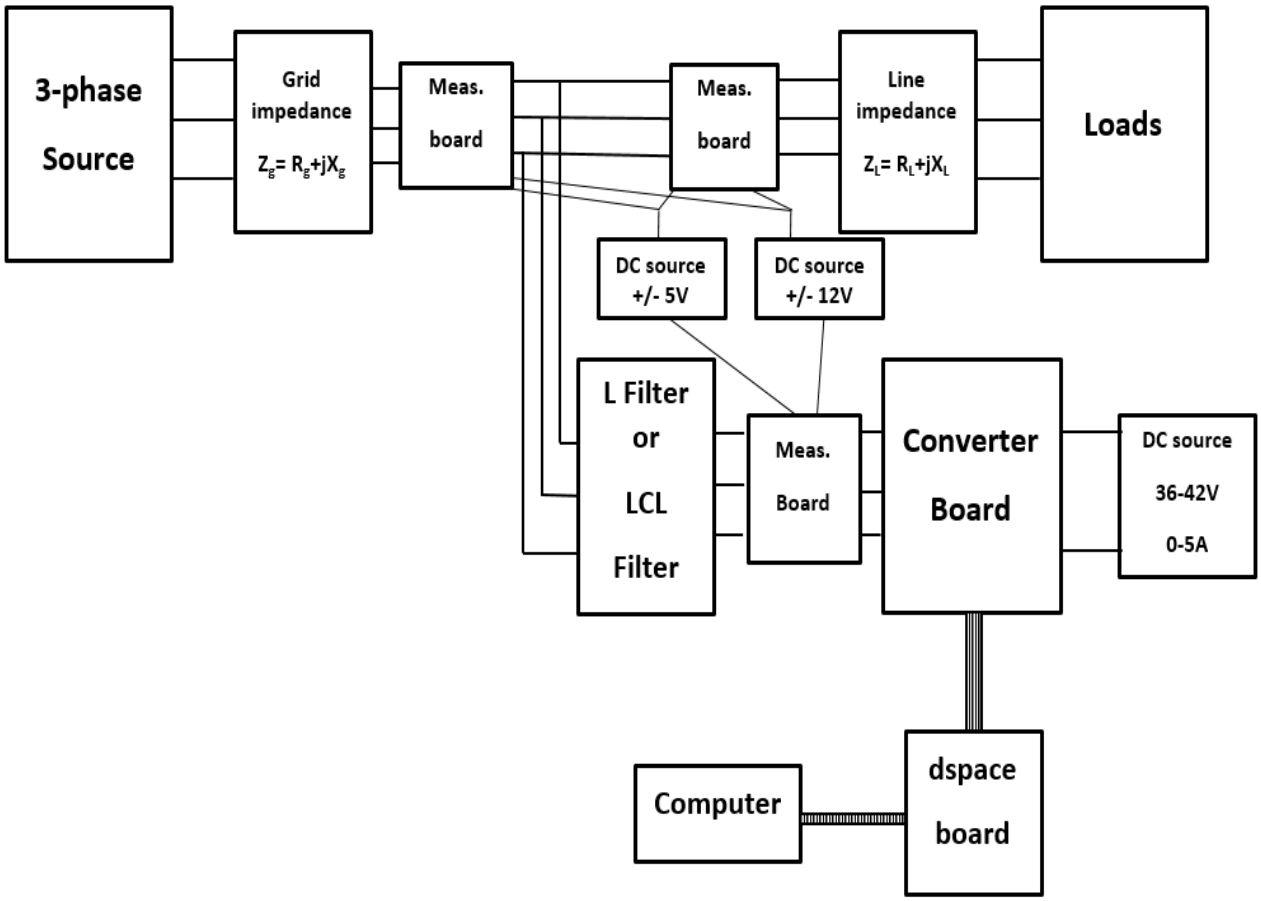

Figure 3.14: Block diagram of the experimental setup.

3.2.1 Power supplies

A three-phase AC source and four DC power supplies were utilized in the experiments. The AC source is NHR 9410 grid simulator manufactured by NH Research Inc. and is shown in Figure 3.15(a). It is a bi-directional AC/DC source and can be operated as single phase or three phase. The parameters of each phase can be adjusted. The frequency is also adjustable. The NHR 9410 is used to test the PV inverters and other grid-connected equipment.

A HP 6030A sytem power DC supply was used as the input for the inverter and is shown in Figure 3.15(b). The maximum voltage and current ratings are 500 VDC and 5 A. A DC power supply of ±12 V was used to power the converter board. The measurement boards were suplied with ± 12 V and ±5 V.

(a)

(b)

Figure 3.15: (a) NHR 9410. (b) HP 6030A sytem power supply.

3.2.2 The inverter board

The board combines two independent three-phase PWM inverters fed from a constant DC voltage source. The board is shown in Figure 3.16. These inverters are three-phase three-leg MOSFET

inverters, and the DC-bus voltage of the inverters must be set between 36 V and 42 V. The board components are powered via a ±12 V DC adapter. It also provides phase A and phase B currents measurements and DC-bus voltage measurement. It interfaces with a DSP-based DS1104 controller, which generates the PWM signals for the inverter.

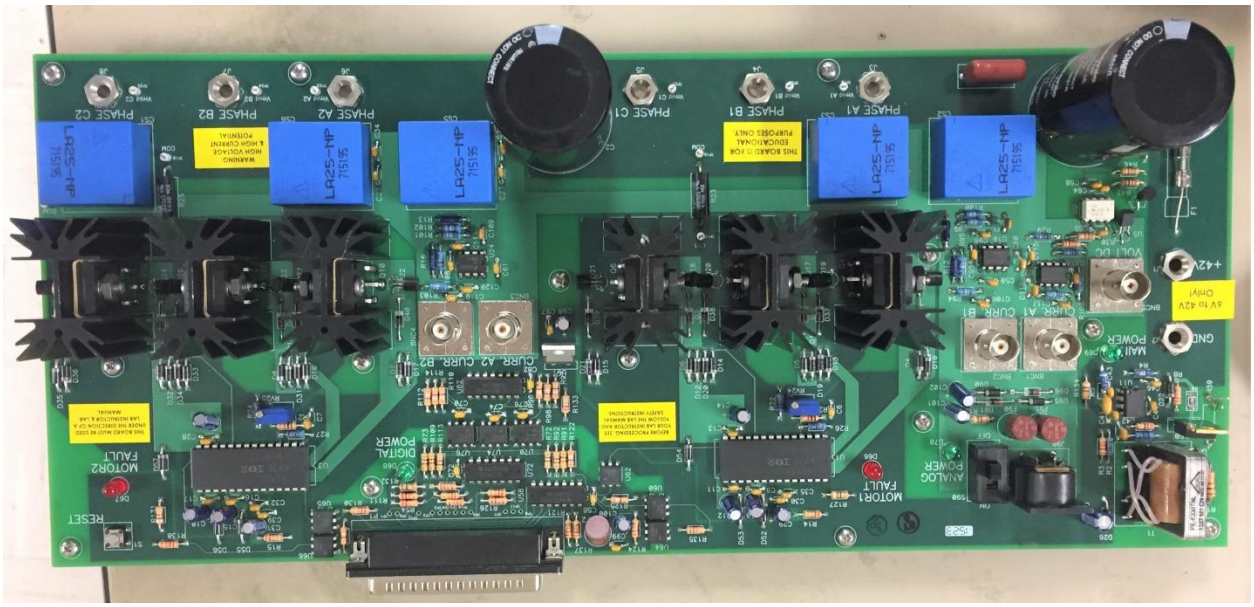

Figure 3.16: The inverter board.

3.2.3 DS1104 R&D controller board and CP 1104 I/O board

The dSpace DS1104 R&D controller board, shown in Figure 3.17, provides inputs/outputs and a real-time processor. It is used to create a control system using the Real-Time Interface (RTI) installed in Simulink. RTI has Simulink blocks for graphical I/O configuration. A Simulink model can be easily transitioned for an application using RTI and a DS1104 R&D controller board.

The implementation of a real-time control loop using dSpace and MATLAB/Simulink required the dSpace DS1104 R&D controller board, connector panel CP1104 and a cable connected between the CP1104 and the inverter board. BNC cables were used to connect the measurements to analog-to-digital-converter (ADC) of the controller board. The voltage and current measurements should be within the voltage range of the ADCs, which are ± 10V. They are

then used via the dSpace block installed in Simulink. The output of the model was transmitted though a cable connecting the inverter board with the controller board.

Figure 3.17: DS1104 R&D controller board.

3.2.4 Measurement boards

The system has two measurement boards. Each measurement board has six input connectors and six output connectors. Three inputs and outputs are for measuring the voltages, and the other three inputs and outputs are for the currents. The current measurements and the voltage measurements are independent even though they share the same board. The current sensor utilized is a CSLH3A9 manufactured by Honeywell. The board is powered by ±12 V and ±5 V DC voltage sources. A photo of the measurement board is shown in Figure 3.18.

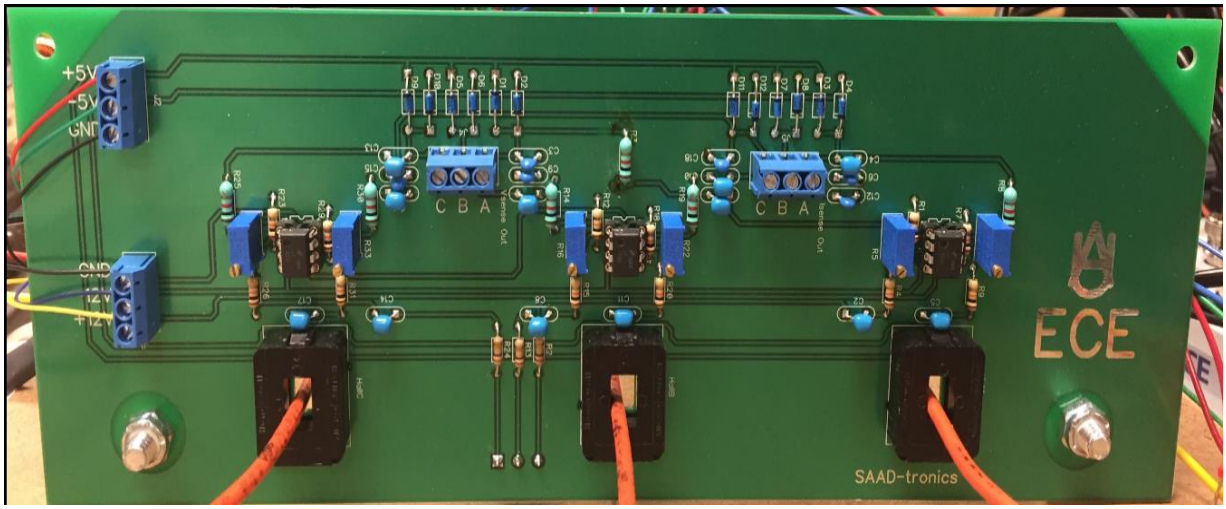

Figure 3.18: Voltage and current measurement boards.

3.2.5 The loads and the inductors of the impedance and the LCL filter

A total of twelve inductors for the grid impedances, the line impedances and the LCL filter were designed. The grid reactances were designed to be adjustable between about 100 µH and 1 mH as seen in Figure 3.19. Two types of loads were employed. Nonlinear loads were built using three-phase diode-bridge rectifier, shown in Figure 3.20, and a resistor. The linear loads were built from resistors with different values as seen in Figure 3.21.

Figure 3.19: Adjustable inductor for the grid impedance.

Figure 3.20: Three-phase diode-bridge rectifier.

Figure 3.21: Sample of the used resistors.

CHAPTER 4: RESULTS AND DISCUSSION

The last two chapters presented the proposed methods for controlling the shunt APF and the description of the simulation and hardware setups. This chapter presents the experimental results for these methods. Several studies were performed to tests the performance of the proposed methods under different conditions of grid voltage and loads.

4.1 Validation of the Proposed Filter

The model of the experimental system is shown in Figure 4.1. The test system consists of a three-phase voltage source, grid impedances, measurement board and three resistive loads of 5Ω each. The experimental test is utilized to obtain the measurements of the voltages and the currents through the measurement board. The measured signals were filtered by the proposed filter to generate the positive sequence components. The results were obtained by dSpace ControlDesk as shown in Figure 4.2, 4.3 and 4.4. This experiment was performed under three test cases:

1. Balanced voltages of magnitudes of $12V_{rms}$.
2. Unbalanced magnitudes of 12 V_{rms} , 11 V_{rms} and 15 V_{rms}.
3. Unbalanced magnitudes (12 V_{rms} , 11 V_{rms} and 15 V_{rms}) and phases where phases a and b are displaced by 210° and phases a and c are displaced by 100°.

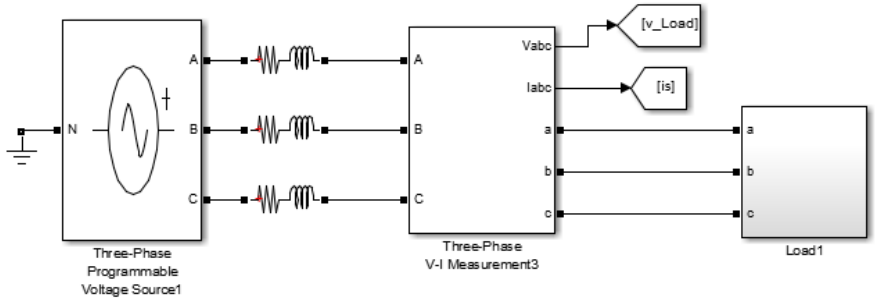

Figure 4.1: Test system for the proposed filter.

Balanced 3-phase quantities:

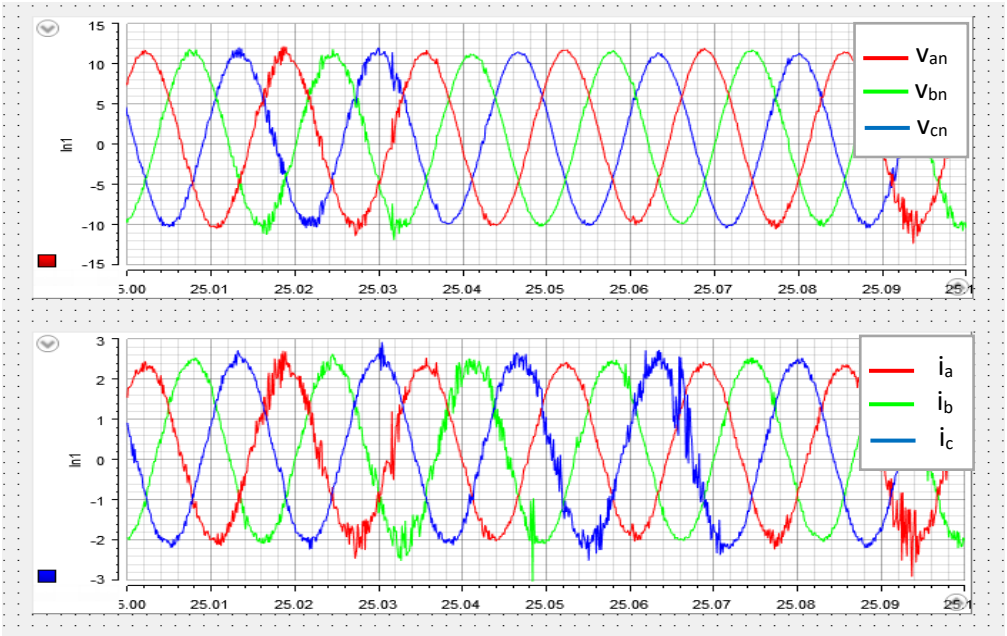

(a)

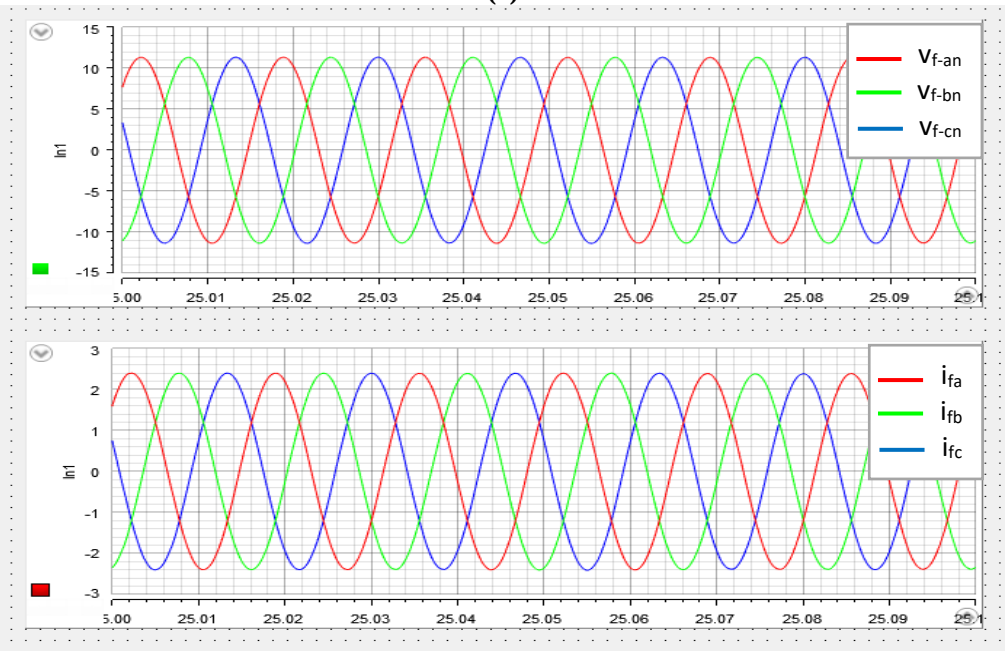

(b)

Figure 4.2: For balanced voltages: (a) measured voltages and measured currents. (b) filtered voltages and filtered currents.

Unbalanced magnitudes:

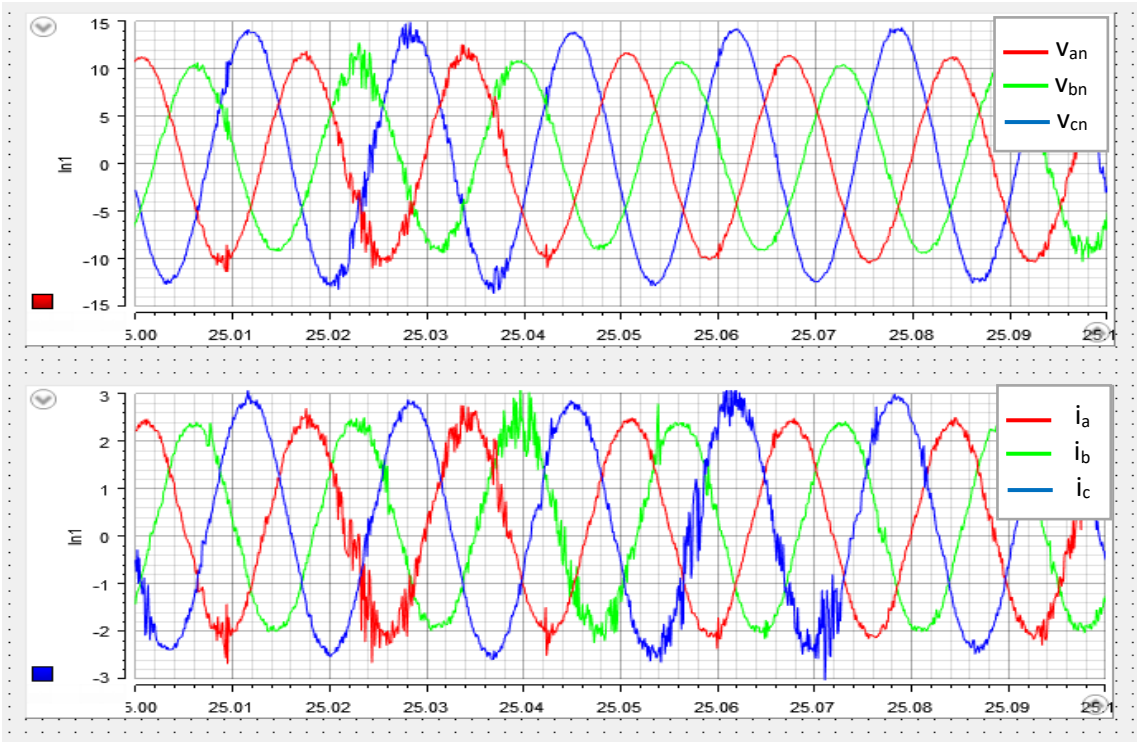

(a)

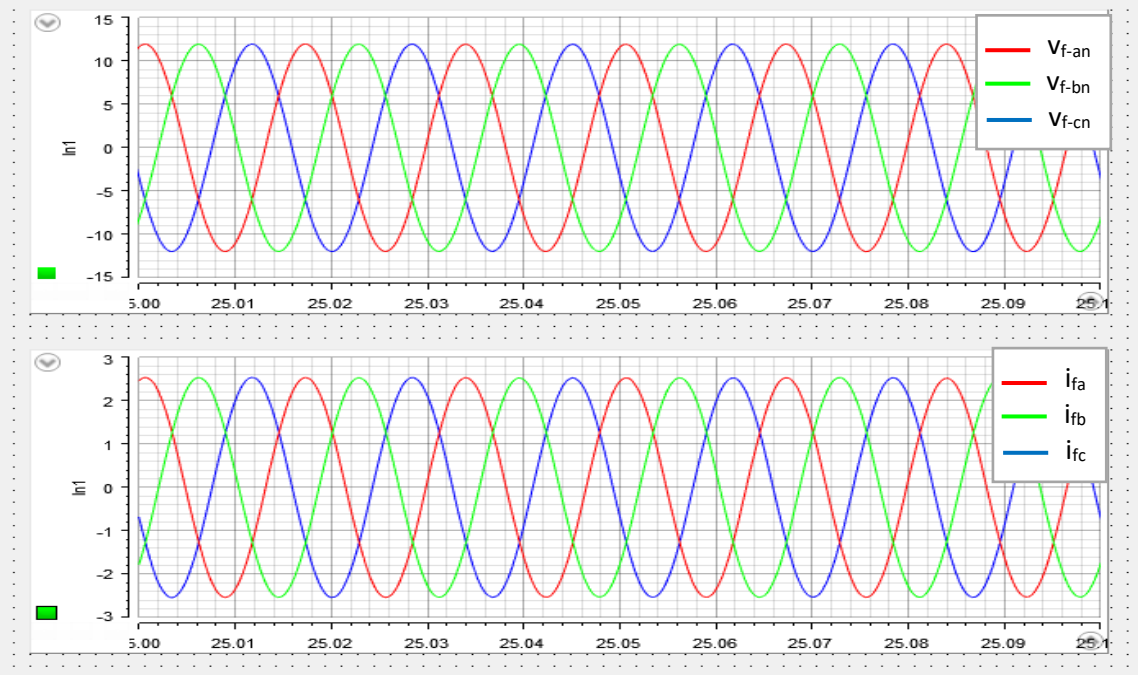

(b)

Figure 4.3: For unbalanced magnitudes: (a) measured voltages and measured currents. (b) filtered voltages and filtered currents.

Unbalanced magnitudes and phases:

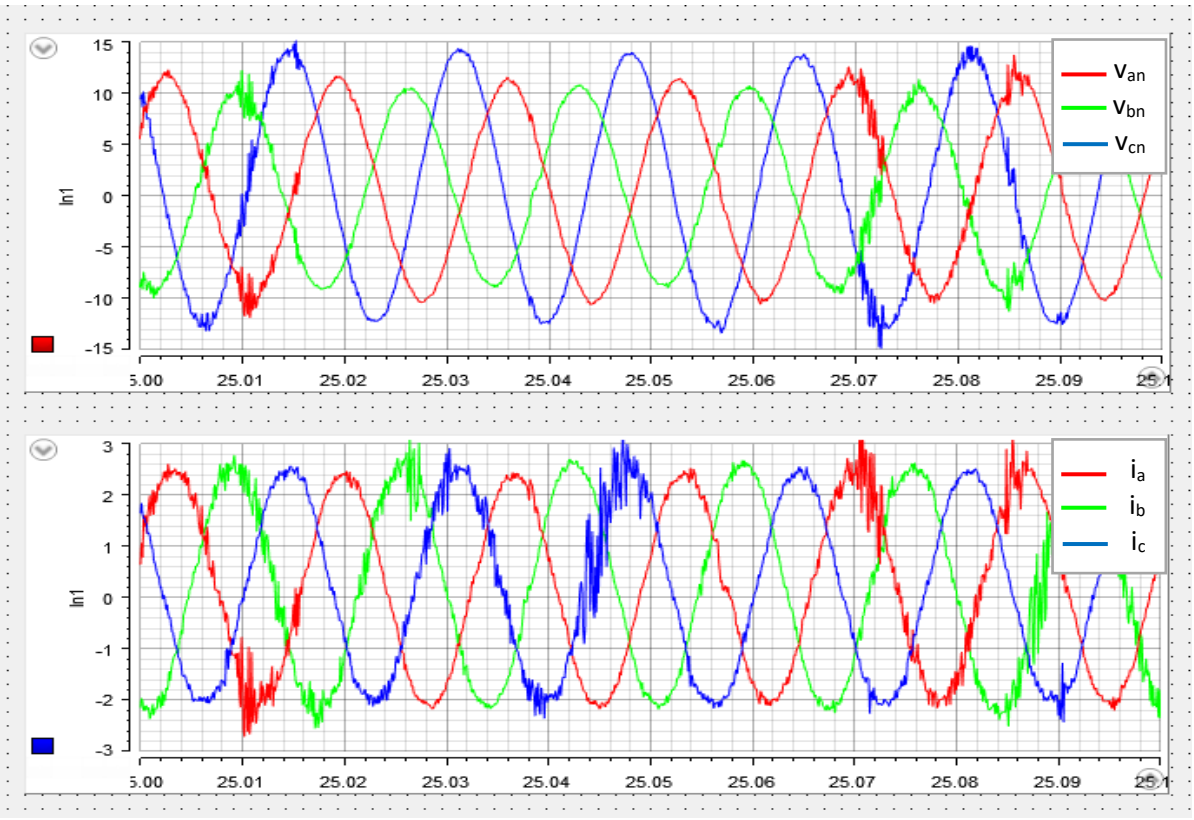

(a)

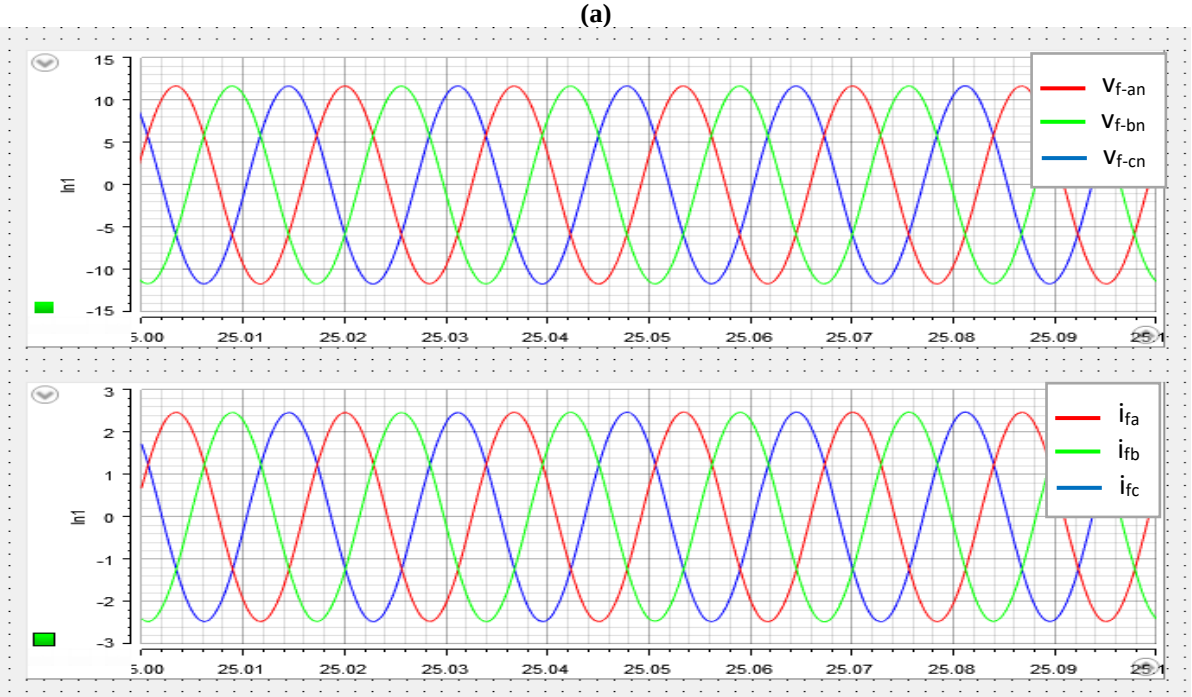

(b)

Figure 4.4: For unbalanced magnitudes and phases: (a) measured voltages and measured currents. (b) filtered voltages and filtered currents.

From the previous figures, the proposed filter maintains balanced voltages and currents under balanced and unbalanced voltages with the presence of the harmonics in the measured signals. The experimental results validated the proposed filter.

4.2 Performance Investigation of the Proposed Control Method

Experimental tests were performed to determine the proposed control method performance. The source currents were observed in order to evaluate this method. The experimental tests were performed under several conditions of the grid voltage and the load. Four different load combinations were utilized: nonlinear load (NL), NL and balanced linear load (BLL), NL and balanced linear load (ULL), and BLL and ULL.

Moreover, each load condition is tested under several grid conditions including: balanced grid voltages, unbalanced grid voltages, and unbalanced grid voltages and unbalanced grid impedances. Three resistors of 5Ω were connected in series with the shunt APF for synchronizing. The performance of the shunt APF was determined by the THD, the magnitudes of the source currents, and the power factor (pf). The results were obtained by a Tektronix MIDO 3024 oscilloscope. The system parameters are shown in Table 4.1.

Table 4.1: Experimental system parameters.

Frequencies	grid f_0= 60 Hz , switching f_{sw}= 20 kHz
Grid voltages	$\overline{V}_{an} = 10.5\lfloor 0°\ V_{rms}$, $\overline{V}_{bn} = 10.5\lfloor -120°\ V_{rms}$, $\overline{V}_{cn} = 10.5\lfloor 120°\ V_{rms}$
DC Voltage	40 V
Grid impedance	adjustable $L_g = 100\ \mu H, 300\ \mu H, 700\ \mu H, 1\ mH$
Line impedance	$R = 0.5\ \Omega, L = 1\ mH$
R load for rectifier	$R = 25\ \Omega$, $R = 12.5\ \Omega$, $R = 5\ \Omega$
Linear load sets	$R = 10\ \Omega$, $R = 12.5\ \Omega$, $R = 25\ \Omega$
LCL filter	$L_i = 4\ mH, C_f = 10\ \mu F, L_g = 300\ \mu H$
L filter	$L_i = 4\ mH$

Case 1: Nonlinear resistive load

Several tests based on the grid conditions were performed. Figure 4.5 shows the configuration of the system for this case.

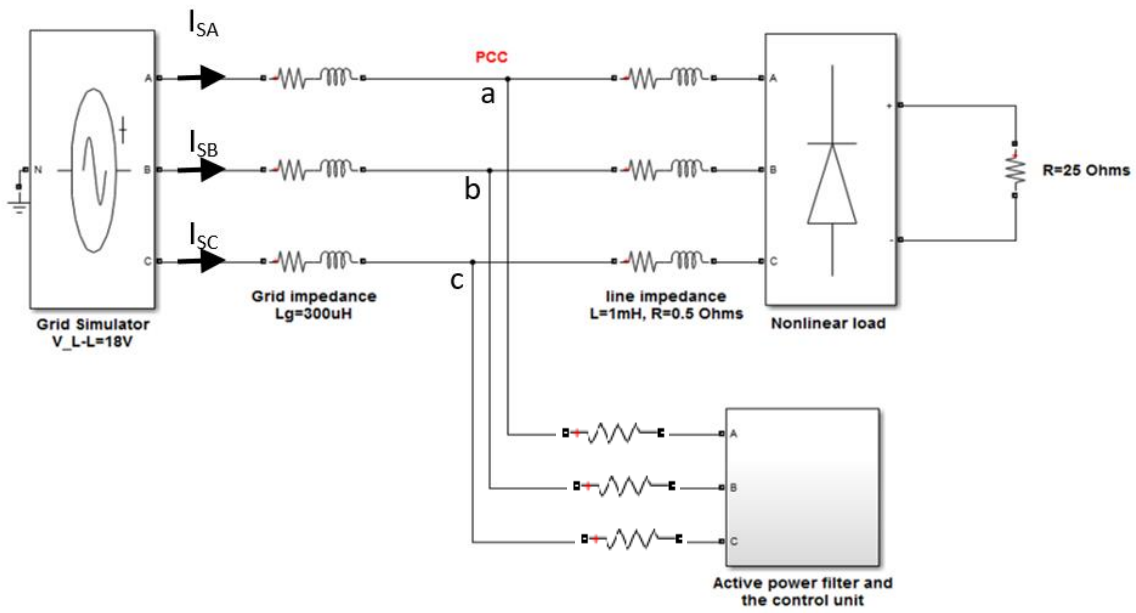

Figure 4.5: The system with NL.

A. Balanced grid voltages

Three different nonlinear loads were tested as listed in A1, A2 and A3. This experiment aimed to evaluate the proposed control system under different nonlinear loads. The results are presented in tables and figures that follow.

A1. R= 25Ω

Table 4.2: Magnitudes of the source currents and the PCC voltage without and with the shunt APF.

$\|I_s\|$ (A_{rms}) w/o APF	$\|I_s\|$ (A_{rms}) w/ APF	$\|V_{ab}\|$ (V_{rms}) w/o APF	$\|V_{ab}\|$ (V_{rms}) w/ APF
0.7	0.964	17.9	17.8

Table 4.3: THD of the source current and the PCC voltage without and with the shunt APF.

THD of I_s w/o APF	THD of I_s w/ APF	THD of V_{ab} w/o APF	THD of V_{ab} w/ APF
19.5%	2.66%	4.7%	3.15%

Table 4.4: Harmonic analysis of the source current and PCC voltage without and with the shunt APF.

f (Hz)	I_s w/o APF	I_s w/ APF	V_{ab} w/o APF	V_{ab} w/ APF
180	1.53%	0.39%	0.99%	1.15%
300	18.4%	0.24%	3.63%	0.57%
420	4.29%	0.19%	1.14%	0.37%

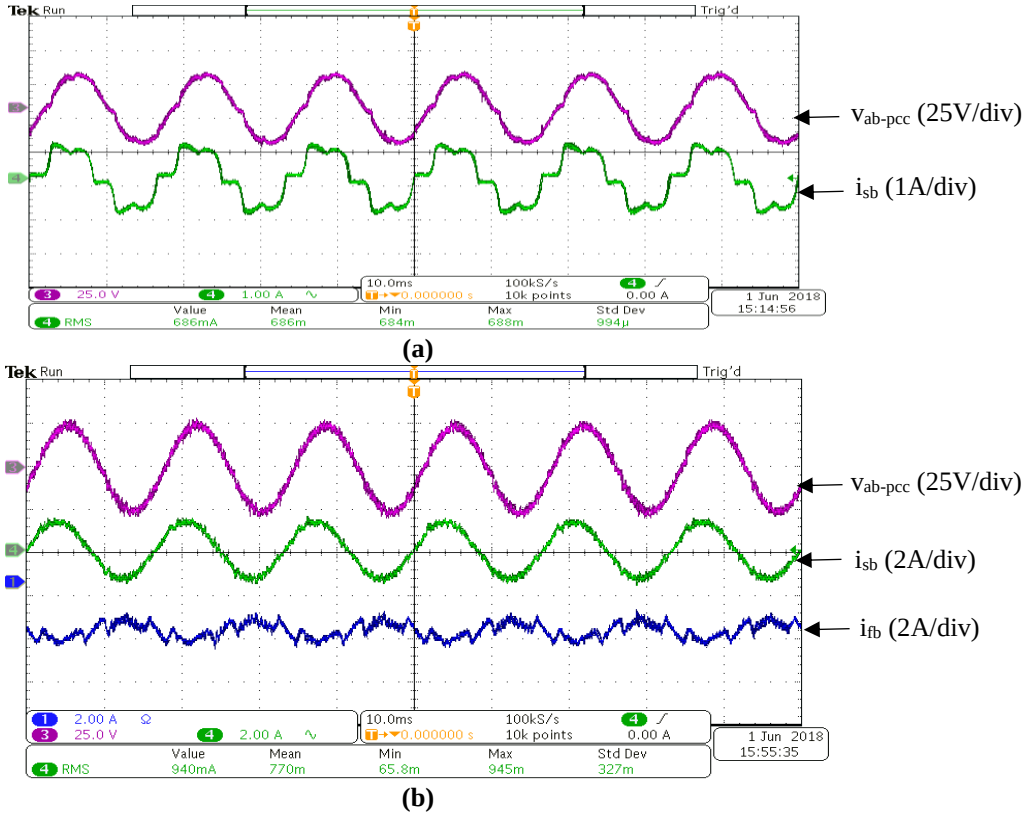

Figure 4.6: (a) $v_{ab\text{-}pcc}$ and i_{sb} without the shunt APF. (b) $v_{ab\text{-}pcc}$,i_{sb} and i_{fb} with the shunt APF. (10ms/div)

A2. R = 12.5 Ω

Table 4.5: Magnitudes of the source currents and the PCC voltage without and with the shunt APF.

$\|I_s\|$ (A_{rms}) w/o APF	$\|I_s\|$ (A_{rms}) w/ APF	$\|V_{ab}\|$ (V_{rms}) w/o APF	$\|V_{ab}\|$ (V_{rms}) w/ APF
1.3	1.57	17.9	18

Table 4.6: THD of the source current and the PCC voltage without and with the shunt APF.

THD of I_s w/o APF	THD of I_s w/ APF	THD of V_{ab} w/o APF	THD of V_{ab} w/ APF
19.5%	3%	13%	3.15%

Table 4.7: Harmonic analysis of the source current and PCC voltage without and with the shunt APF.

f (Hz)	I_s w/o APF	I_s w/ APF	V_{ab} w/o APF	V_{ab} w/ APF
180	0.09%	0.9%	0.33%	0.82%
300	21.8%	1%	8.11%	0.48%
420	7.1%	0.49%	4%	0.37%

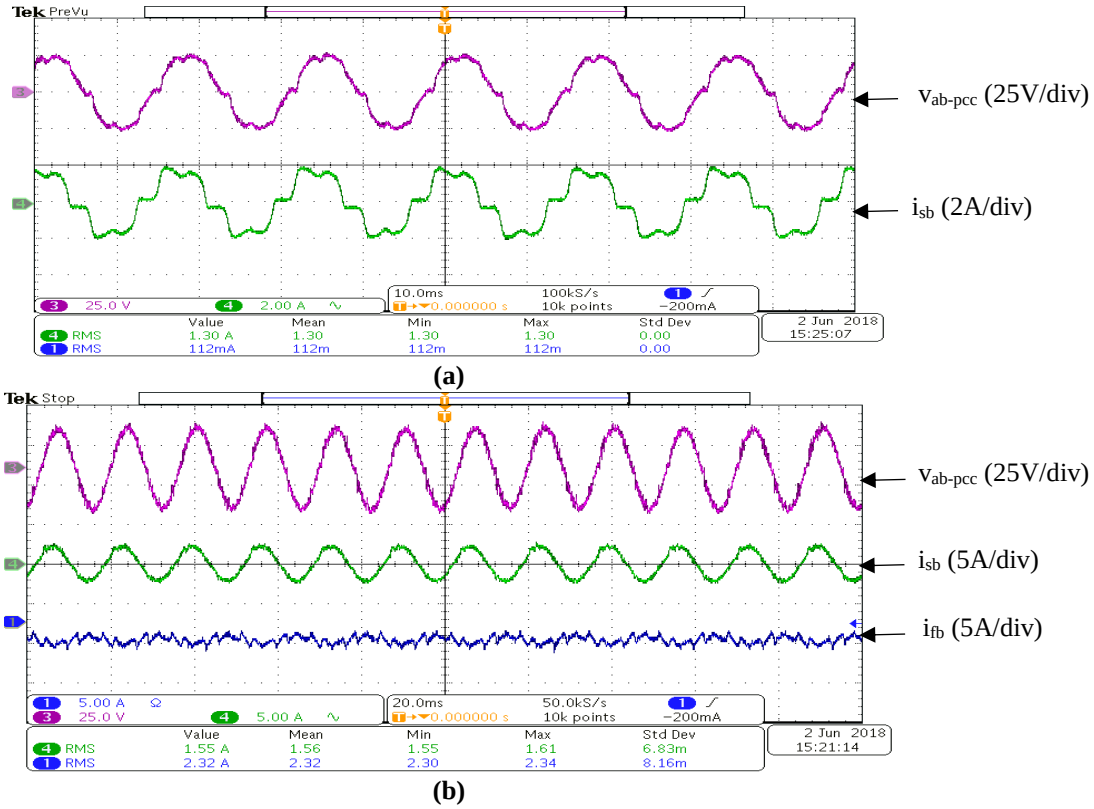

Figure 4.7: (a) $v_{ab\text{-}pcc}$ and i_{sb} without the shunt APF (10ms/div). (b) $v_{ab\text{-}pcc}$,i_{sb} and i_{fb} with the shunt APF (20ms/div).

A3. R = 5 Ω

Table 4.8: Magnitudes of the source currents and the PCC voltage without and with the shunt APF.

$\|I_s\|$ (A_{rms}) w/o APF	$\|I_s\|$ (A_{rms}) w/ APF	$\|V_{ab}\|$ (V_{rms}) w/o APF	$\|V_{ab}\|$ (V_{rms}) w/ APF
2.94	3.38	18	18

Table 4.9: THD of the source current and the PCC voltage without and with the shunt APF.

THD of I_s w/o APF	THD of I_s w/ APF	THD of V_{ab} w/o APF	THD of V_{ab} w/ APF
19.5%	4.09%	15%	6.8%

Table 4.10: Harmonic analysis of the source current and PCC voltage without and with the shunt APF.

f (Hz)	I_s w/o APF	I_s w/ APF	V_{ab} w/o APF	V_{ab} w/ APF
180	1.1%	1.88%	0.82%	1.1%
300	15%	0.42%	11.1%	1.94%
420	4.22%	0.51%	4.78%	0.99%

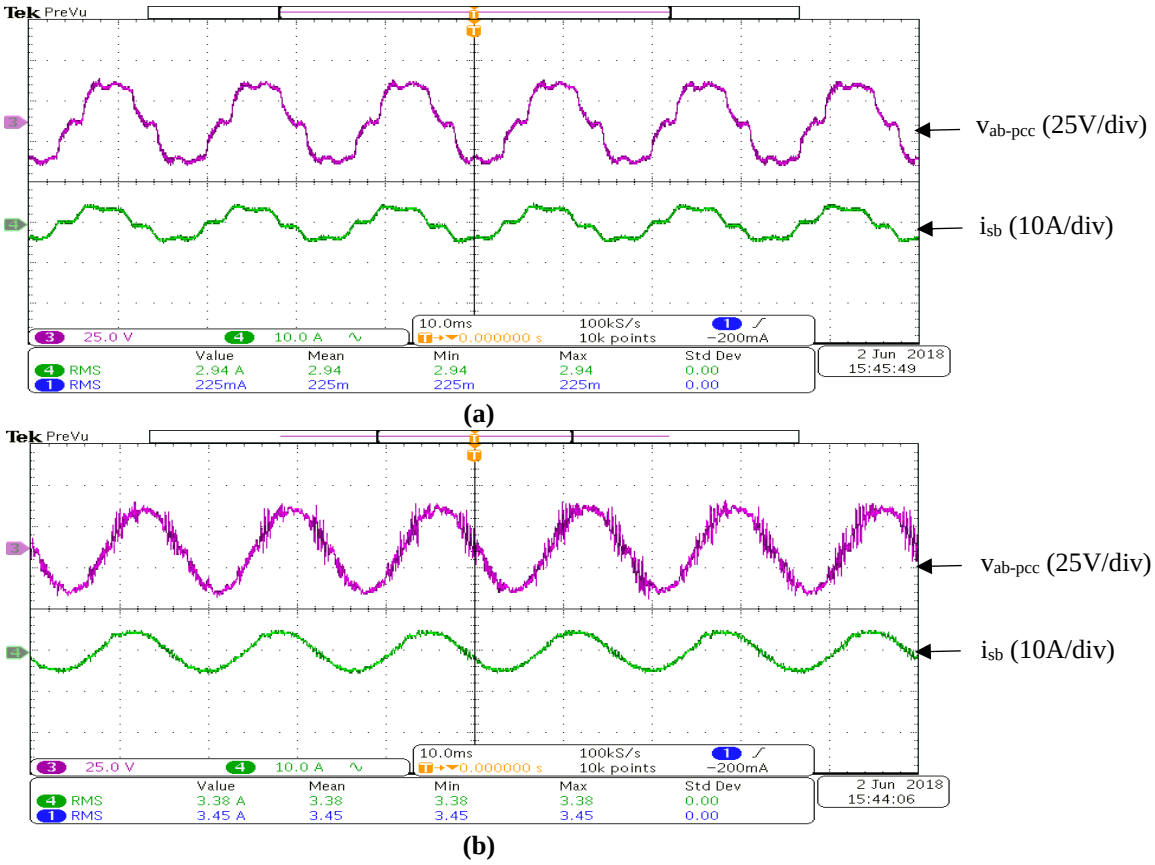

Figure 4.8: (a) $v_{ab\text{-}pcc}$ and i_{sb} without the shunt APF. (b) $v_{ab\text{-}pcc}$,i_{sb} with the shunt APF. (10ms/div)

For Test case A, the source currents were almost equal with the shunt APF as shown in Tables 4.2, 4.5 and 4.8. The THDs of the source currents were small as seen in Tables 4.3, 4.6 and 4.9. Figures 4.6 (b), 4.7 (b) and 4.8 (b) shows the source currents were balanced and sinusoidal.

B. Unbalanced magnitudes and phase angles ($\overline{V}_{an}$= 10.5∠0° V_{rms}, $\overline{V}_{bn}$= 11.5∠-110° V_{rms}, $\overline{V}_{cn}$= 13.5∠110° V_{rms}).

The results were obtained without and with the proposed control system as shown in Tables 4.11, 4.12, and 4.13. The source currents were balanced with a low THD of 3.4%. Figure 4.9 (b) shows that the source currents were balanced and sinusoidal.

Table 4.11: Magnitudes of the source currents and the PCC voltage without and with the shunt APF.

$\|I_{sa}\|$,$\|I_{sb}\|$ (A_{rms}) w/o APF	$\|I_{sa}\|$,$\|I_{sb}\|$ (A_{rms}) w/ APF	$\|V_{ab}\|$ (V_{rms}) w/o APF	$\|V_{ab}\|$ (V_{rms}) w/ APF
0.68, 0.88	1.1, 1.19	18.8	18.5

Table 4.12: THD of the source current and the PCC voltage without and with the shunt APF.

THD of I_s w/o APF	THD of I_s w/ APF	THD of V_{ab} w/o APF	THD of V_{ab} w/ APF
Min = 19.7% Max= 29%	3.66%	4.84%	2.98%

Table 4.13: Harmonic analysis of the source current and PCC voltage without and with the shunt APF.

f (Hz)	I_s w/o APF	I_s w/ APF	V_{ab} w/o APF	V_{ab} w/ APF
180	Min= 12.1% Max= 17.5%	0.72%	1.2%	1.08%
300	Min= 13.8% Max= 22.6%	0.46%	3.56%	0.59%
420	Min= 4.1% Max= 6.71%	0.41%	1.44%	0.32%

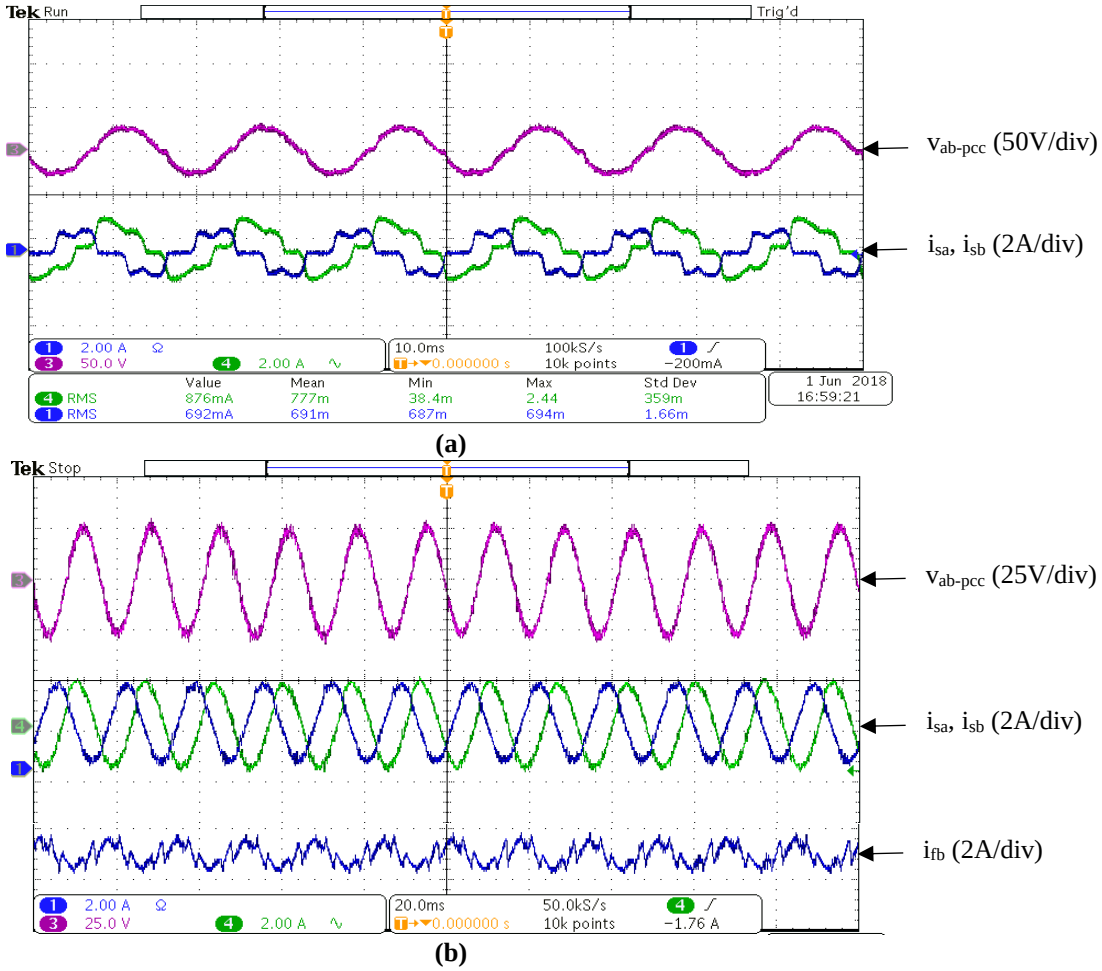

Figure 4.9: (a) $v_{ab\text{-}pcc}$, i_{sa} and i_{sb} without the filter (10ms/div). (b) $v_{ab\text{-}pcc}$, i_{sa}, i_{sb} and i_{fb} with the filter (20ms/div).

As seen from the above tables and figure, the shunt APF was able to eliminate the negative sequence components from the source currents.

C. Unbalanced grid impedances ($L_{ga} \approx 100$ µH, $L_{gb} \approx 700$ µH, $L_{gc} \approx 1000$ µH) and voltages ($\overline{V}_{an} = 10.5\angle 0°$ V_{rms}, $\overline{V}_{bn} = 12.5\angle -120°$ V_{rms}, $\overline{V}_{cn} = 11.63\angle 111.43°$ V_{rms})

The results of the source currents are presented in Tables 4.14, 4.15 and 4.16. The source currents were balanced with low THD of 3.4%. Figure 4.10 (b) shows that the source current was sinusoidal.

Table 4.14: Magnitudes of the source currents and the PCC voltage without and with the shunt APF.

$\|I_{sa}\|$,$\|I_{sb}\|$ (A_{rms}) w/o APF	$\|I_{sa}\|$,$\|I_{sb}\|$ (A_{rms}) w/ APF	$\|V_{ab}\|$ (V_{rms}) w/o APF	$\|V_{ab}\|$ (V_{rms}) w/ APF
07, 0.9	1.1, 1.15	18.4	20

Table 4.15: THD of the source current and the PCC voltage without and with the shunt APF.

THD of I_s w/o APF	THD of I_s w/ APF	THD of V_{ab} w/o APF	THD of V_{ab} w/ APF
Min= 18.4% Max= 23.1%	3.4%	3.36%	4.74%

Table 4.16: Harmonic analysis of the source current and PCC voltage without and with the shunt APF.

f (Hz)	I_s w/o APF	I_s w/ APF	V_{ab} w/o APF	V_{ab} w/ APF
180	Min= 5.9% Max= 6.6%	0.9%	1.2%	1.39%
300	Min= 15.8% Max= 21.9%	0.725%	0.68%	3.74%
420	Min= 1.69% Max= 5.84%	0.54%	0.5%	1%

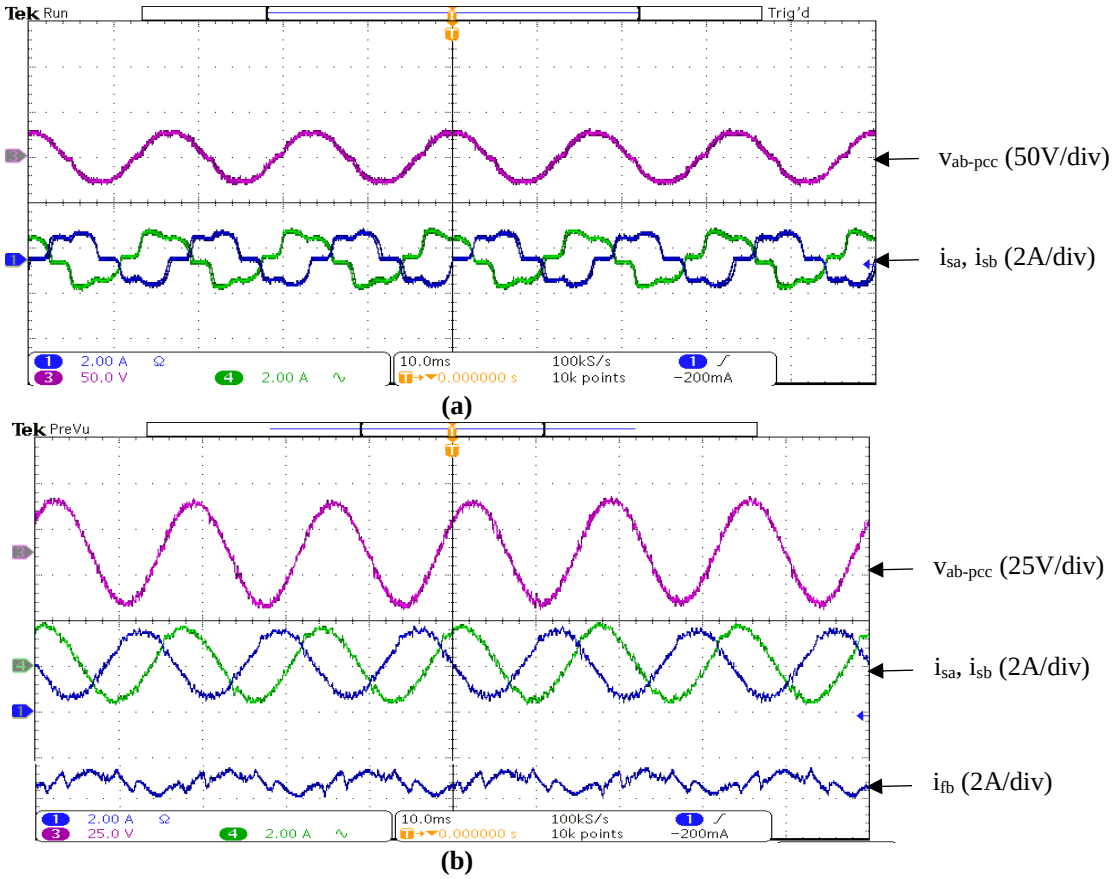

Figure 4.10: (a) $v_{ab\text{-}pcc}$, i_{sa} and i_{sb} without the filter. (b) $v_{ab\text{-}pcc}$, i_{sa}, i_{sb} and i_{fb} with the filter. (10ms/div)

From the above results of *Case 1*, the nonlinear load with smaller load resulted in a higher THD as seen in cases A1, A2, and A3. The THD of the source current and the pcc voltage were decreased sharply. Figures 4.6-4.10 show the source current waveforms and pcc voltage were corrected to sinusoidal waveforms with the shunt APF. The source current magnitudes were also close to each other. For balanced and unbalanced grid conditions, the source currents were balanced sinusoidal when the load was nonlinear.

Case 2: Nonlinear resistive load (25 Ω) and balanced linear resistive load (25 Ω, 25 Ω, 25 Ω)

The system with nonlinear and balanced linear loads was investigated under balanced and unbalanced grid conditions. This case is divided into three divisions based on the grid conditions. The results are shown in the tables and figures that follow. Figure 4.11 is a diagram for the setup.

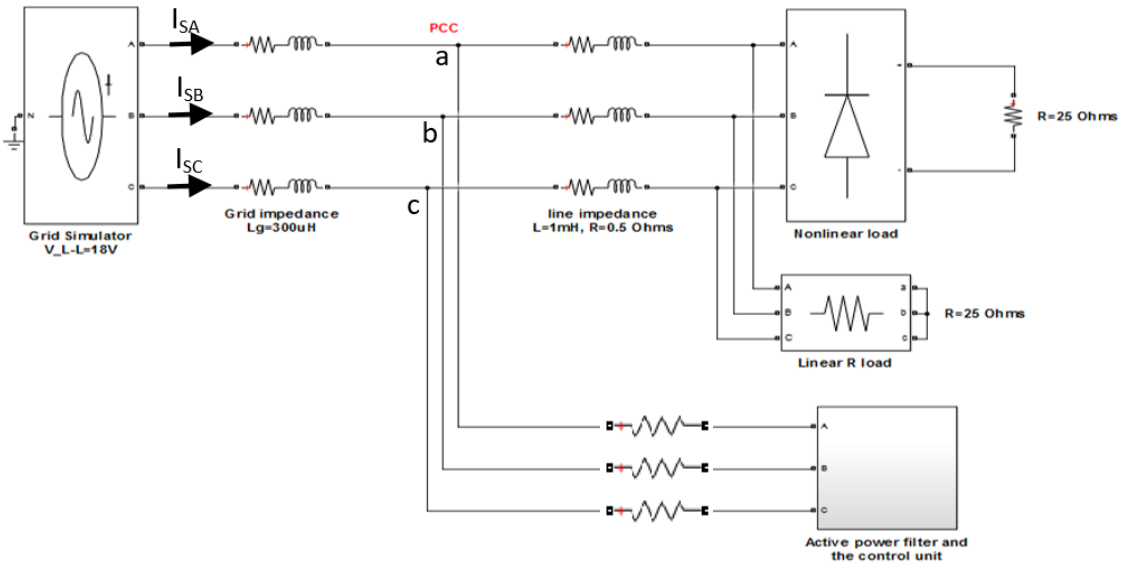

Figure 4.11: The system with nonlinear load and linear load.

A. Balanced grid voltages

Under balanced grid voltages, the source current magnitudes remained balanced with magnitude of 1.44 A_{rms} as shown in Table 4.17 and Figure 4.12. As shown in Table 4.18, the THD was

decrease from 14.8% to 2.69%. The amounts of the 5th and 7th harmonic orders were decreased to less than 1% as shown in Table 4.19.

Table 4.17: Magnitudes of the source currents and the PCC voltage without and with the shunt APF.

$\|I_s\|$ (A_{rms}) w/o APF	$\|I_s\|$ (A_{rms}) w/ APF	$\|V_{ab}\|$ (V_{rms}) w/o APF	$\|V_{ab}\|$ (V_{rms}) w/ APF
1.08	1.44	18	18.2

Table 4.18: THD of the source current and the PCC voltage without and with the shunt APF.

THD of I_s w/o APF	THD of I_s w/ APF	THD of V_{ab} w/o APF	THD of V_{ab} w/ APF
14.8%	2.69%	6.13%	4.56%

Table 4.19: Harmonic analysis of the source current and PCC voltage without and with the shunt APF.

f (Hz)	I_s w/o APF	I_s w/ APF	V_{ab} w/o APF	V_{ab} w/ APF
180	0.65%	1.26%	0.47%	2.32%
300	13%	0.1%	4.2%	0.73%
420	4.34%	0.25%	2.73%	0.39%

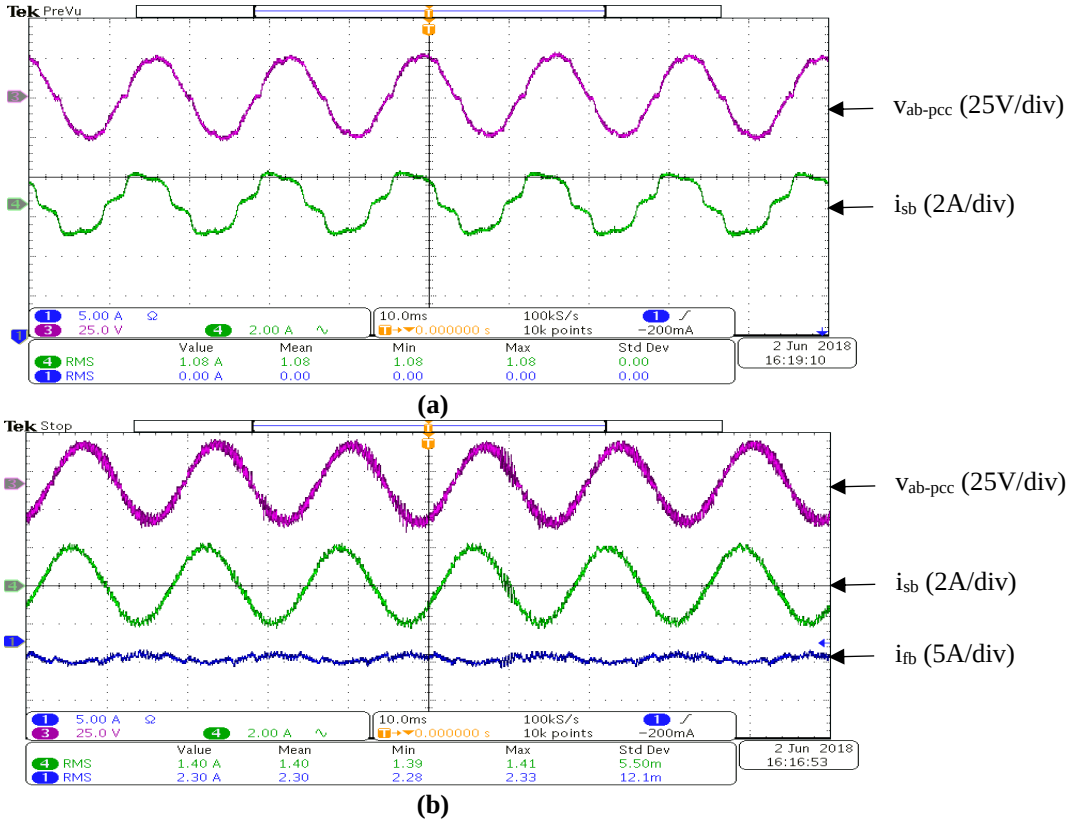

Figure 4.12: (a) $v_{ab\text{-}pcc}$ and i_{sb} without the filter. (b) $v_{ab\text{-}pcc}$,i_{sb} and i_{fb} with the filter. (10ms/div)

B. Unbalanced grid voltages ($\overline{V}_{an}$= 10.5∠0° V_{rms}, $\overline{V}_{bn}$= 11.5∠-110° V_{rms}, $\overline{V}_{cn}$= 13.5∠110° V_{rms})

For unbalanced grid voltages, Table 4.20 and Figure 4.13 show that the source current magnitudes were balanced with a magnitude of about 1.5 A_{rms}. The THD was reduced sharply to 3.59% as seen in Table 4.21. The amounts of the 3rd, 5th and 7th harmonic orders were decreased as shown in Table 4.22.

Table 4.20: The source current magnitudes and the PCC voltage without and with the shunt APF.

$\|I_{sa}\|$,$\|I_{sb}\|$ (A_{rms}) w/o APF	$\|I_{sa}\|$,$\|I_{sb}\|$ (A_{rms}) w/ APF	$\|V_{ab}\|$ (V_{rms}) w/o APF	$\|V_{ab}\|$ (V_{rms}) w/ APF
1, 1.4	1.53, 1.59	18	17.6

Table 4.21: THD of the source current and the PCC voltage without and with the shunt APF.

THD of I_s w/o APF	THD of I_s w/ APF	THD of V_{ab} w/o APF	THD of V_{ab} w/ APF
Min= 19.7% Max= 29%	3.59%	5.2%	4.16%

Table 4.22: Harmonic analysis of the source current and PCC voltage without and with the shunt APF.

f (Hz)	I_s w/o APF	I_s w/ APF	V_{ab} w/o APF	V_{ab} w/ APF
180	6.52%	1.12%	1.7%	1.32%
300	8.6%	1.96%	4.23%	0.94%
420	4.3%	0.72%	1.3%	0.57%

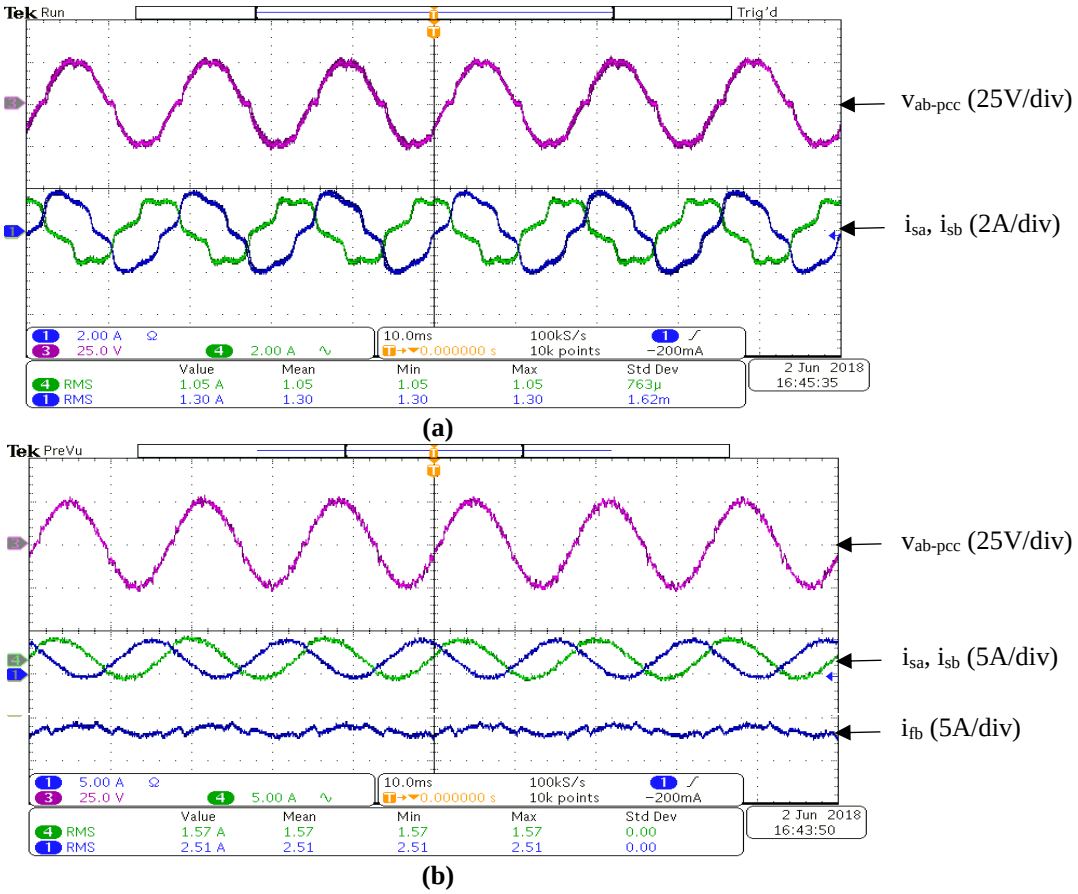

Figure 4.13: (a) $v_{ab\text{-}pcc}$, i_{sa} and i_{sb} without the filter. (b) $v_{ab\text{-}pcc}$, i_{sa}, i_{sb} and i_{fb} with the filter. (10ms/div)

C. Unbalanced grid impedances ($L_{ga} \approx 100$ µH, $L_{gb} \approx 700$ µH, $L_{gc} \approx 1000$ µH) and voltages ($\overline{V}_{an} = 10.5\angle 0°$ V_{rms}, $\overline{V}_{bn} = 12.5\angle -120°$ V_{rms}, $\overline{V}_{cn} = 11.63\angle 111.43°$ V_{rms})

For unbalanced grid impedances and grid voltages, Table 4.23 and Figure 4.14 show that the source current magnitudes were nearly equal with a magnitude of about 1.6 A_{rms}. As shown in Table 4.24, the THD was reduced sharply to 3.59%. The 3rd, 5th and 7th harmonic orders amounts were decreased as shown in Table 4.25.

Table 4.23: The source current magnitudes and the PCC voltage without and with the shunt APF.

$\lvert I_{sa}\rvert$,$\lvert I_{sb}\rvert$ (A_{rms}) w/o APF	$\lvert I_{sa}\rvert$,$\lvert I_{sb}\rvert$ (A_{rms}) w/ APF	$\lvert V_{ab}\rvert$ (V_{rms}) w/o APF	$\lvert V_{ab}\rvert$ (V_{rms}) w/ APF
1.1, 1.31	1.54, 1.6	19.6	19.7

Table 4.24: THD of the source current and the PCC voltage without and with the shunt APF.

THD of I_s w/o APF	THD of I_s w/ APF	THD of V_{ab} w/o APF	THD of V_{ab} w/ APF
10.3%	3.9%	5.1%	3%

Table 4.25: Harmonic analysis of the source current and PCC voltage without and with the shunt APF.

f (Hz)	I_s w/o APF	I_s w/ APF	V_{ab} w/o APF	V_{ab} w/ APF
180	3.9%	2%	0.63%	0.6%
300	8.17%	1.14%	3.67%	0.27%
420	3.17%	0.47%	1.16%	0.32%

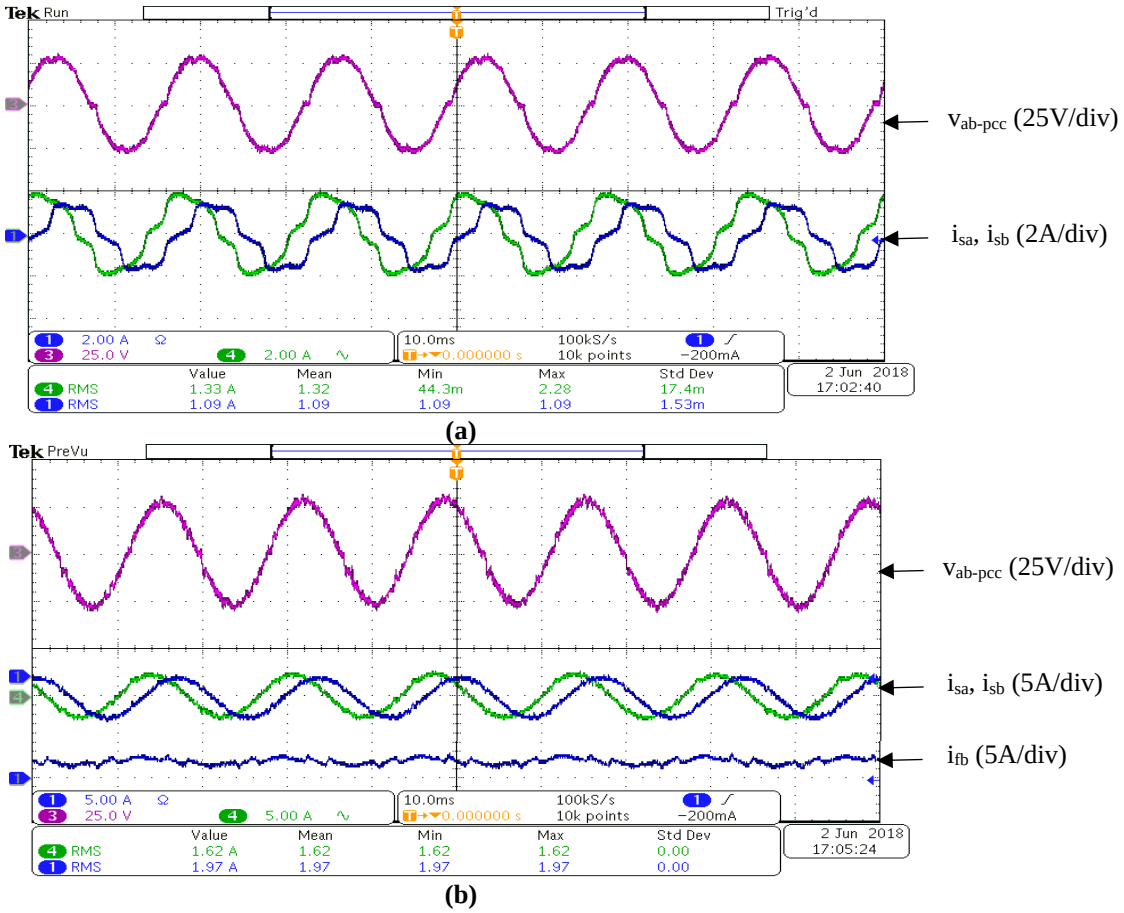

Figure 4.14: (a) $v_{ab\text{-}pcc}$, i_{sa} and i_{sb} without the filter. (b) $v_{ab\text{-}pcc}$, i_{sa}, i_{sb} and i_{fb} with the filter. (10ms/div)

The results from *Case 2* show that the proposed system was able to maintain sinusoidal waveforms of the pcc voltage and the source currents. The THDs of the pcc voltage and the source current were less than 5%. The source current amplitudes have almost equal values. As seen in

Figures 4.12, 4.13 and 4.14, the source currents were balanced sinusoidal waveforms under balanced and unbalanced grid conditions with nonlinear and linear balanced loads.

Case 3: Nonlinear resistive load (25 Ω) and unbalanced linear resistive loads (12.5 Ω, 25 Ω, 25 Ω)

The system with nonlinear and unbalanced linear loads was investigated under balanced and unbalanced grid conditions. This case is divided into 3 divisions based on the grid conditions. The results are shown in tables and figures.

A. Balanced grid voltages

Table 4.26 and Figure 4.15 show that the source current magnitudes were balanced with a magnitude of about 1.6 A_{rms}. The THD of the source current was reduced from 11.1% to 3.1% as shown in Table 4.27. The amounts of the 3rd, 5th and 7th harmonic orders were decreased sharply as shown in Table 4.28.

Table 4.26: The source current magnitudes and the PCC voltage without and with the shunt APF.

$\|I_{sa}\|$,$\|I_{sb}\|$ (A_{rms}) w/o APF	$\|I_{sa}\|$,$\|I_{sb}\|$ (A_{rms}) w/ APF	$\|V_{ab}\|$ (V_{rms}) w/o APF	$\|V_{ab}\|$ (V_{rms}) w/ APF
1.17, 1.3	1.55, 1.55	17.9	17.9

Table 4.27: THD of the source current and the PCC voltage without and with the shunt APF.

THD of I_s w/o APF	THD of I_s w/ APF	THD of V_{ab} w/o APF	THD of V_{ab} w/ APF
11.1%	3.1%	4.33%	3.75%

Table 4.28: Harmonic analysis of the source current and PCC voltage without and with the shunt APF.

f (Hz)	I_s w/o APF	I_s w/ APF	V_{ab} w/o APF	V_{ab} w/ APF
180	0.33%	0.6%	1.1%	0.78%
300	10.4%	1.1%	3.29%	0.922%
420	3%	0.66%	1.58%	0.342%

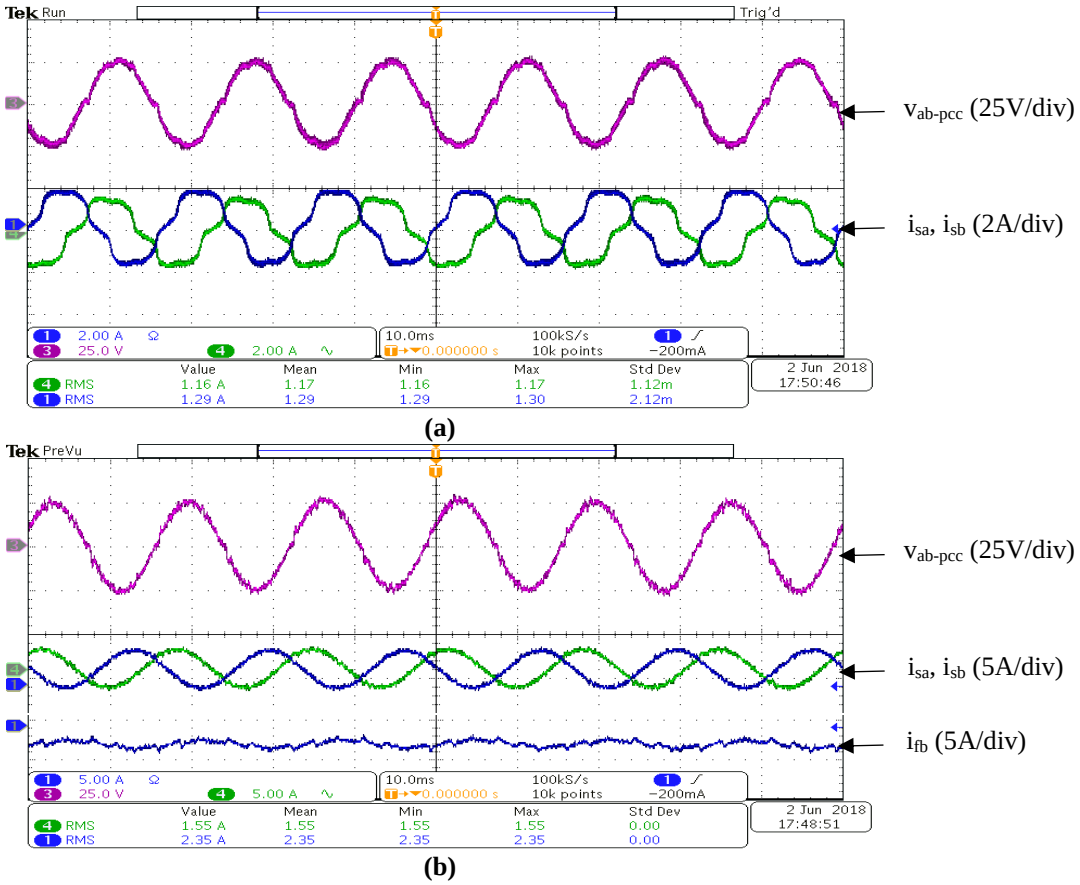

Figure 4.15: (a) $v_{ab\text{-}pcc}$, i_{sa} and i_{sb} without the filter. (b) $v_{ab\text{-}pcc}$, i_{sa}, i_{sb} and i_{fb} with the filter. (10ms/div)

B. Unbalanced grid voltages ($\overline{V}_{an}$= 10.5∠0° V_{rms}, $\overline{V}_{bn}$= 10.5∠-120° V_{rms}, $\overline{V}_{cn}$= 14∠120° V_{rms})

The source current magnitudes were almost equal with magnitude of about 1.7 A_{rms} as shown in Table 4.29 and Figure 4.16. The THD of the source current was reduced from 13.3% to 4.3% as shown in Table 4.30. The amounts of the 3rd, 5th and 7th harmonic orders were decreased sharply as shown in Table 4.31.

Table 4.29: The source current magnitudes and the PCC voltage without and with the shunt APF.

$\|I_{sa}\|$,$\|I_{sb}\|$ (A_{rms}) w/o APF	$\|I_{sa}\|$,$\|I_{sb}\|$ (A_{rms}) w/ APF	$\|V_{ab}\|$ (V_{rms}) w/o APF	$\|V_{ab}\|$ (V_{rms}) w/ APF
1.22, 1.4	1.69, 1.71	18	18

Table 4.30: THD of the source current and the PCC voltage without and with the shunt APF.

THD of I_s w/o APF	THD of I_s w/ APF	THD of V_{ab} w/o APF	THD of V_{ab} w/ APF
13.3%	4.3%	5%	4.07%

Table 4.31: Harmonic analysis of the source current and PCC voltage without and with the shunt APF.

f (Hz)	I_s w/o APF	I_s w/ APF	V_{ab} w/o APF	V_{ab} w/ APF
180	4.19%	0.52%	0.06%	1.27%
300	12.1%	1.17%	4.32%	0.86%
420	2.3%	0.438%	1.18%	0.38%

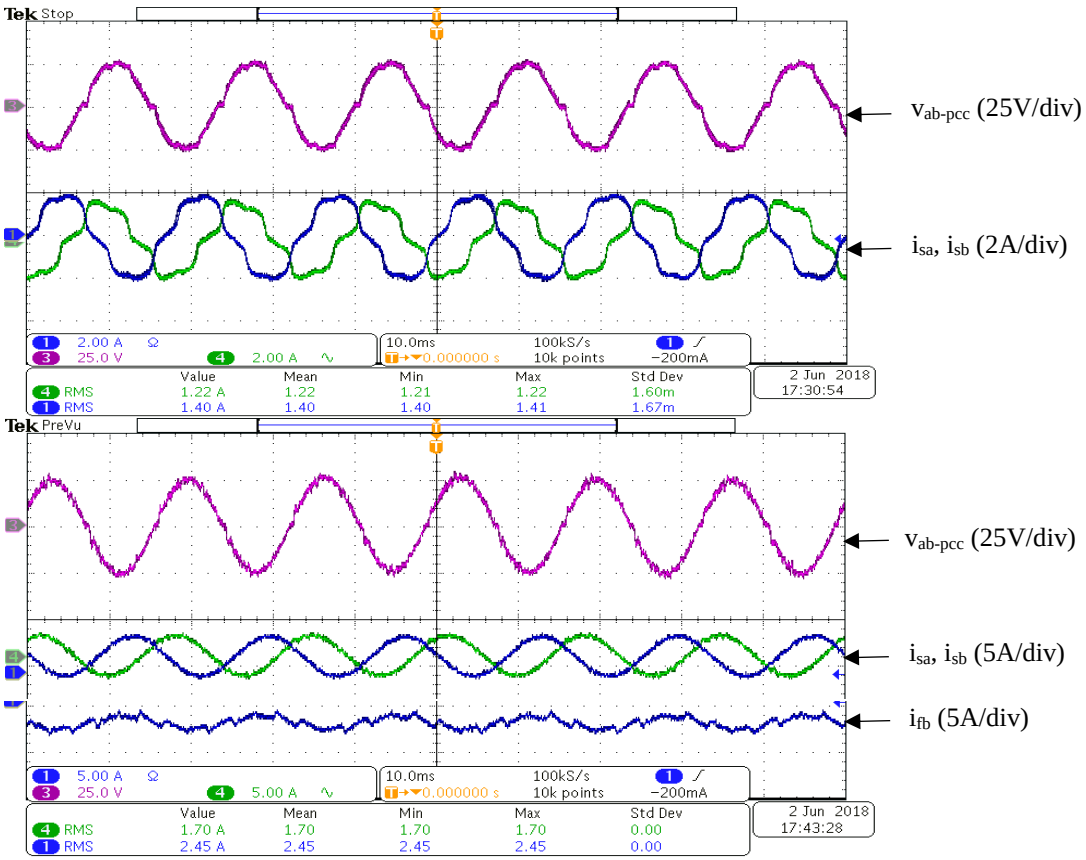

(b)

Figure 4.16: (a) $v_{ab\text{-}pcc}$, i_{sa} and i_{sb} without the filter. (b) $v_{ab\text{-}pcc}$, i_{sa}, i_{sb} and i_{fb} with the filter.

The results of *Case 3* show that the waveforms of the source current and the pcc voltage were sinusoidal for balanced and unbalanced conditions. The THDs of the pcc voltage and the source current were reduced to less than 5%. The source current magnitudes were nearly equal and

were considered balanced under balanced and unbalanced grid voltages as shown in Figures 4.15 and 4.16.

Case 4: Balanced linear resistive loads

In this case, the proposed control method was applied to the system shown in Figure 4.17. The case consists of three divisions A, B and C based on the grid condition. In division A where the grid voltages were balanced, three different loads were tested in order to examine the effectiveness of the proposed control method with big and small loads. Divisions B and C show the results when the grid conditions were unbalanced. The results were obtained with and without the shunt APF.

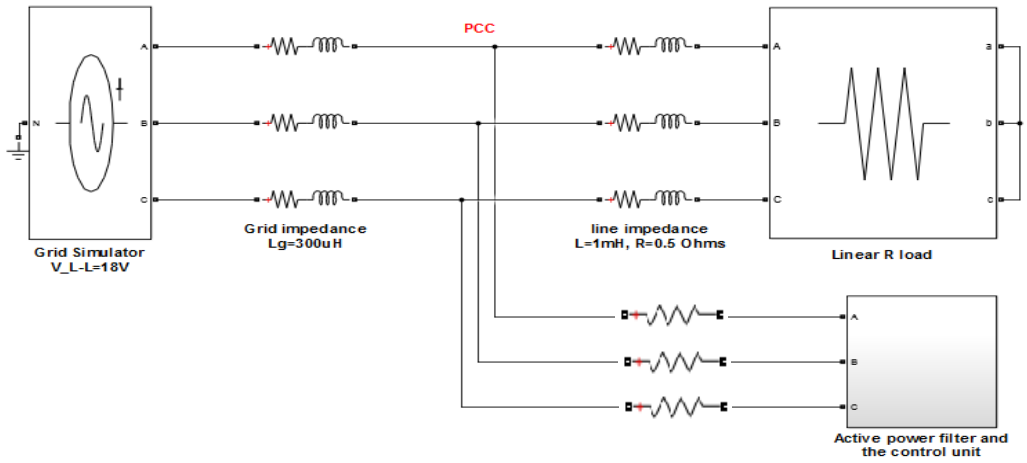

Figure 4.17: The system with nonlinear load and linear load.

A. Balanced grid voltages

A1. $R_1 = R_2 = R_3 = 25\ \Omega$

Table 4.32: Magnitudes of the source currents and the PCC voltage without and with the shunt APF.

$\|I_s\|$ (A_{rms}) w/o APF	$\|I_s\|$ (A_{rms}) w/ APF	$\|V_{ab}\|$ (V_{rms}) w/o APF	$\|V_{ab}\|$ (V_{rms}) w/ APF
0.425	0.67	18	18

Table 4.33: THD of the source current and the PCC voltage without and with the shunt APF.

THD of I_s w/o APF	THD of I_s w/ APF	THD of V_{ab} w/o APF	THD of V_{ab} w/ APF
2.15%	3.78%	2.81%	2.85%

Table 4.34: Harmonic analysis of the source current and PCC voltage without and with the shunt APF.

f (Hz)	I_s w/o APF	I_s w/ APF	V_{ab} w/o APF	V_{ab} w/ APF
180	1.21%	1.82%	1%	0.8%
300	0.15%	0.09%	0.52%	0.4%
420	0.18%	0.11%	0.4%	0.26%

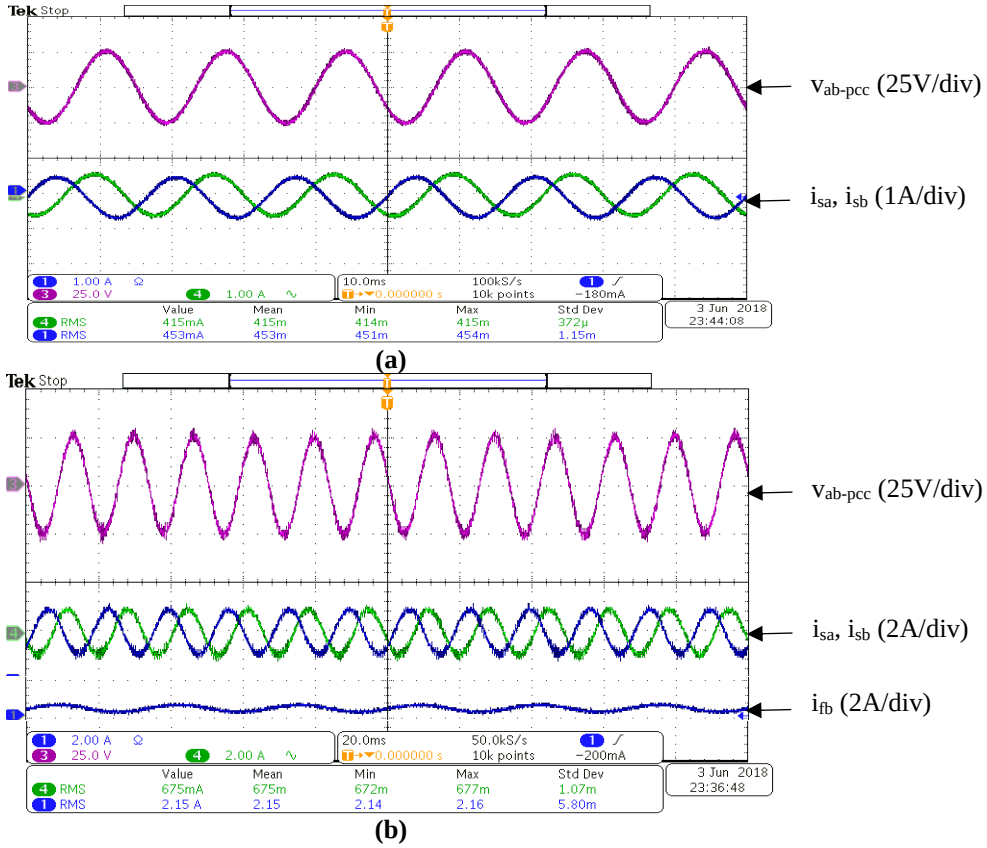

Figure 4.18: (a) $v_{ab\text{-}pcc}$ and i_{sb} without the filter (10ms/div). (b) $v_{ab\text{-}pcc}$,i_{sb} and i_{fb} with the filter (20ms/div).

A2. $R_1 = R_2 = R_3 = 10\ \Omega$

Table 4.35: Magnitudes of the source currents and the PCC voltage without and with the shunt APF.

$\lvert I_s \rvert$ (A_{rms}) w/o APF	$\lvert I_s \rvert$ (A_{rms}) w/ APF	$\lvert V_{ab} \rvert$ (V_{rms}) w/o APF	$\lvert V_{ab} \rvert$ (V_{rms}) w/ APF
1	1.28	18	18

Table 4.36: THD of the source current and the PCC voltage without and with the shunt APF.

THD of I_s w/o APF	THD of I_s w/ APF	THD of V_{ab} w/o APF	THD of V_{ab} w/ APF
1.81%	3%	2.39%	1.9%

Table 4.37: Harmonic analysis of the source current and PCC voltage without and with the shunt APF.

f (Hz)	I_s w/o APF	I_s w/ APF	V_{ab} w/o APF	V_{ab} w/ APF
180	0.36%	1.7%	1.1%	0.75%
300	0.9%	0.5%	0.95%	0.43%
420	0.6%	0.26%	0.6%	0.2%

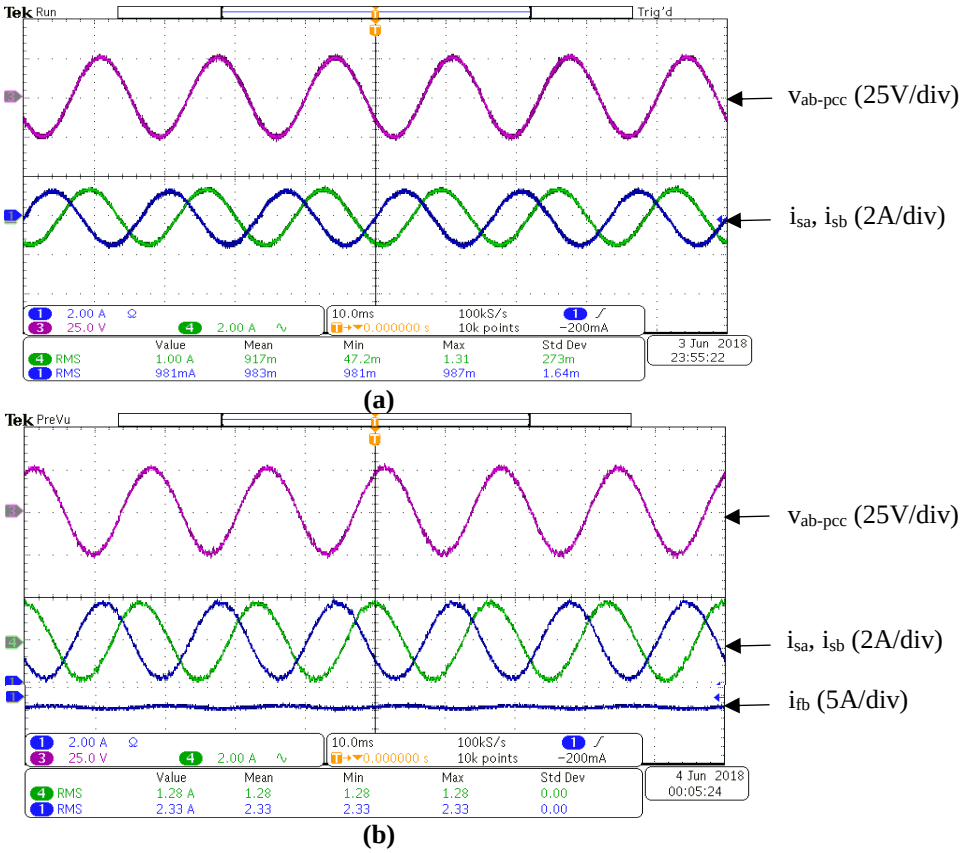

Figure 4.19: (a) $v_{ab\text{-}pcc}$, i_{sa} and i_{sb} without the filter. (b) $v_{ab\text{-}pcc}$, i_{sa}, i_{sb} and i_{fb} with the filter. (10ms/div)

For the results of division A, the source current magnitudes were almost equal as shown in Tables 4.32 and 4.35 and Figures 4.16 and 4.17. The THDs of the source current were low as shown in Tables 4.33 and 4.36. The amounts of 3rd, 5th and 7th harmonic orders were decreased sharply as shown in Tables 4.34 and 4.37.

B. Unbalanced magnitudes and phase angles ($\overline{V}_{an}$= 10.5∠0° V_{rms}, $\overline{V}_{bn}$= 11.5∠-110° V_{rms}, $\overline{V}_{cn}$= 13.5∠110° V_{rms})

Table 4.38 and Figure 4.20 show that the source current magnitudes were balanced with a magnitude of about 1.4 A_{rms}. The THD of the source current was low as shown in Table 4.39. The amount of the 3rd, 5th and 7th harmonic orders were also low as shown in Table 4.40.

Table 4.38: Magnitudes of the source currents and the PCC voltage without and with the shunt APF.

$\|I_{sa}\|,\|I_{sb}\|,\|I_{sc}\|$ (A_{rms}) w/o APF	$\|I_{sa}\|,\|I_{sb}\|,\|I_{sc}\|$ (A_{rms}) w/ APF	$\|V_{ab}\|$ (V_{rms}) w/o APF	$\|V_{ab}\|$ (V_{rms}) w/ APF
1.17, 0.93,1.26	1.4,1.4,1.4	18	17.6

Table 4.39: THD of the source current and the PCC voltage without and with the shunt APF.

THD of I_s w/o APF	THD of I_s w/ APF	THD of V_{ab} w/o APF	THD of V_{ab} w/ APF
2.16%	2.83%	2.07%	1.81%

Table 4.40: Harmonic analysis of the source current and PCC voltage without and with the shunt APF.

f (Hz)	I_s w/o APF	I_s w/ APF	V_{ab} w/o APF	V_{ab} w/ APF
180	1.31%	1.42%	1%	0.9%
300	0.9%	0.42%	0.92%	0.44%
420	0.34%	0.35%	0.26%	0.2%

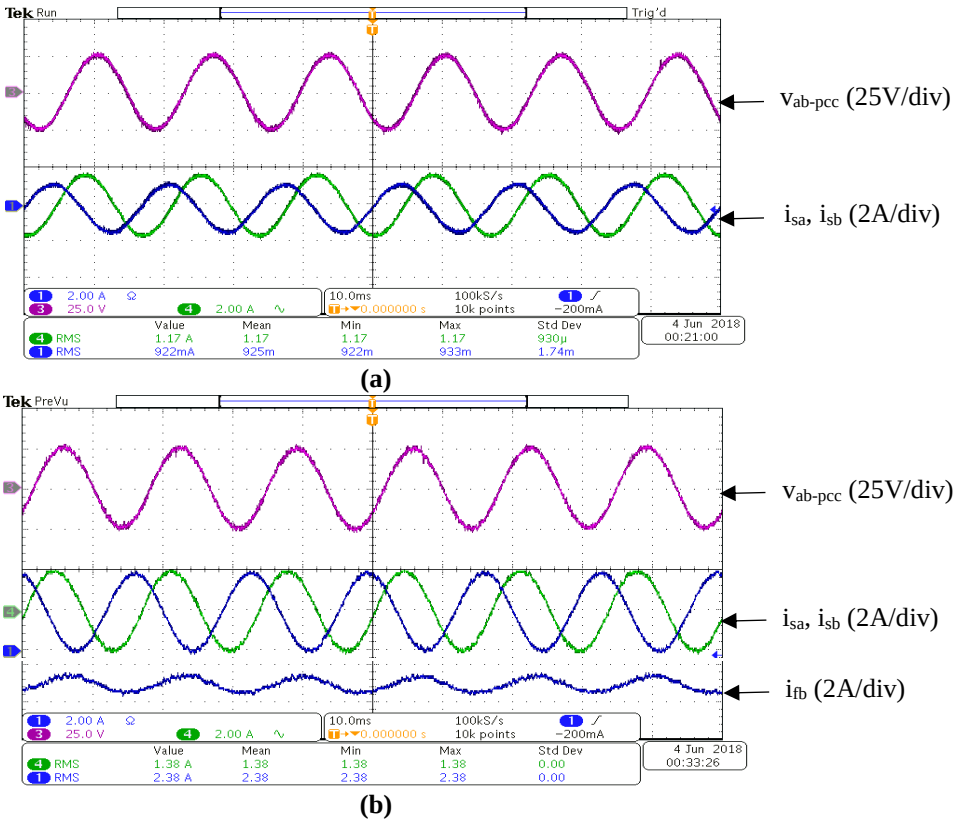

Figure 4.20: (a) $v_{ab\text{-}pcc}$, i_{sa} and i_{sb} without the filter. (b) $v_{ab\text{-}pcc}$, i_{sa}, i_{sb} and i_{fb} with the filter. (10ms/div)

C. Unbalanced grid impedance ($L_{ga} \approx 100$ µH, $L_{gb} \approx 700$ µH, $L_{gc} \approx 1000$ µH) and voltages ($\overline{V}_{an} = 10.5\angle 0°$ V_{rms}, $\overline{V}_{bn} = 12.5\angle -120°$ V_{rms}, $\overline{V}_{cn} = 11.63\angle 111.43°$ V_{rms})

For unbalanced grid impedances and grid voltages, Table 4.41 and Figure 4.21 show that the source current magnitudes were nearly equal with a magnitude of about 1.4 A_{rms}. As shown in Table 4.42, the THD was reduced sharply to 2.3%. The 3rd, 5th and 7th harmonic orders amounts were decreased as shown in Table 4.43.

Table 4.41: Magnitudes of the source currents and the PCC voltage without and with the shunt APF.

$\|I_{sa}\|$,$\|I_{sb}\|$,$\|I_{sc}\|$ (A_{rms}) w/o APF	$\|I_{sa}\|$,$\|I_{sb}\|$,$\|I_{sc}\|$ (A_{rms}) w/ APF	$\|V_{ab}\|$ (V_{rms}) w/o APF	$\|V_{ab}\|$ (V_{rms}) w/ APF
0.98,1.2,1.1	1.38,1.4,1.38	19.8	19.7

Table 4.42: THD of the source current and the PCC voltage without and with the shunt APF.

THD of I_s w/o APF	THD of I_s w/ APF	THD of V_{ab} w/o APF	THD of V_{ab} w/ APF
2.2%	2.3%	2.4%	2.5%

Table 4.43: Harmonic analysis of the source current and PCC voltage without and with the shunt APF.

f (Hz)	I_s w/o APF	I_s w/ APF	V_{ab} w/o APF	V_{ab} w/ APF
180	0.83%	0.9%	1%	0.6%
300	1.31%	0.23%	1%	0.6%
420	0.8%	0.3%	0.4%	0.33%

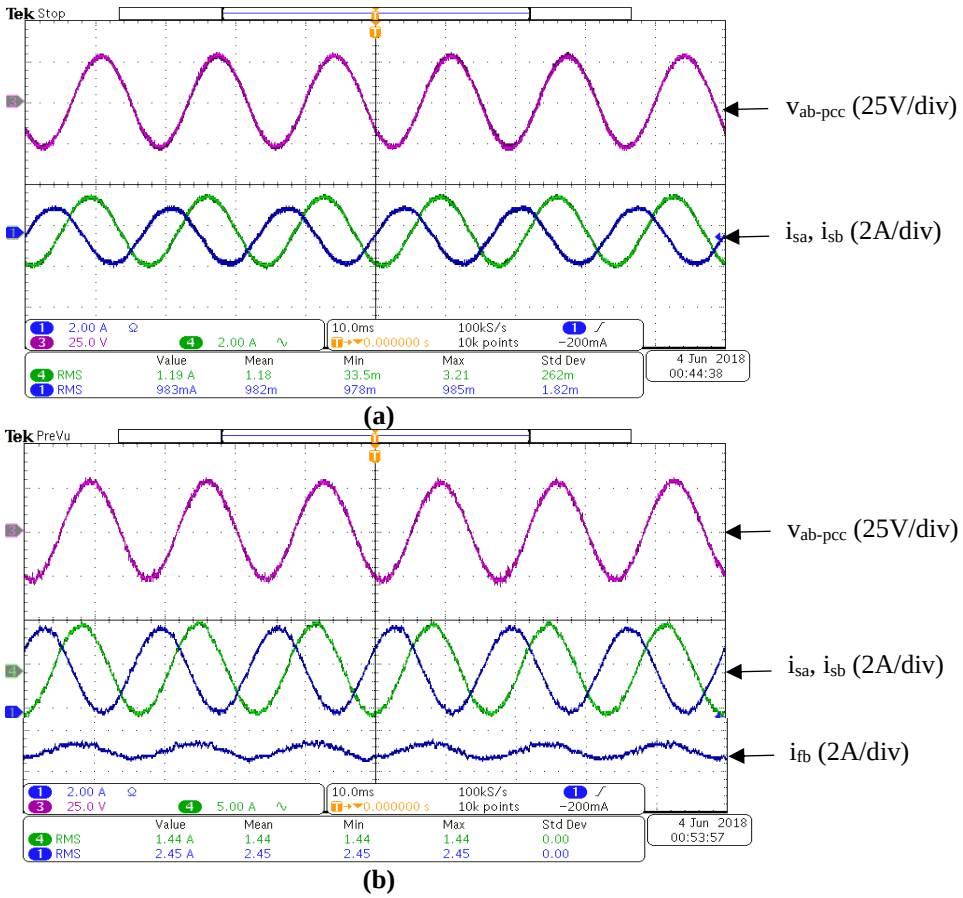

Figure 4.21: (a) $v_{ab\text{-}pcc}$, i_{sa} and i_{sb} without the filter. (b) $v_{ab\text{-}pcc}$, i_{sa}, i_{sb} and i_{fb} with the filter. (10ms/div)

For balanced grid voltages, three sets of balanced loads were used as seen in divisions A1 and A2. The pcc voltages and the source currents remained balanced with very small THD. Under unbalanced grid conditions, the source currents were balanced as shown in Figures 4.18, 4.19, 4.20 and 4.21. The results of *Case 4* show that the source currents were balanced sinusoidal under balanced and unbalanced conditions.

Case 5: Unbalanced linear resistive loads (25 Ω, 10 Ω, 10 Ω)

The configuration of this case is shown in Figure 4.17. This case consists of three divisions, which are A, B and C and based on the grid condition. In division A where the grid voltages were balanced, three different loads were tested in order to examine the effectiveness of the proposed

control method with big and small loads. Divisions B and C show the results when the grid conditions were unbalanced. The results were obtained with and without the shunt APF.

A. Balanced grid voltages

Table 4.44 and Figure 4.22 show that the source current magnitudes were balanced with a magnitude of 1 A_{rms}. The THD of the source current was low as shown in Table 4.45. The amount of the 3rd, 5th and 7th harmonic orders were also low as shown in Table 4.46.

Table 4.44: Magnitudes of the source currents and the PCC voltage without and with the shunt APF.

$\|I_{sa}\|,\|I_{sb}\|,\|I_{sc}\|$ (A_{rms}) w/o APF	$\|I_{sa}\|,\|I_{sb}\|,\|I_{sc}\|$ (A_{rms}) w/ APF	$\|V_{ab}\|$ (V_{rms}) w/o APF	$\|V_{ab}\|$ (V_{rms}) w/ APF
0.54,0.91,0.89	1,0.99,1	18.2	18

Table 4.45: THD of the source current and the PCC voltage without and with the shunt APF.

THD of I_s w/o APF	THD of I_s w/ APF	THD of V_{ab} w/o APF	THD of V_{ab} w/ APF
2.44%	3%	2.53%	3%

Table 4.46: Harmonic analysis of the source current and PCC voltage without and with the shunt APF.

f (Hz)	I_s w/o APF	I_s w/ APF	V_{ab} w/o APF	V_{ab} w/ APF
180	1.84%	1.66%	1.37%	0.77%
300	0.64%	0.57%	0.86%	0.8%
420	0.36%	0.24%	0.23%	0.42%

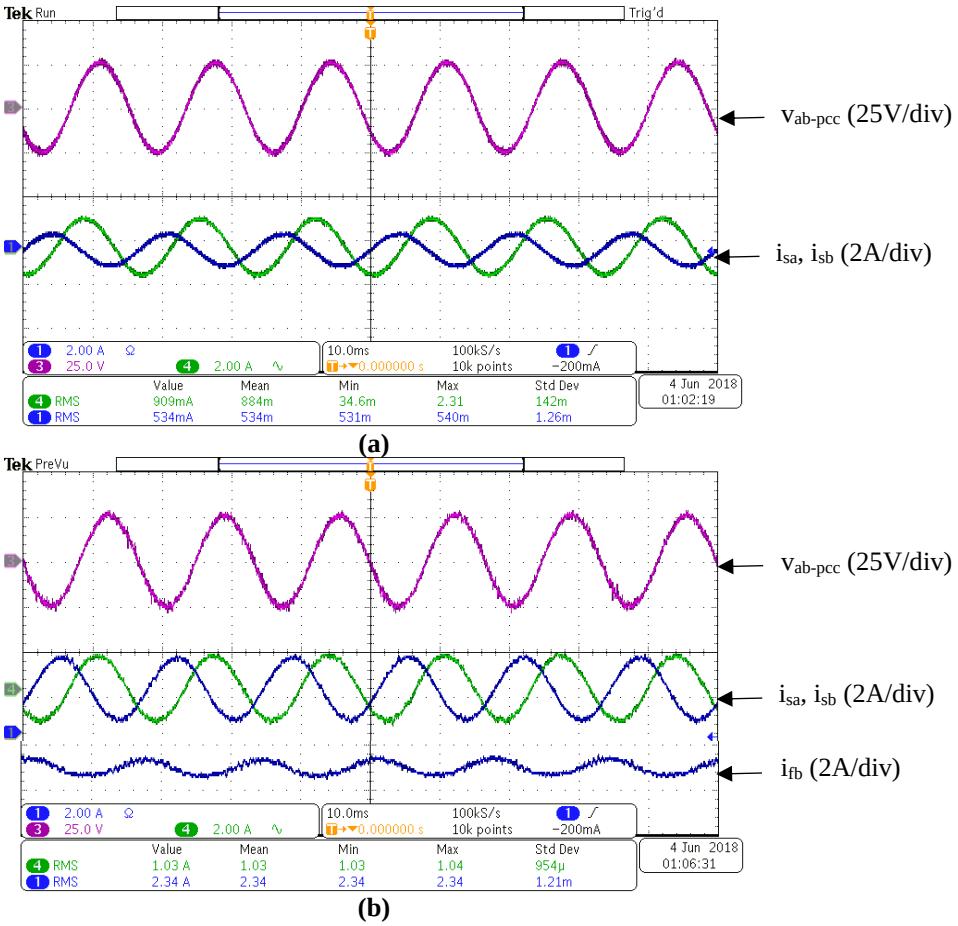

Figure 4.22: (a) $v_{ab\text{-}pcc}$, i_{sa} and i_{sb} without the filter. (b) $v_{ab\text{-}pcc}$, i_{sa}, i_{sb} and i_{fb} with the filter. (10ms/div)

B. Unbalanced grid impedance ($L_{ga} \approx 100$ µH, $L_{gb} \approx 700$ µH, $L_{gc} \approx 1000$ µH) and voltages ($\overline{V}_{an} = 10.5\angle 0°$ V_{rms}, $\overline{V}_{bn} = 12.5\angle -120°$ V_{rms}, $\overline{V}_{cn} = 11.63\angle 111.43°$ V_{rms})

Table 4.47 and Figure 4.23 (b) show that the source current magnitudes were balanced with a magnitude of about 1.2 A_{rms}. The THD of the source current was low as shown in Table 4.48. The amount of the 3rd, 5th and 7th harmonic orders were also low as shown in Table 4.49.

Table 4.47: Magnitudes of the source currents and the PCC voltage without and with the shunt APF.

$\|I_{sa}\|$,$\|I_{sb}\|$,$\|I_{sc}\|$ (A_{rms}) w/o APF	$\|I_{sa}\|$,$\|I_{sb}\|$,$\|I_{sc}\|$ (A_{rms}) w/ APF	$\|V_{ab}\|$ (V_{rms}) w/o APF	$\|V_{ab}\|$ (V_{rms}) w/ APF
0.51,1.13,1.18	1.15,1.2,1.18	18.1	17.8

Table 4.48: THD of the source current and the PCC voltage without and with the shunt APF.

THD of I_s w/o APF	THD of I_s w/ APF	THD of V_{ab} w/o APF	THD of V_{ab} w/ APF
2.77%	2.39%	2.39%	2.77%

Table 4.49: Harmonic analysis of the source current and PCC voltage without and with the shunt APF.

f (Hz)	I_s w/o APF	I_s w/ APF	V_{ab} w/o APF	V_{ab} w/ APF
180	2.29%	0.82%	1.36%	0.87%
300	0.72%	0.54%	0.63%	0.42%
420	0.2%	0.51%	0.27%	0.2%

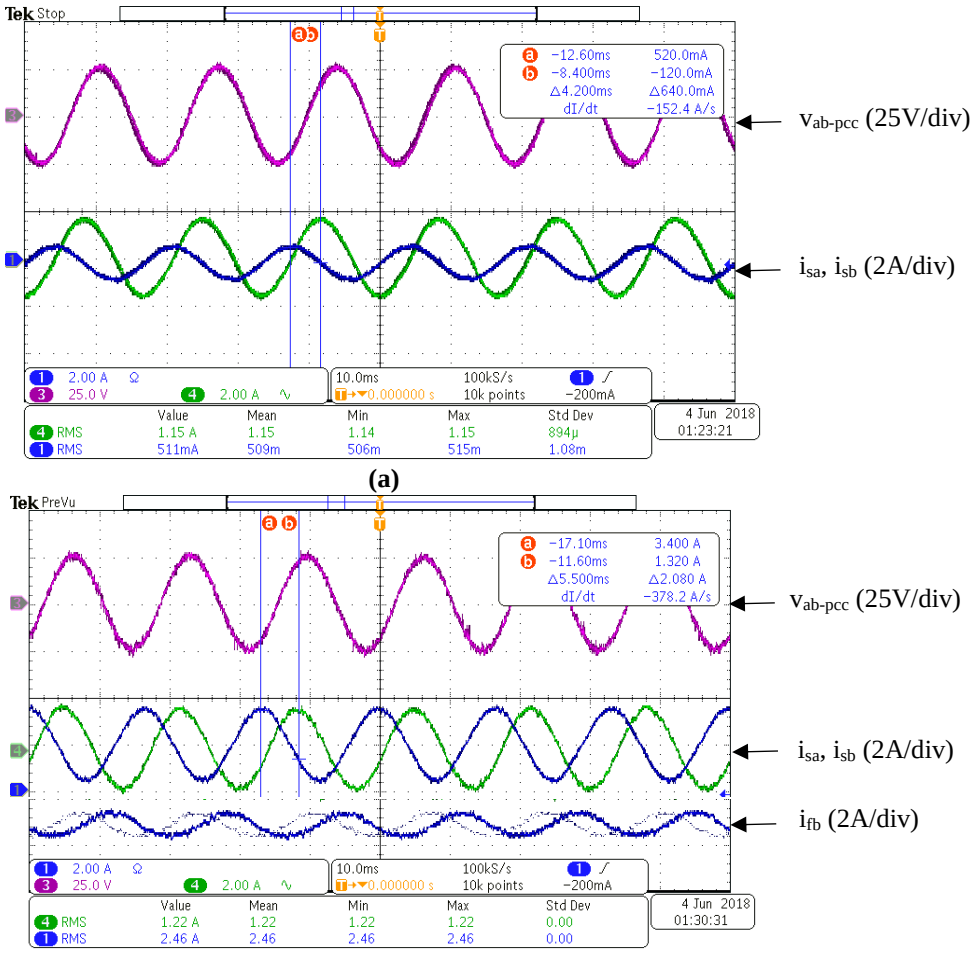

(a)

(b)

Figure 4.23: (a) $v_{ab\text{-}pcc}$, i_{sa} and i_{sb} without the filter. (b) $v_{ab\text{-}pcc}$, i_{sa}, i_{sb} and i_{fb} with the filter. (10ms/div)

For Case 5, unbalanced loads were tested under balanced and unbalanced grid conditions. Balanced source currents were obtained under all conditions. The THDs of the source currents

were less than 5%. Therefore, the shunt APF with the proposed control system operates effectively with unbalanced loads under balanced and unbalanced grid conditions.

Power factor analysis

The power factor (pf) was determined by the Tektronix oscilloscope to evaluate the performance of the shunt APF. It was determined for three load conditions and two grid voltage conditions. In all cases, the pf was almost unity when the proposed shunt APF was operating. The results are presented in Tables 4.50, 4.51, and 4.52.

Table 4.50: Power factor with balanced linear loads.

Balanced grid voltages		Unbalanced grid voltages	
Without the Shunt APF	With the Shunt APF	Without the Shunt APF	With the Shunt APF
0.988	0.99	0.993	0.993

Table 4.51: Power factor with unbalanced linear loads.

Balanced grid voltages		Unbalanced grid voltages	
Without the Shunt APF	With the Shunt APF	Without the Shunt APF	With the Shunt APF
0.993	0.992	0.992	0.991

Table 4.52: Power factor with nonlinear load.

Balanced grid voltages		Unbalanced grid voltages	
Without the Shunt APF	With the Shunt APF	Without the Shunt APF	With the Shunt APF
0.915	0.99	0.92	0.973

4.2.1 Summary

The proposed control method was applied to a system with different operating conditions. The experimental results have shown that the shunt APF with the proposed control method was able to inject three phase currents in order to cancel the unwanted components from the source currents. For all conditions, the source currents were balanced and had a very small THD value. The pcc voltages were maintained sinusoidal when the load was nonlinear. The power factor

achieved almost unity in all cases and conditions. The experimental results validated the simulation results. Therefore, the proposed control method is an effective control method for balanced and unbalanced power system conditions with the presence of harmonics.

4.3 Investigation of the proposed control method under frequency deviation

The purpose of this study was to test the response of the shunt APF with the proposed control method when the system frequency deviates from the nominal system frequency under balanced and unbalanced power system conditions. The system configuration is shown in Figure 4.17. For the study of the control methods, the frequency was set to five different values 58 Hz, 59 Hz, 60 Hz, 61 Hz and 62 Hz. For the frequency detection method, the frequency was selected as 40 Hz, 50 Hz, 60 Hz and 70 Hz. Three sets of results are presented to study and analyze the control system under system frequency variations. The proposed control method in the previous section was tested when the system frequency changed. The performance of utilizing the proposed system was determined by the magnitude of the source currents and the THD of the source currents. The results of the proposed frequency detection method was then provided. Finally, the study of the proposed frequency adaptive control method was presented in order to develop the performance of the shunt APF under a change of the system frequency.

4.3.1 Results of the proposed control method under frequency change

The results were obtained with and without the shunt APF to detect the response of the proposed control system under the frequency deviation. The system was evaluated under balanced and unbalanced conditions. The experimental system parameters are shown in Table 4.1. The unbalanced conditions include ULL (three unequal resistors as 25 Ω, 10 Ω, and 10 Ω) and unbalanced grid voltages which are $\overline{V}_{an}$=14∠0° V_{rms}, $\overline{V}_{bn}$= 11∠-110° V_{rms} , $\overline{V}_{cn}$= 10.5∠110° V_{rms}.

Table 4.53: Experimental results from changing the frequency without the shunt APF.

System condition	Without the shunt APF		
	f (Hz)	$\|I_{sa}\|,\|I_{sb}\|,\|I_{sc}\|$ (A_{rms})	$THD_{\%}$
Balanced system	58	1, 1, 1	2, 2, 2
	59	1, 1, 1	2, 2, 2
	60	1, 1, 1	2, 2, 2
	61	1, 1, 1	2, 2, 2
	62	1, 1, 1	2, 2, 2
Unbalanced system	58	0.56, 1, 1	2, 2, 2
	59	0.56, 1, 1	2, 2, 2
	60	0.56, 1, 1	2, 2, 2
	61	0.56, 1, 1	2, 2, 2
	62	0.56, 1, 1	2, 2, 2

Table 4.54: Experimental results from changing the frequency with the shunt APF.

System condition	With the shunt APF		
	f (Hz)	$\|I_{sa}\|,\|I_{sb}\|,\|I_{sc}\|$ (A_{rms})	$THD_{\%}$
Balanced system	58	1.33, 1.26, 1.24	1.5, 1.4, 1.5
	59	1.34, 1.3, 1.27	1.5, 1.4, 1.5
	60	1.33, 1.33, 1.33	1.4, 1.5, 1.5
	61	1.3, 1.34, 1.26	1.4, 1.4, 1.5
	62	1.27, 1.33, 1.25	1.7, 1.8, 1.6
Unbalanced system	58	1.17, 1.12, 1.05	1.4, 1.3, 1.4
	59	1.18, 1.15, 1.12	1.4, 1.6, 1.6
	60	1.18, 1.17, 1.17	1.4, 1.6, 1.5
	61	1.16, 1.18, 1.13	1.4, 1.7, 1.8
	62	1.13, 1.16, 1	1.3, 1.7, 1.8

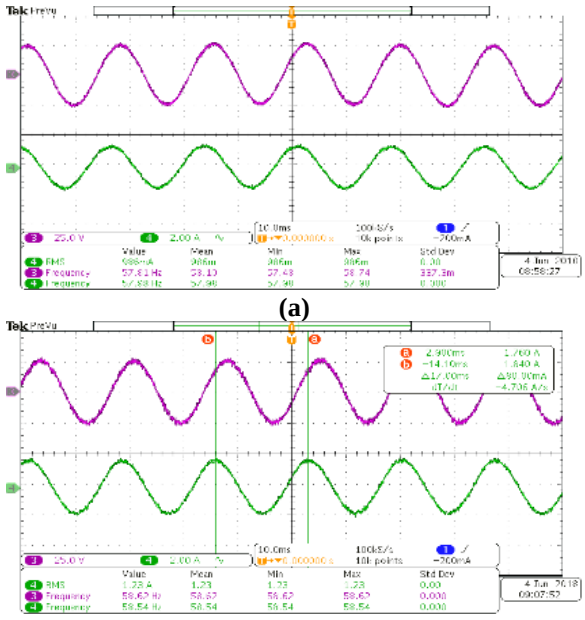

(a)

(b)

For balanced system at f=58 Hz, (a) $v_{ab\text{-}pcc}$ and i_{sb} without the shunt APF. (b) $v_{ab\text{-}pcc}$ and i_{sb} with the shunt APF.

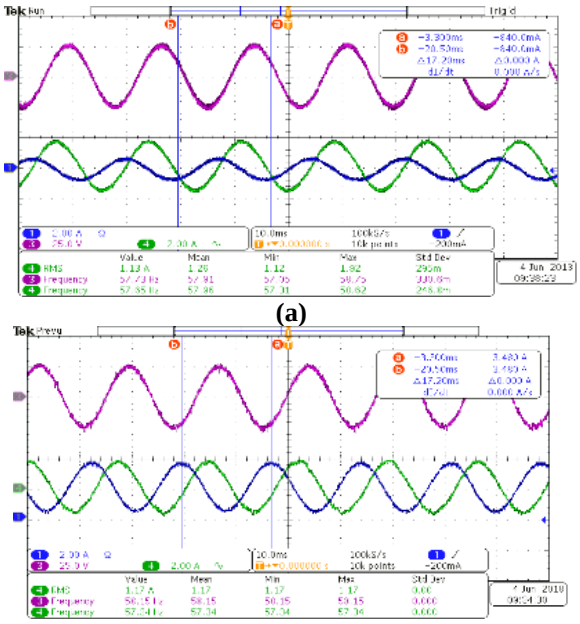

(a)

(b)

For unbalanced system at f=58 Hz, (a) $v_{ab\text{-}pcc}$, i_{sa} and i_{sb} without the shunt APF. (b) $v_{ab\text{-}pcc}$, i_{sa} and i_{sb} with the shunt APF.

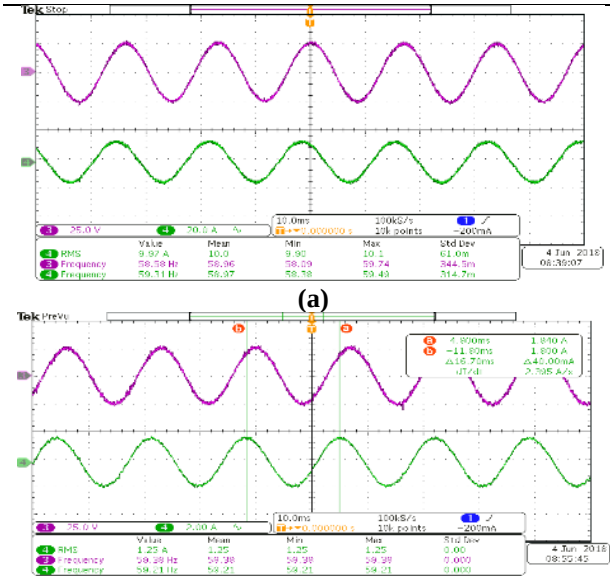

(a)

(b)

For balanced system at f=59 Hz, (a) $v_{ab\text{-}pcc}$ and i_{sb} without the shunt APF. (b) $v_{ab\text{-}pcc}$ and i_{sb} with the shunt APF.

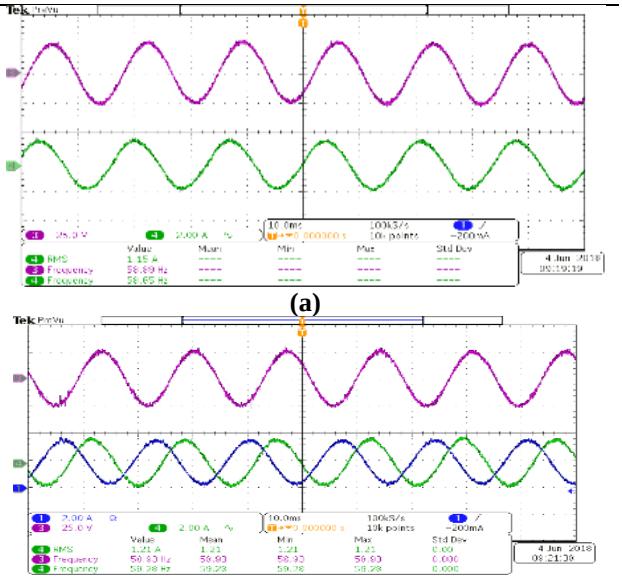

(a)

(b)

For unbalanced system at f=59 Hz, (a) $v_{ab\text{-}pcc}$, i_{sa} and i_{sb} without the shunt APF. (b) $v_{ab\text{-}pcc}$, i_{sa} and i_{sb} with the shunt APF.

Figure 4.24: Experimental results without and with the proposed control method for 58 Hz and 59 Hz when the system is balanced and unbalanced.

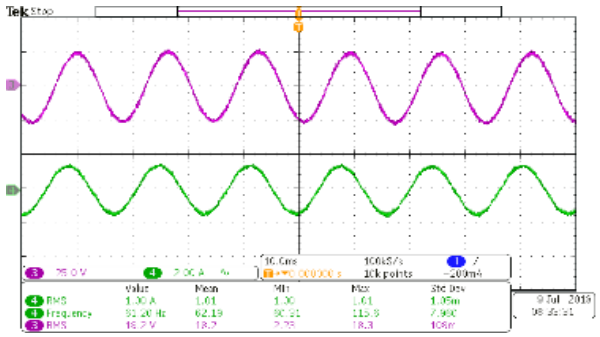

(a)

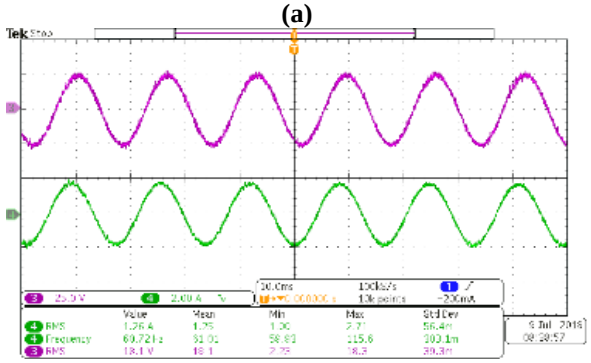

(b)

For balanced system at f=61 Hz, (a) $v_{ab\text{-}pcc}$ and i_{sb} without the shunt APF. (b) $v_{ab\text{-}pcc}$ and i_{sb} with the shunt APF.

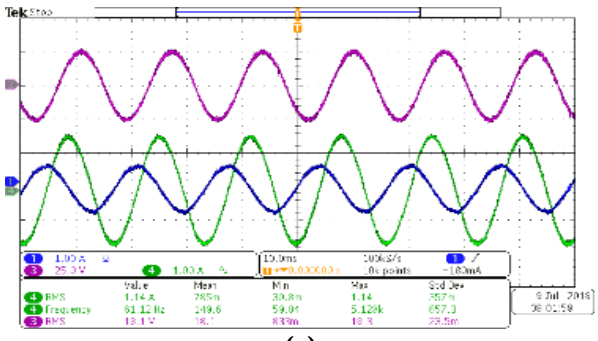

(a)

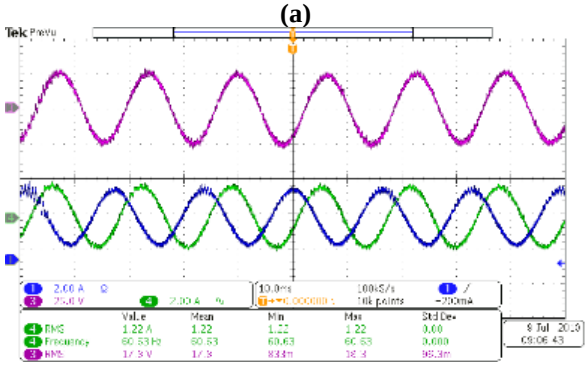

(b)

For unbalanced system at f=61 Hz, (a) $v_{ab\text{-}pcc}$, i_{sa} and i_{sb} without the shunt APF. (b) $v_{ab\text{-}pcc}$, i_{sa} and i_{sb} with the shunt APF.

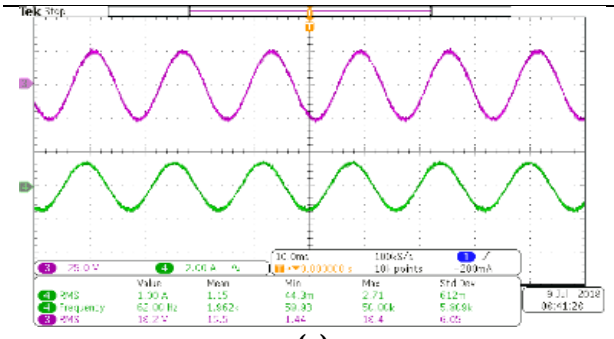

(a)

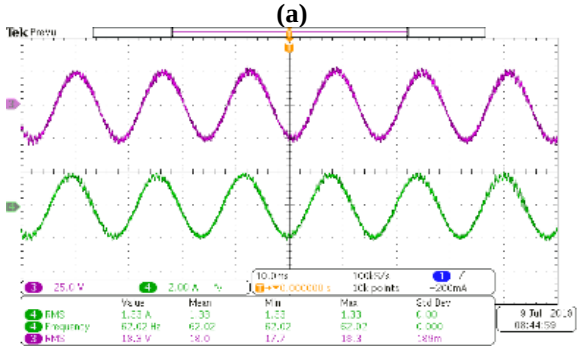

(b)

For balanced system at f=62 Hz, (a) $v_{ab\text{-}pcc}$ and i_{sb} without the shunt APF. (b) $v_{ab\text{-}pcc}$ and i_{sb} with the shunt APF.

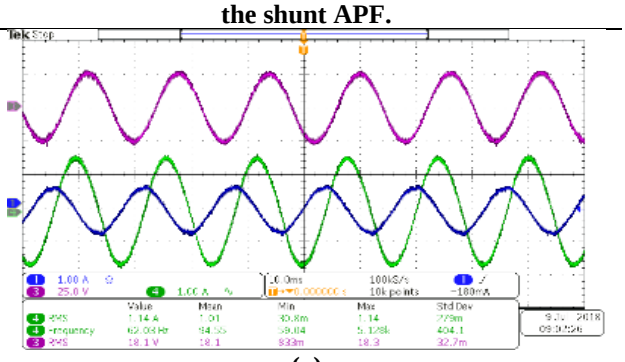

(a)

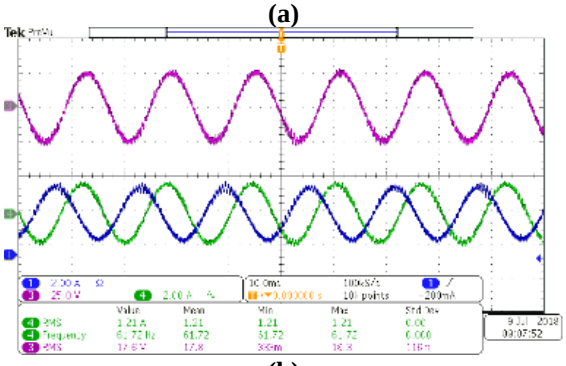

(b)

For unbalanced system at f=62 Hz, (a) $v_{ab\text{-}pcc}$, i_{sa} and i_{sb} without the shunt APF. (b) $v_{ab\text{-}pcc}$, i_{sa} and i_{sb} with the shunt APF.

Figure 4.25: Experimental results without and with the proposed control method for 61 Hz and 62 Hz when the system is balanced and unbalanced.

The experimental results show that the shunt APF with the proposed control method maintained sinusoidal currents as the frequency changes as shown in Figures 4.24 and 4.25. The source currents were almost balanced source currents under balanced and unbalanced power system conditions. However, the differences between the magnitudes of the source currents were enlarged as the frequency deviation increased as seen in Table 4.54. The THDs increased as the frequency deviation increased as shown in Table 4.53. Based on the above results the shunt APF shows acceptable performance under frequency variations, but it does not change the system frequency to the desired frequency of 60 Hz. The frequency fluctuated between the system frequency and the control system frequency.

4.3.2 Results of the proposed frequency detection method

The proposed frequency detection method was evaluated in software and in hardware. It employed a three-phase AC source. The frequency is set initially at 40 Hz. It was increased by 10 Hz until it reaches 70 Hz. The simulation is executed in 4 seconds where the frequency increases 10 Hz each second. The experimental results were obtained by increasing the source frequency manually by 10 Hz. The simulation and experimental outputs are shown in Figure 4.26. It can be seen from the results that the proposed detection method works properly. The response time of this method to the frequency change is about 0.2 sec.

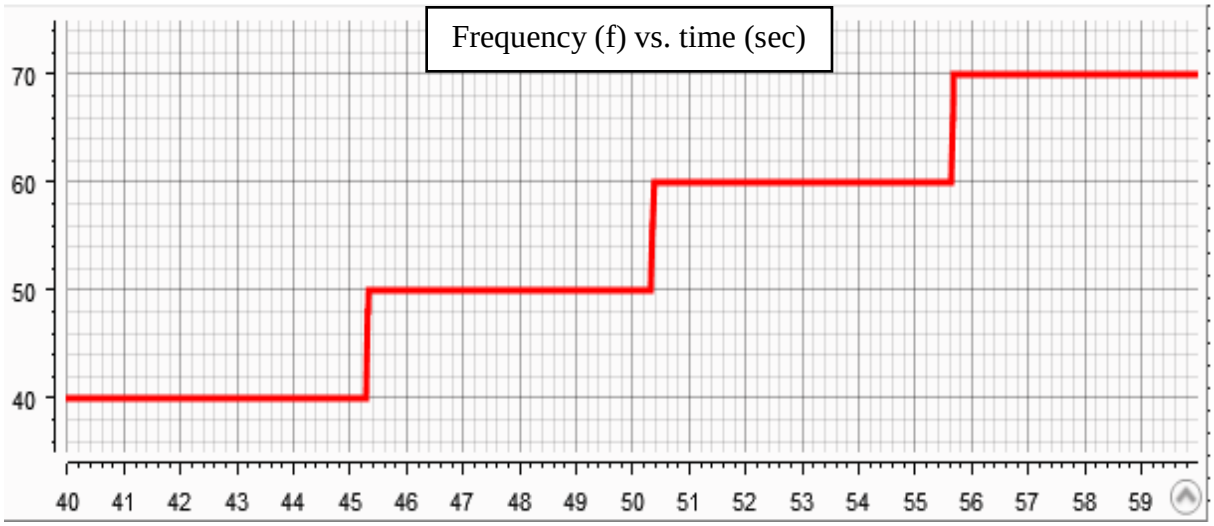

Figure 4.26: Experimental result of measuring the system frequency using the proposed frequency detection method.

4.3.3 Experimental results of the proposed frequency adaptive control method

The performance of the proposed frequency adaptive control method with the shunt APF can be determined from the experimental results. The experimental results are shown in Table 4.55 and Figures 4.27 and 4.28.

Table 4.55: Experimental results for the magnitude and the THD of the source current.

	f (Hz)	$\|I_s\|$ (A_{rms})	$THD_{\%}$
Balanced system	58	1.31, 1.33, 1.33	2, 2, 2
	59	1.32, 1.33, 1.32	2, 2, 2
	60	1.33, 1.33, 1.33	2, 2, 2
	61	1.33, 1.32, 1.32	2.1, 2.1, 2.1
	62	1.33, 1.31, 1.33	2, 2, 2
Unbalanced system	58	1.18, 1.17, 1.16	2, 2.2, 2.4
	59	1.18, 1.18, 1.17	2.2, 2.1, 2.2
	60	1.18, 1.17, 1.17	2, 2, 2
	61	1.17, 1.17, 1.17	1.9, 2.2, 2.2
	62	1.16, 1.17, 1.17	2, 2.1, 2

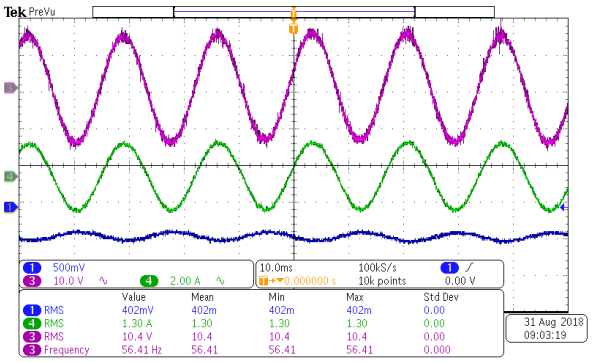

For balanced system: from top, v_{bn}, i_{sb} and i_{fb} when f= 58 Hz.

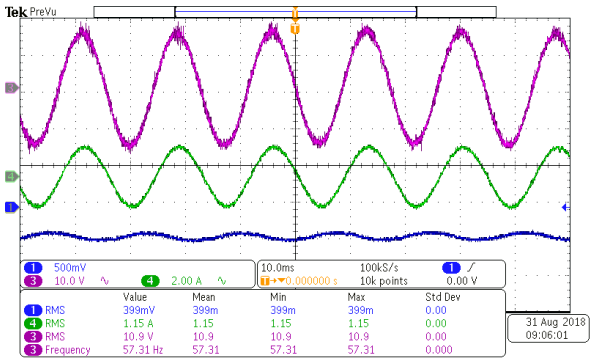

For unbalanced system: from top, v_{bn}, i_{sb} and i_{fb} when f= 58 Hz.

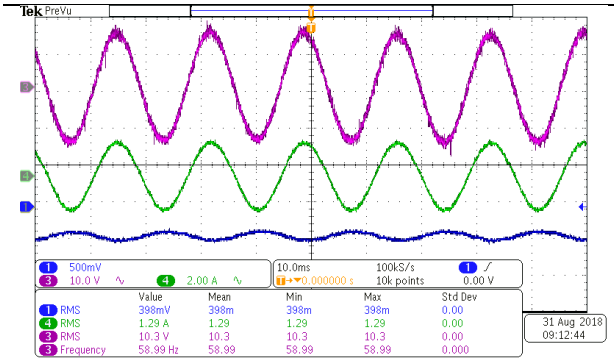

For balanced system: from top, v_{bn}, i_{sb} and i_{fb} when f= 59 Hz.

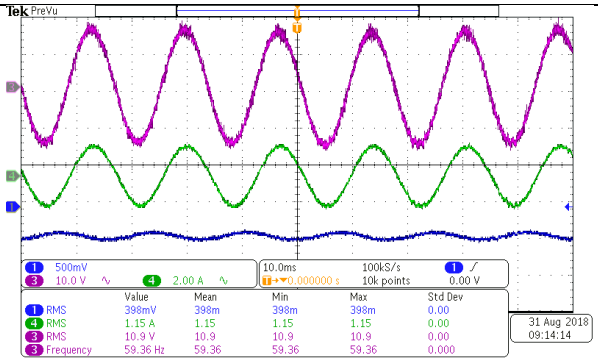

For unbalanced system: from top, v_{bn}, i_{sb} and i_{fb} when f= 59 Hz.

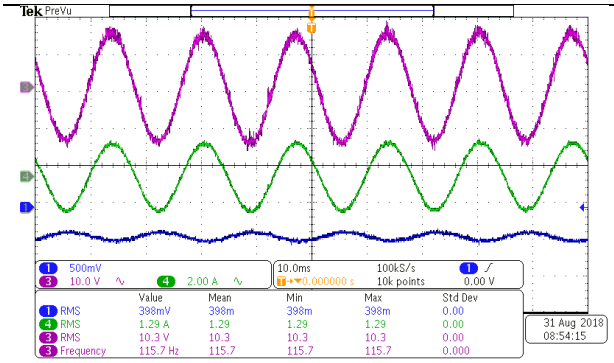

For balanced system: from top, v_{bn}, i_{sb} and i_{fb} when f= 60 Hz.

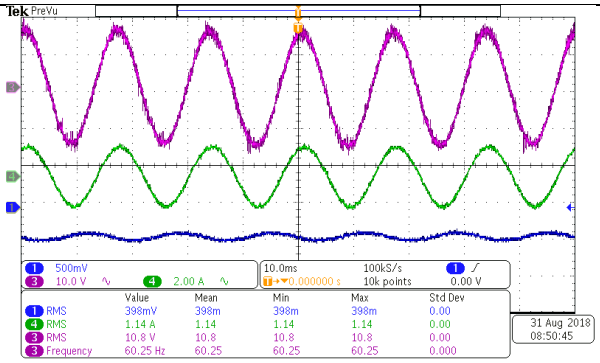

For unbalanced system: from top, v_{bn}, i_{sb} and i_{fb} when f= 60 Hz.

Figure 4.27: Experimental results of the proposed frequency adaptive control system for 58 Hz, 59 Hz, and 60 Hz.

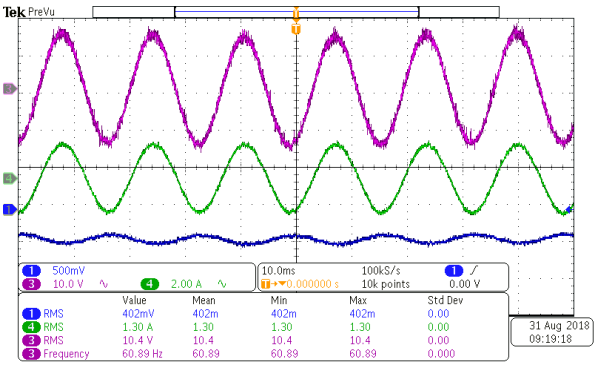

For balanced system: from top, v_{bn}, i_{sb} and i_{fb} when f= 61 Hz.

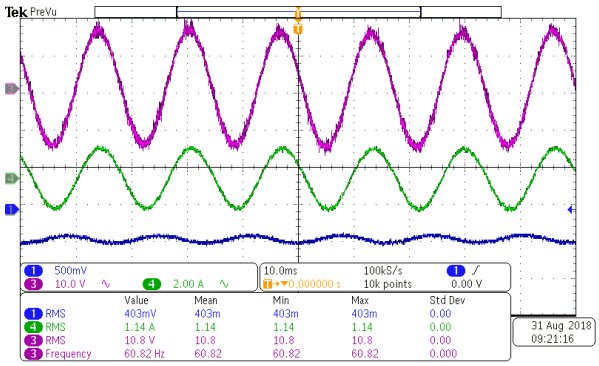

For unbalanced system: from top, v_{bn}, i_{sb} and i_{fb} when f= 61 Hz.

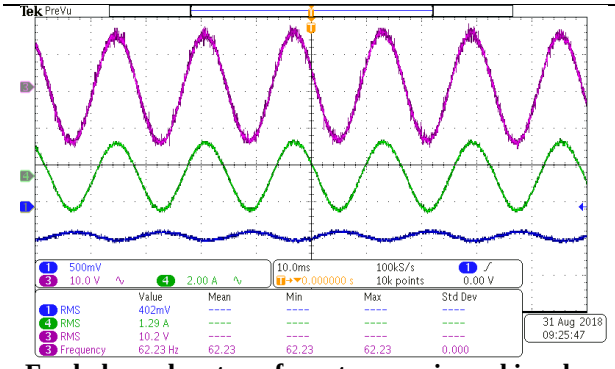

For balanced system: from top, v_{bn}, i_{sb} and i_{fb} when f= 62 Hz.

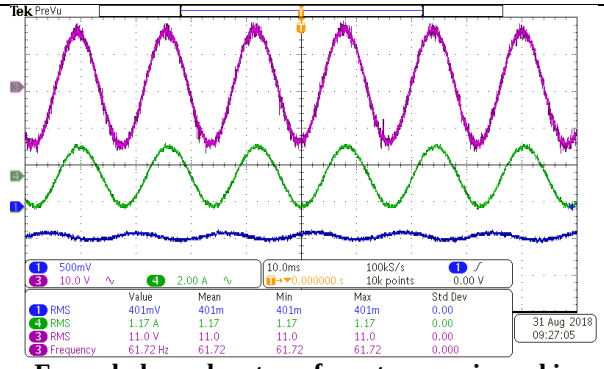

For unbalanced system: from top, v_{bn}, i_{sb} and i_{fb} when f= 62 Hz.

Figure 4.28: Experimental results of the proposed frequency adaptive control system for 61 Hz and 62 Hz.

The experimental results show that the shunt APF injected currents that eliminate the negative sequence components from currents as the frequency changes. The source currents were almost balanced under balanced and unbalanced power system conditions. The THDs were low for all cases. The shunt APF shows appropriate performance under frequency change.

4.4 Experimental Study of the Proposed Sensoless Control Method

The proposed sensorless control method was investigated for different power system conditions. Several experimental tests were undertaken to determine its performance. The outputs of the source currents were observed and analyzed to evaluate the feasibility of this method.

The experimental study was executed in several tests. These tests were undertaken under several conditions of the grid voltages and the loads. The loads have three conditions that are BLL,

ULL, and NL. The BLL consists of three 25 Ω resistors. The combination of the ULL is three unequal resistors of 25 Ω, 12.5 Ω, and 25 Ω. The NL has a resistor with a value of 25 Ω. Additionally, each load condition is tested under two grid conditions that are balanced grid voltages, where the magnitude of each phase is 10.5 V_{rms}, and unbalanced grid voltages which are $\overline{V}_{an}$=10.5∠0° V_{rms}, $\overline{V}_{bn}$= 11.5∠-110° V_{rms} , $\overline{V}_{cn}$= 13.5∠110° V_{rms}. The performance of the shunt APF was determined from the THD, the magnitudes of the source currents, and the power factor (pf).

System with Linear resistive loads:

A. Balanced loads

For balanced loads, the source currents were balanced with the shunt APF as shown in Table 4.56. Table 4.57 shows low THD of the source current with the shunt APF. The amount of 3rd, 5th and 7th harmonic orders were acceptable as shown in Table 4.58. The power factor was also found as shown in Table 4.59. The power factor was almost unity with the shunt APF. Figures 4.29 and 4.30 show that the waveforms for the source currents were balanced and sinusoidal under balanced and unbalanced grid voltages.

Table 4.56: Magnitudes of the source currents without and with the shunt APF

Balanced grid voltages		Unbalanced grid voltages	
$\|I_{sa}\|,\|I_{sb}\|,\|I_{sc}\|$ (A_{rms}) w/o shunt APF	$\|I_{sa}\|,\|I_{sb}\|,\|I_{sc}\|$ (A_{rms}) w/ shunt APF	$\|I_{sa}\|,\|I_{sb}\|,\|I_{sc}\|$ (A_{rms}) w/o shunt APF	$\|I_{sa}\|,\|I_{sb}\|,\|I_{sc}\|$ (A_{rms}) w/ shunt APF
0.42, 0.42, 0.42	1, 1, 1	0.39, 0.49, 0.52	1.1, 1.1, 1.2

Table 4.57: THD of I_s without and with the shunt APF.

Balanced grid voltages		Unbalanced grid voltages	
THD w/o shunt APF	THD w/ shunt APF	THD w/o shunt APF	THD w/ shunt APF
3.33%	2.72%	3.4%	3.68%

Table 4.58: Harmonic analysis of the source current without and with the shunt APF.

	Balanced grid voltages		Unbalanced grid voltages	
f (Hz)	% of fundamental w/o shunt APF	% of fundamental w/ shunt APF	% of fundamental w/o shunt APF	% of fundamental w/ shunt APF
180	1.66%	1.25%	1.46%	2.16%
300	0.67%	1.07%	0.8%	0.6%
420	0.43%	0.1%	0.18%	0.47%

Table 4.59: Power factor without and with the shunt APF

Balanced grid voltages		Unbalanced grid voltages	
Without shunt APF	With shunt APF	Without shunt APF	With shunt APF
0.993	0.99	0.996	0.994

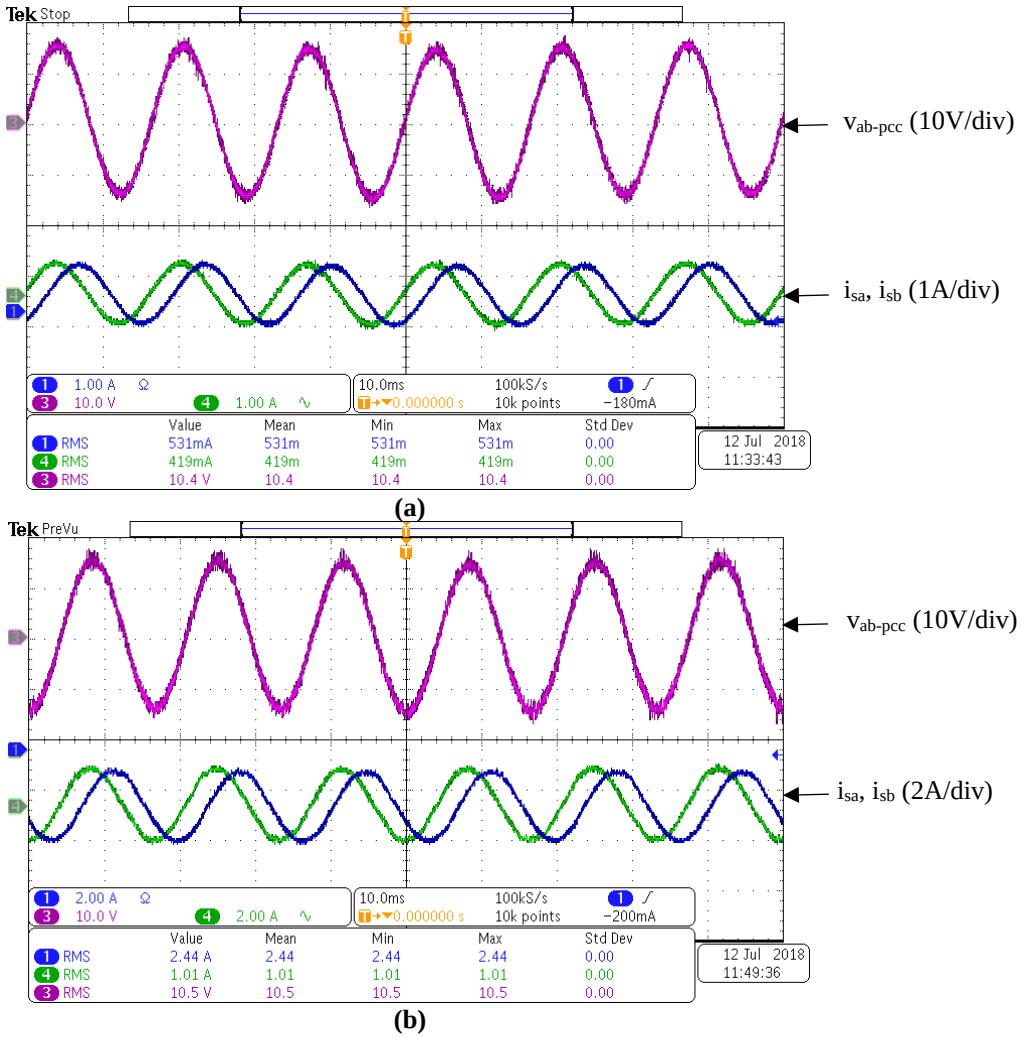

Figure 4.29: For balanced voltages: (a) $v_{bn\text{-}pcc}$ i_{sa} and i_{sb} without the shunt APF. (b) $v_{bn\text{-}pcc}$,i_{sa} and i_{sb} with the shunt APF. (10ms/div)

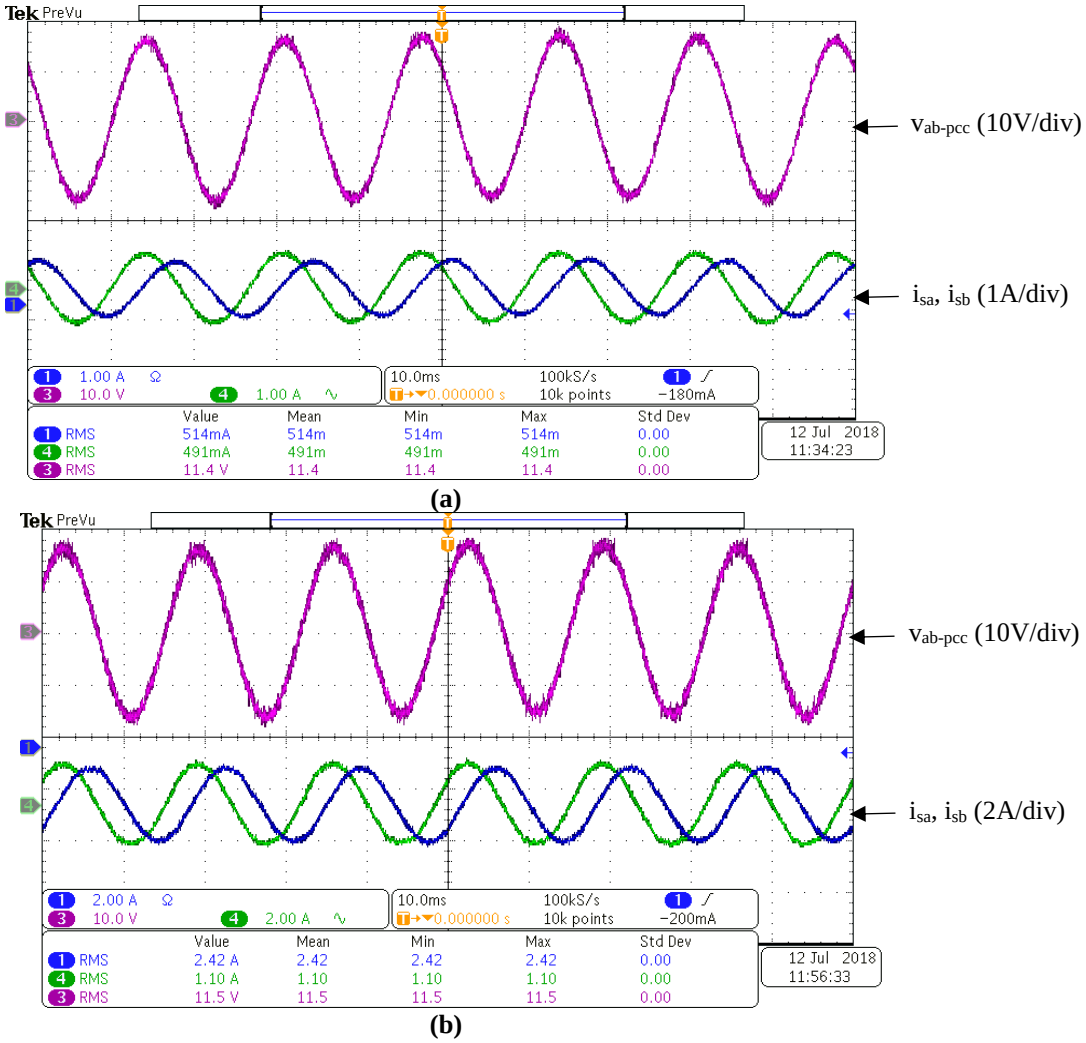

Figure 4.30: For unbalanced voltages: (a) $v_{bn\text{-}pcc}$ i_{sa} and i_{sb} without the shunt APF. (b) $v_{bn\text{-}pcc}$,i_{sa} and i_{sb} with the shunt APF. (10ms/div)

B. Unbalanced loads

For unbalanced loads, the source current magnitudes were nearly equal with the shunt APF as shown in Table 4.60. Table 4.61 shows low THD of the source current with the shunt APF. The amount of 3rd, 5th and 7th harmonic orders were acceptable as shown in Table 4.62. The power factor was almost unity with the shunt APF as shown in Table 4.63. The waveforms the source currents were balanced and sinusoidal under balanced and unbalanced grid voltages as seen in Figures 4.31 and 4.32.

Table 4.60: Magnitudes of the source currents with and without the shunt APF

Balanced grid voltages		Unbalanced grid voltages	
$\|I_{sa}\|,\|I_{sb}\|,\|I_{sc}\|$ (A_{rms}) w/o shunt APF	$\|I_{sa}\|,\|I_{sb}\|,\|I_{sc}\|$ (A_{rms}) w/ shunt APF	$\|I_{sa}\|,\|I_{sb}\|,\|I_{sc}\|$ (A_{rms}) w/o shunt APF	$\|I_{sa}\|,\|I_{sb}\|,\|I_{sc}\|$ (A_{rms}) w/ shunt APF
0.48, 0.62, 0.47	1.1, 1.1, 1	0.45, 0.72, 0.61	1.2, 1.1, 1.2

Table 4.61: THD of I_s without and with the shunt APF.

Balanced grid voltages		Unbalanced grid voltages	
THD w/o shunt APF	THD w/ shunt APF	THD w/o shunt APF	THD w/ shunt APF
2.85%	3.26%	2.49%	2.61%

Table 4.62: Harmonic analysis of the source current without and with the shunt APF.

	Balanced grid voltages		Unbalanced grid voltages	
f (Hz)	% of fundamental w/o shunt APF	% of fundamental w/ shunt APF	% of fundamental w/o shunt APF	% of fundamental w/ shunt APF
180	1.13%	2%	0.618%	0.36%
300	0.74%	0.94%	0.48%	1.1%
420	0.62%	0.51%	0.35%	0.9%

Table 4.63: Power factor without and with the shunt APF

Balanced grid voltages		Unbalanced grid voltages	
Without shunt APF	With shunt APF	Without shunt APF	With shunt APF
0.994	0.995	0.996	0.997

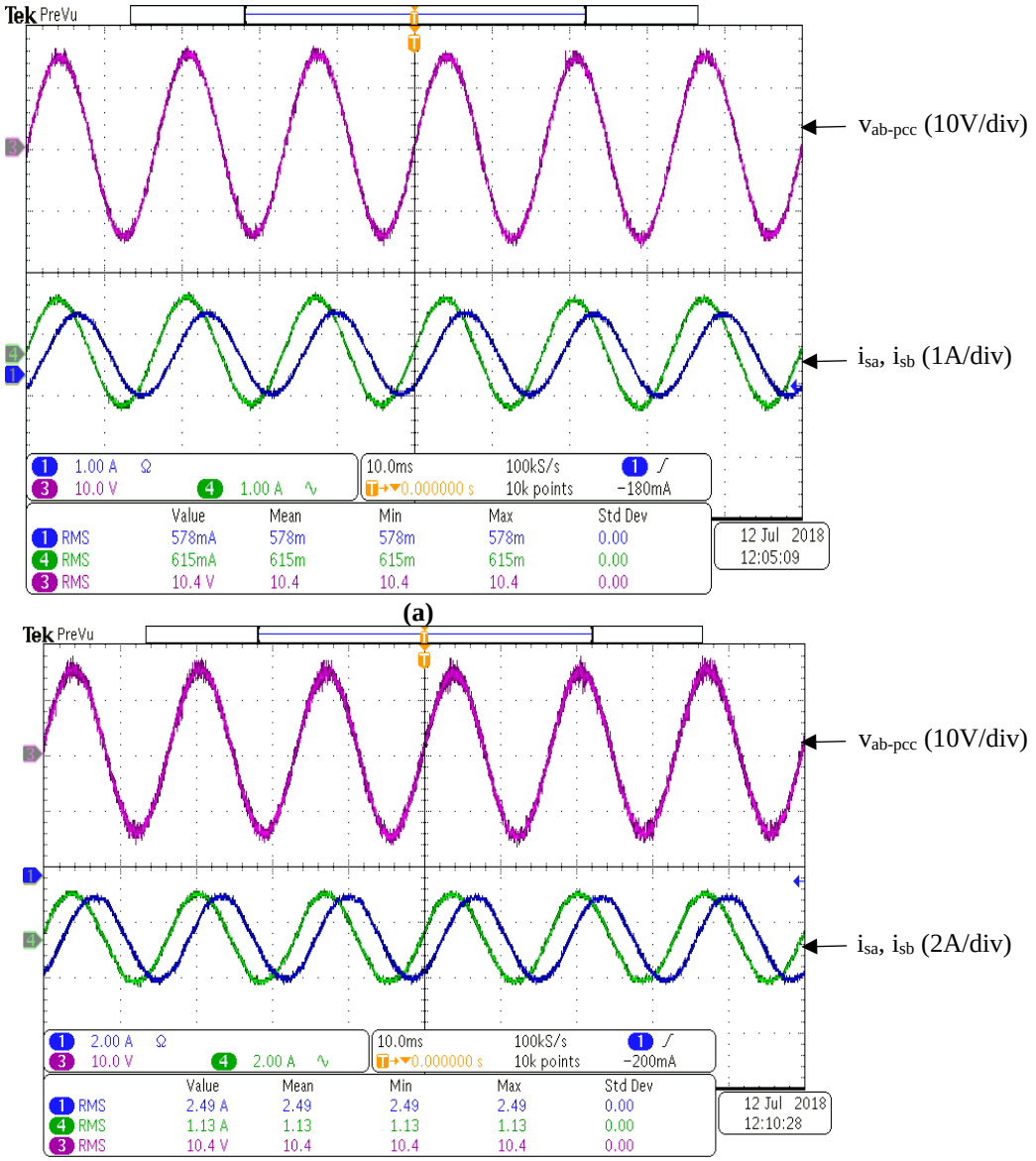

Figure 4.31: For balanced voltages: (a) $v_{bn\text{-}pcc}$ i_{sa} and i_{sb} without the shunt APF. (b) $v_{bn\text{-}pcc}$,i_{sa} and i_{sb} with the shunt APF. (10ms/div)

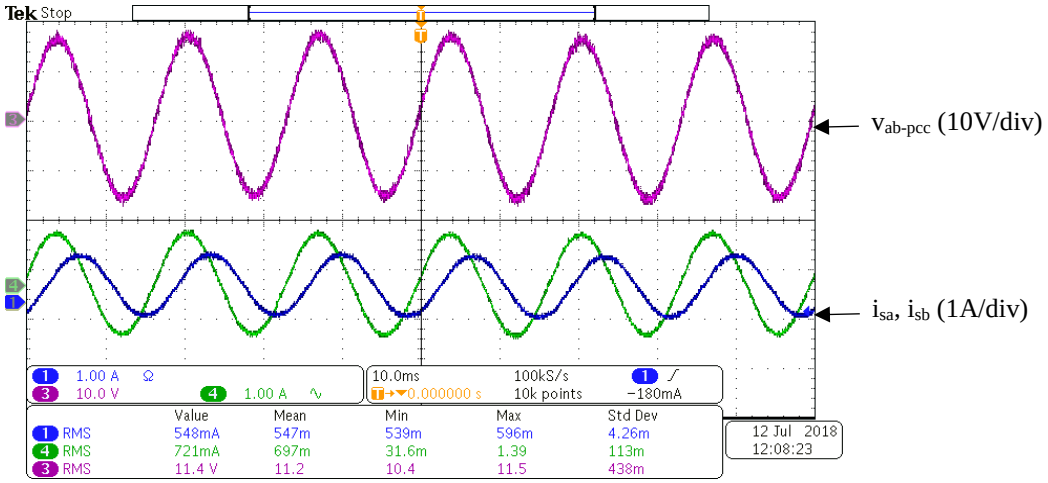

(a)

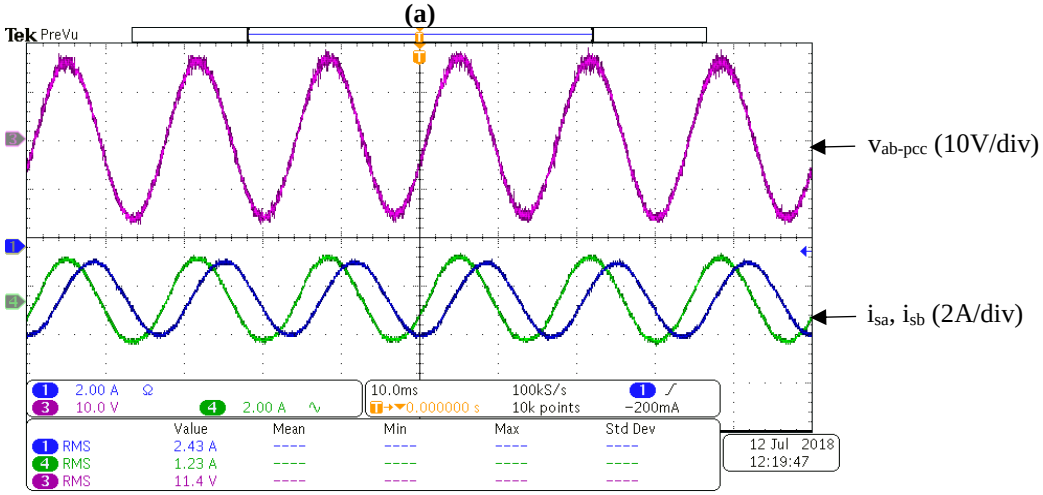

(b)

Figure 4.32: For unbalanced voltages: (a) $v_{bn\text{-}pcc}$ i_{sa} and i_{sb} without the shunt APF. (b) $v_{bn\text{-}pcc}$,i_{sa} and i_{sb} with the shunt APF. (10ms/div)

System with nonlinear load:

The source current magnitudes were balanced with the shunt APF and nonlinear load as shown in Table 4.64. The THD of the source current with the shunt APF was low as shown in Table 4.65. The 3rd, 5th and 7th harmonics were satisfactory as shown in Table 4.66. The power factors were about 0.98 under balanced and unbalanced grid voltages with the shunt APF as shown in Table 4.67. The waveforms for the source currents were balanced and sinusoidal under balanced and unbalanced grid voltages as seen in Figures 4.33 and 4.34.

Table 4.64: Magnitudes of the source currents with and without the shunt APF

Balanced grid voltages		Unbalanced grid voltages	
$\|I_{sa}\|,\|I_{sb}\|,\|I_{sc}\|$ (A_{rms}) w/o shunt APF	$\|I_{sa}\|,\|I_{sb}\|,\|I_{sc}\|$ (A_{rms}) w/ shunt APF	$\|I_{sa}\|,\|I_{sb}\|,\|I_{sc}\|$ (A_{rms}) w/o shunt APF	$\|I_{sa}\|,\|I_{sb}\|,\|I_{sc}\|$ (A_{rms}) w/ shunt APF
0.67, 0.67, 0.67	1, 1, 1	0.67, 0.79, 0.86	1.1, 1.1, 1.05

Table 4.65: THD of I_s without and with the shunt APF.

Balanced grid voltages		Unbalanced grid voltages	
THD w/o shunt APF	THD w/ shunt APF	THD w/o shunt APF	THD w/ shunt APF
18.6%	4.96%	20.4%	5.13%

Table 4.66: Harmonic analysis of the source current without and with the shunt APF.

	Balanced grid voltages		Unbalanced grid voltages	
f (Hz)	% of fundamental w/o shunt APF	% of fundamental w/ shunt APF	% of fundamental w/o shunt APF	% of fundamental w/ shunt APF
180	0.94%	1.79%	11.3%	2.17%
300	17.4%	2.47%	15%	2.98%
420	5.26%	1.27%	6.74%	1.37%

Table 4.67: Power factor without and with the shunt APF

Balanced grid voltages		Unbalanced grid voltages	
Without shunt APF	With shunt APF	Without shunt APF	With shunt APF
0.92	0.98	0.912	0.977

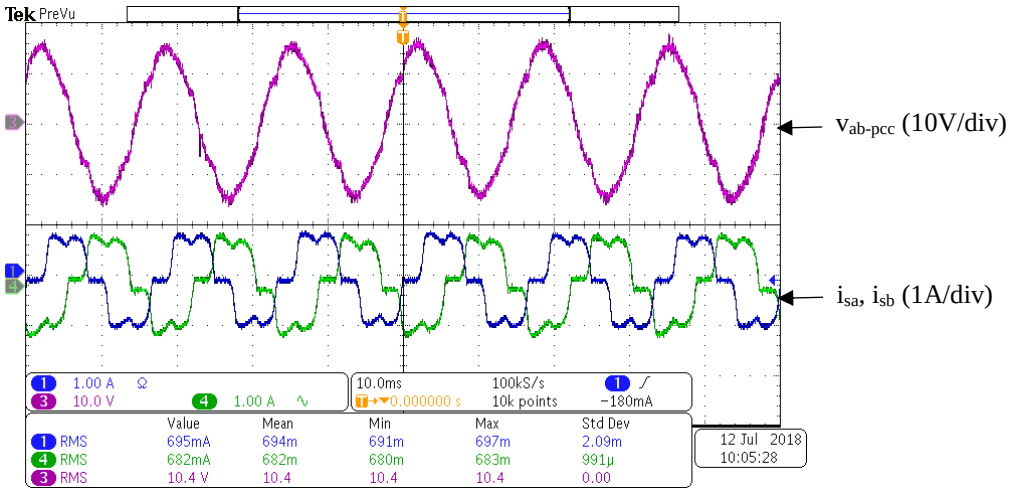

(a)

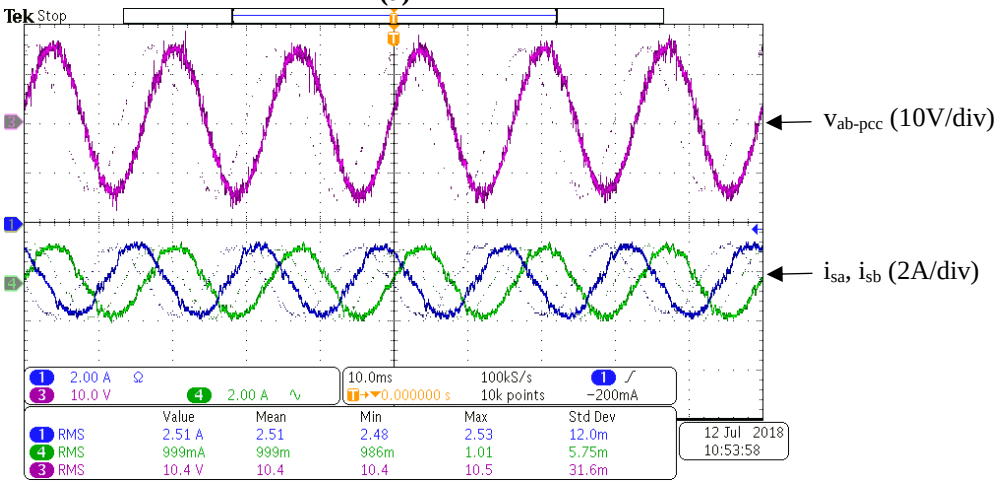

(b)

Figure 4.33: For balanced voltages: (a) $v_{bn\text{-}pcc}$ i_{sa} and i_{sb} without the shunt APF. (b) $v_{bn\text{-}pcc}$,i_{sa} and i_{sb} with the shunt APF. (10ms/div)

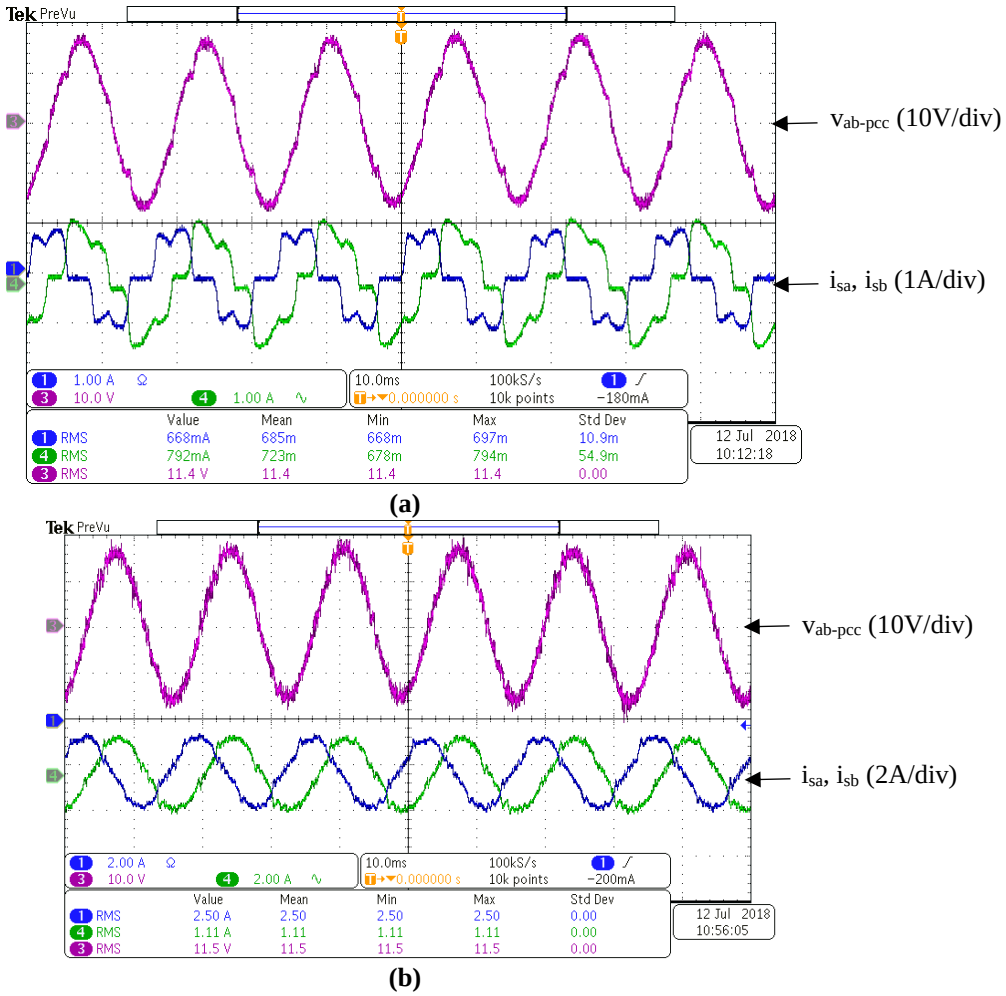

Figure 4.34: For unbalanced voltages: (a) $v_{bn\text{-}pcc}$ i_{sa} and i_{sb} without the shunt APF. (b) $v_{bn\text{-}pcc}$,i_{sa} and i_{sb} with the shunt APF. (10ms/div)

The experimental results show that the harmonics in the source current have been reduced. Under different grid voltage and load conditions, the THD of the source current was satisfactory. The magnitudes of the source currents were balanced with low UB ratio under unbalanced conditions of the source voltage and loads. The power factor was almost unity for all cases. For that, the shunt APF with the proposed sensorless control method operated suitably under different power system conditions.

4.4.1 Summary

The proposed PCC voltage sensorless control method was employed to eliminate the power quality problems related to the source currents. Experimental results have shown that the filtered source currents had balanced sinusoidal waveforms. For all conditions, the source currents had a THD value less than 5%. The magnitudes of the source currents were nearly balanced. The harmonics in the PCC voltages were also eliminated when the load is nonlinear. The experimental results validate the simulation results. Therefore, the proposed control method is a suitable control method for balanced and unbalanced power system conditions with the presence of harmonics.

CHAPTER 5: FUTURE PLAN AND CONCLUSION

5.1 Conclusion

The increase of power electronics devices on the grid and the variable nature of the loads can lead to serious disturbances on power system. Passive and active filters are used to solve power quality problems, especially harmonics. With the increase of the number of the harmonic orders, passive filters are insufficient solutions because of their large size, resonance, and fixed compensation behaviors. Active power filters have been employed because they are adjustable with the system conditions in terms of harmonic elimination and reactive power compensation. A proper and suitable control system of shunt APFs are very important to eliminate power quality problems related to source current.

Among several control methods, instantaneous reactive power theory (IRPT) is a well-known method in the field of controlling shunt APFs. It has a suitable performance and a simple implementation. But, it has poor performance under unbalanced power system conditions. Moreover, the extraction of the positive sequence components and negative sequence components has an important role in the control system of shunt APF. Traditionally, low-pass filters (LPF), high-pass filters (HPF), and a phase-locked loop (PLL) are used for extracting the harmonic components. However, these devices cause some issues which degrade the performance of the control system.

The main purpose of this research is to design and build a control system that is able to operate properly under balanced and unbalanced power system conditions with and without the presence of the harmonics. For that, a new positive and negative sequence components filter was designed and analyzed. It is intended to separate the positive sequence components from three-

phase quantities under any power system conditions. This filter produces balanced three-phase quantities, which are utilized with IRPT. This allows the elimination of other types of filters and PLL. Algorithm analyses demonstrated the operation of the control system. The simulation and experimental results show that the source currents were balanced and sinusoidal under ideal and non-ideal power system conditions. For that, the shunt APF with the proposed control system has been successfully demonstrated. Additionally, the control system was tested under different values of the system frequency. The results show that the control system was able to handle different values of the frequency. The differences between the source current magnitudes increased as the frequency deviation increased. The frequency of the source currents under frequency deviation followed the system frequency not the filter frequency, which is 60 Hz.

The consideration of the system frequency in controlling shunt APFs is important to guarantee suitable operation and synchronization of APFs. Variations in the frequency could cause adverse impacts to the control system and the power system. Therefore, these variations should be controlled in order to obtain stable and proper performance of the system. A frequency detection technique with the proposed filter was evaluated in simulation and in experiment. It shows its ability to measure the frequency with a wide range. Then, it was added to the proposed control system in order to overcome the issues of the frequency variations. The simulation results show the new control system adapted the system frequency. From the experimental results, the frequency of the proposed filter was adjusted to be similar to the system frequency. The results show effective operation under frequency change.

Conventional control systems require information of the voltage magnitude and phase. However, some control techniques can be mathematically modified that allows reducing or eliminating a number of sensors. Therefore, it is possible to perform sensorless control systems.

This can offer some advantages such as eliminating sensor offset, resolution limitation and sensor noise, robustness against sensor failures, improving the system reliability and lowering the costs. For that, a voltage sensorless control method was proposed in this thesis. It is purposed to generate the reference current signals without sensing the grid voltages. It is mainly depends on the proposed positive and negative sequence filter to generated the reference signals. The simulation and experimental results show that this method is compatible under different power system condition.

The results show that the proposed control techniques operate suitbly under ideal and non-ideal grid and load conditions. The following points summarize the operation of the proposed techniques:

- Generating the fundamental components by extracting the positive sequence in any grid or load conditions.
- Generating the negative sequence components to balance the source currents and to compensate for the harmonics.
- Generating the reactive components to compensate for the reactive power.
- No need for PLL.
- No dq transformation needed.
- Adequate performance in steady state and in transient.
- No phase delay at fundamental frequency.
- Reducing the calculations greatly.
- Easy to implement in digital controllers.

5.2 Future Plan

The research and work in this dissertation have given new ideas for future work regarding power quality problems and controlling APFs. Future research can be performed in the following areas:

- Comparing the performance of available positive sequence components detection and reference signal generation methods with the proposed sequence component detection and control method.
- Applying the proposed control system to a renewable energy system such as a PV system.
- Investigating the operation of the proposed control system in a weak grid.
- Estimating voltage of sensorless control.
- Applying the proposed filter to different control strategies.
- Investigating the work of the proposed control with some modifications for series APFs.
- Applying other frequency detection techniques to the proposed control system for comparison purposes.

REFERENCE

[1] Ali A., Aydin S., "Designing, Modeling, and Simulating a Single-phase Active Power Filter for Harmonic Compensation and Reactive Power" *Bulletin of Environment, Pharmacology and Life Sciences, 2014 Academy for Environment and Life Sciences*, India, Vol. 4, pp 80-89.

[2] P. Neves, D. Gonçalves, J. G. Pinto, R. Alves and J. L. Afonso, "Single-phase Shunt Active Filter interfacing renewable energy sources with the power grid," *Industrial Electronics, 2009. IECON '09. 35th Annual Conference of IEEE*, Porto, Portugal, 2009, pp. 3264-3269.

[3] F. Pottker de Souza and I. Barbi, "Single-phase active power filters for distributed power factor correction," *2000 IEEE 31st Annual Power Electronics Specialists Conference. Conference Proceedings (Cat. No.00CH37018)*, Galway, Ireland, 2000, pp. 500-505 vol.1.

[4] S. Biricik, S. Redif, O. C. Ozerdem and M. Basu, "Control of the shunt Active Power Filter under non-ideal grid voltage and unbalanced load conditions," *Power Engineering Conference (UPEC), 2013 48th International Universities*, Dublin, Ireland, 2013, pp. 1-5.

[5] S. Biricik, S. Redif, Ö C. Ozerdem, S. K. Khadem and M. Basu, "Real-time control of shunt active power filter under distorted grid voltage and unbalanced load condition using self-tuning filter," *IET Power Electronics*, vol. 7, no. 7, pp. 1895-1905, July 2014.

[6] T. Demirdelen, M. İnci, K. Ç. Bayindir and M. Tümay, "Review of hybrid active power filter topologies and controllers," *4th International Conference on Power Engineering, Energy and Electrical Drives*, Istanbul, Turkey, 2013, pp. 587-592.

[7] A. Mortezaei, C. Lute, M. G. Simões, F. P. Marafão and A. Boglia, "PQ, DQ and CPT control methods for shunt active compensators — A comparative study," *2014 IEEE Energy Conversion Congress and Exposition (ECCE)*, Pittsburgh, PA, 2014, pp. 2994-3001.

[8] S. Khalid, B. Dwivedi and V. M. Mishra, "Constant instantaneous power based controller for a shunt active power filter under balanced, unbalanced, and distorted supply conditions," *Computing, Communication & Automation (ICCCA), 2015 International Conference*, Noida, India, 2015, pp. 963-967.

[9] N. Gupta, S. P. Singh and S. P. Dubey, "Neural network based shunt active filter for harmonic and reactive power compensation under non-ideal mains voltage," *2010 5th IEEE Conference on Industrial Electronics and Applications*, Taichung, Taiwan, 2010, pp. 370-375.

[10] "IEEE Recommended Practice and Requirements for Harmonic Control in Electric Power Systems," *IEEE Std 519-2014 (Revision of IEEE Std 519-1992)*, vol., no., pp.1-29, 11 June 2014.

[11] A. Teke, "Unified power quality conditioner: design, simulation and experimental analysis," PhD dissertation, University Of Cukurova, Institute of natural and applied science, Adana, Turkey, 2011.

[12] "Definitions of Voltage Unbalance," *IEEE Power Engineering Review*, vol. 22, no. 11, pp. 49-50, Nov. 2002.

[13] "IEEE Recommended Practice for Electric Power Distribution for Industrial Plants," *IEEE Std 141-1993*, pp.1-768, April 29 1994.

[14] P. Pillay and M. Manyage, "California Electricity Situation," *IEEE Power Engineering Review*, vol. 21, no. 5, pp. 10-12, May 2001.

[15] R. K. Varma, R. M. Mathur, G. J. Rogers and P. Kundur, "Modeling effects of system frequency variation in long-term stability studies," *IEEE Transactions on Power Systems*, vol. 11, no. 2, pp. 827-832, May 1996.

[16] R. Verma, P. Sahu, "Frequency fluctuation in power system: sources, control and minimizing techniques," *International Journal of Advanced Research in Electrical, Electronics and Instrumentation Engineering (IJAREEIE),* Vol. 3, No. 8, Aug 2014.

[17] M. Kmail, "Investigation of shunt active power filter for power quality improvement," MS Thesis, Near East university, Nicosia, Cyprus, 2012.

[18] Kerry L., "Application Note 779 A Basic Introduction to Filters - Active, Passive, and Switched Capacitor" National Semiconductor, Texas Instruments, 2010.

[19] S. Ahmed, G. Madjid, M. Youcef, T. Hamza, "Real Time Control of an Active Power Filter under Distorted Voltage Condition," *IJPEDS*, Vol.2, No.4, Dec 2012, pp. 424~433

[20] D. C. Bhonsle and R. B. Kelkar, "Design and simulation of single phase shunt active power filter using MATLAB," Recent Advancements in Electrical, *Electronics and Control Engineering, 2011 International Conference*, Sivakasi, India, 2011, pp. 237-241.

[21] G. S. Raj and K. Rathi, "P-Q theory based Shunt Active Power Filter for power quality under ideal and non-ideal grid voltage conditions," *2015 International Conference on Power, Instrumentation, Control and Computing (PICC),* Thrissur, India, 2015, pp. 1-5.

[22] Jeevananthan K. S., "Designing of Single Phase Shunt Active Filter Using Instantaneous Power Theory" *International Journal of Electrical and Electronics Research*, 2014, Vol. 2, pp: 1-10. ISSN 2348-6988 (online).

[23] Hong-Seok Song and Kwanghee Nam, "Dual current control scheme for PWM converter under unbalanced input voltage conditions," *IEEE Transactions on Industrial Electronics*, vol. 46, no. 5, pp. 953-959, Oct 1999.

[24] S. Kothuru, J. Kotturu and C. H. Kumar Reddy, "Reduction of harmonics in 3-phase, 3-wire system by the use of shunt active filter," *2014 International Conference on Circuits, Power and Computing Technologies [ICCPCT-2014]*, Nagercoil, India, 2014, pp. 7-12.

[25] S. Karimi, P. Poure and S. Saadate, "High performances reference current generation for shunt active filter under distorted and unbalanced conditions," *2008 IEEE Power Electronics Specialists Conference*, Rhodes, Greece, 2008, pp. 195-201.

[26] H. M. Ebrahim, "Power quality improvement using active power filter," PhD dissertation, Minoufiya University, Egypt, 2010.

[27] H. Akagi, Y. Kanazawa, A. Nabae, "Generalized Theory of the Instantaneous Reactive Power in Three-Phase Circuits," *IPEC'83 - International Power Electronics Conference*, Tokyo, Japan, 1983, pp. 1375-1386.

[28] S. Karimi, P. Poure and S. Saadate, "Reference current generation without PLL for shunt active filter under distorted and unbalanced conditions," *2008 IEEE International Symposium on Industrial Electronics*, Cambridge, UK, 2008, pp. 363-368.

[29] N. D. Tuyen, G. Fujita, M. N. B. Muhtazaruddin and T. Funabashi, "Shunt Active Power Filter for 3-phase 3-wire nonlinear load under unbalanced and distorted PCC voltage using Notch Adaptive Filter," *2014 IEEE PES T&D Conference and Exposition*, Chicago, IL, USA, 2014, pp. 1-5.

[30] H. Carneiro, B. Exposto and J. L. Afonso, “Evaluation of two fundamental Positive-Sequence Detectors for highly distorted and unbalanced systems,” *11th International Conference on Electrical Power Quality and Utilisation*, Lisbon, Portugal, 2011, pp. 1-6.

[31] T. C. Green and J. H. Marks, “Control techniques for active power filters,” *IEE Proceedings - Electric Power Applications*, vol. 152, no. 2, pp. 369-381, 4 March 2005.

[32] W. C. Duesterhoeft; Max W. Schulz; Edith Clarke, “Determination of Instantaneous Currents and Voltages by Means of Alpha, Beta, and Zero Components,” *Transactions of the American Institute of Electrical Engineers*. 1248–1255, 1951.

[33] S. Chattopadhyay; M. Mitra; S. Sengupta, “Area Based Approach for Three Phase Power Quality Assessment in Clarke Plane,” Journal of Electrical Systems, 2008.

[34] F. Tahri, A.Tahri, Eid A. AlRadadi and A. Draou Senior, “Analysis and Control of Advanced Static VAR compensator Based on the Theory of the Instantaneous Reactive Power,” *ACEMP*, Bodrum, Turkey, 2007.

[35] R. Musa, “Improving the safety operation of three-phase shunt active filter,” MSc Thesis, University of Quebec, Montreal, Canada, 2017.

[36] A. A. Rockhill and T. A. Lipo, “A generalized transformation methodology for polyphase electric machines and networks,” *2015 IEEE International Electric Machines & Drives Conference (IEMDC)*, Coeur d'Alene, ID, 2015, pp. 27-34.

[37] M. Abdusalam, P. Poure and S. Saadate, “Hardware implementation of a three-phase active filter system with harmonic isolation based on self-tuning-filter,” *2008 IEEE Power Electronics Specialists Conference*, Rhodes, Greece, 2008, pp. 2875-2881.

[38] E. Samadaei, H. Vahedi, A. Sheikholeslami and S. Lesan, "Using STF-PQ algorithm and hysteresis current control in hybrid active power filter to eliminate source current harmonic," *2010 First Power Quality Conferance*, Tehran, Iran, 2010, pp. 1-6.

[39] F. M. Hasan and A. R. Beig, "An improved active filter for distorted voltage conditions," *Applied Power Electronics Conference and Exposition (APEC), 2013 Twenty-Eighth Annual IEEE*, Long Beach, CA, 2013, pp. 3186-3193.

[40] E. Robles, S. Ceballos, J. Pou, J. L. Martín, J. Zaragoza and P. Ibañez, "Variable-Frequency Grid-Sequence Detector Based on a Quasi-Ideal Low-Pass Filter Stage and a Phase-Locked Loop," *IEEE Transactions on Power Electronics*, vol. 25, no. 10, pp. 2552-2563, Oct. 2010.

[41] S. R. Nam, S. H. Kang, S. H. Kang "Real-Time Estimation of Power System Frequency Using a Three-Level Discrete Fourier Transform Method," *Energies*, Vol. 8, No. 1, pp 97-93, 2015.

[42] Shilpa Y. Sondkar, Santosh Dudhane, Hemant K. Abhyankar, "Frequency Measurement Methods by Signal Processing Techniques," *Procedia Engineering*, Vol. 38, pp 2590-2594, 2012.

[43] R. Kennel, P. Szczupak and T. Boller, "Sensorless Control of 3-Phase PWM Rectifier in Case of Grid Phase Disconnection," *2005 IEEE 36th Power Electronics Specialists Conference*, Recife, Brazil, 2005, pp. 2019-2022.

[44] M. B. Ketzer and C. B. Jacobina, "Sensorless PWM rectifiers with active filter action," *2015 IEEE 24th International Symposium on Industrial Electronics (ISIE)*, Buzios, Brazil, 2015, pp. 405-410.

[45] Hong-Seok Song, In-Won Joo and Kwanghee Nam, “Source voltage sensorless estimation scheme for PWM rectifiers under unbalanced conditions,” *IEEE Transactions on Industrial Electronics*, vol. 50, no. 6, pp. 1238-1245, Dec. 2003.

[46] D. Wojciechowski and R. Strzelecki, “Sensorless predictive control of three-phase parallel active filter,” *AFRICON 2007*, Windhoek, Namibia, 2007, pp. 1-7.

[47] Manikandan, “Measure the Frequency of given input Square wave,” Mathworks, 2016, https://www.mathworks.com/matlabcentral/fileexchange/55456-measure-the-frequencyof-given-input-square-wave?focused=fc1c9377-6cd2-6dd4-5885 e83aeb9d60f1&tab=model

[48] Fei Liu, Xiaoming Zha, Yan Zhou and Shanxu Duan, “Design and research on parameter of LCL filter in three-phase grid-connected inverter,” *2009 IEEE 6th International Power Electronics and Motion Control Conference*, Wuhan, China, 2009, pp. 2174-2177.

[49] M. Liserre, F. Blaabjerg and S. Hansen, "Design and control of an LCL-filter-based three-phase active rectifier,", *IEEE Transactions on Industry Applications*, vol. 41, no. 5, pp. 1281-1291, Sept.-Oct. 2005.

[50] A. Kahlane , L. Hassaine, M. Kherchi, “LCL filter design for photovoltaic grid connected systems,” *Revue des Energies Renouvelables SIENR’14 Ghardaïa*, 2014, pp 227 – 232.

[51] Y. Tang, P. C. Loh, P. Wang, F. H. Choo, F. Gao and F. Blaabjerg, “Design, control, and implementation of LCL-filter-based shunt active power filters,” *2011 Twenty-Sixth Annual IEEE Applied Power Electronics Conference and Exposition (APEC)*, Fort Worth, TX, 2011, pp. 98-105.

[52] G. E. M. Ruiz, N. Muñoz and J. B. Cano, "Modeling, analysis and design procedure of LCL filter for grid connected converters," *2015 IEEE Workshop on Power Electronics and Power Quality Applications (PEPQA)*, Bogota, Colombia, 2015, pp. 1-6.

[53] A. Reznik, M. G. Simões, A. Al-Durra and S. M. Muyeen, “LCL Filter Design and Performance Analysis for Grid-Interconnected Systems,” *IEEE Transactions on Industry Applications*, vol. 50, no. 2, pp. 1225-1232, March-April 2014.